DAMAGE MODELING AND DAMAGE DETECTION FOR STRUCTURES USING A PERTURBATION METHOD

A Thesis
Presented to
The Academic Faculty

by

Akash Dixit

In Partial Fulfillment
of the Requirements for the Degree
Doctor of Philosophy in the
Daniel Guggenheim School of Aerospace Engineering

Georgia Institute of Technology
May, 2012

DAMAGE MODELING AND DAMAGE DETECTION FOR STRUCTURES USING A PERTURBATION METHOD

Approved by:

Professor Sathya Hanagud, Advisor
Daniel Guggenheim School of Aerospace
Engineering
Georgia Institute of Technology

Professor Dewey H. Hodges
Daniel Guggenheim School of Aerospace
Engineering
Georgia Institute of Technology

Professor George Kardomateas
Daniel Guggenheim School of Aerospace
Engineering
Georgia Institute of Technology

Professor Massimo Ruzzene
Daniel Guggenheim School of Aerospace
Engineering
Georgia Institute of Technology

Professor Leroy Z. Emkin
Department of Civil and Environmental
Engineering
Georgia Institute of Technology

Date Approved: 22nd December, 2011

To my Father,

Shri Suresh Kumar Dixit,

And To my Mother,

Shrimati Hem Lata Dixit,

ACKNOWLEDGEMENTS

I found writing this section to be the most difficult of all the chapters of my dissertation. All along, I have been trained to be logical and analytical, but it is difficult to do the same here. There are no precise parameters, no theoretical formulations which would give closed form or even approximate solutions, by which I can adjudge who all should be included in this section. There are no experiments that can be conducted to validate my beliefs. The chapter is based on conjectures, memories and beliefs, so, at the outset, I would like to acknowledge the inherent lack of science, as is generally understood, of this chapter and therefore apologize for errors of inclusion or omission.

I have been lucky to come across a lot of extraordinary people in my life. Among these extraordinary people, the most extraordinary have been my parents. My father is the strongest person that I came across and was my first and the best teacher. He initiated my education through a poetic creation of 'Pariyon ki rani ki kahani.' He nurtured me to become a 'world citizen.' I am always awestruck by his extraordinary ability to tame his physical faculties by his mental resoluteness. Next, I acknowledge my mother who made immense sacrifices for me. I acknowledge, a lot of my ability to do things in life are due to her constant encouragement, support and overall positive parenting, in spite of the difficulties she had to go through. This may appear a bit uncanny, but I thank myself for not giving up too. In this paragraph, I would also acknowledge God, who created the world around me to help me improve.

Next, I would like to acknowledge other people who have left an indelible mark on my future life and also rendered active help during my PhD. I would like to start with, by thanking my co-advisor Professor Hodges for his help in the preparation of this thesis. I would consider myself successful if I am able to emulate some of his characteristics as a researcher and an educator, even if partially. I would like to acknowledge my advisor Professor Hanagud, for his wisdom in guiding me through the course of this thesis preparation.

His pithy advice to me about research and life would be treasured and held in high esteem by me for the rest of my life. I acknowledge Professor Emkin, for his kind mentorship throughout my stay at Georgia Tech and his ever ready helping hand with my problems. Next, I acknowledge Mr. Stewart, for his kind heart and exemplary managerial skills which I saw as he coordinated all the sections in the Engineering Graphics and Visualization class. I would also like to acknowledge Professor Kardomateas for his kindness and support during the course of my PhD. This acknowledgement section would not be complete without my thanks to the Aerospace engineering, School as represented by Professors Jagoda and Yang, for its financial and academic support during the course of my PhD. I feel proud and lucky to be able to witness these extraordinary people and hope to imbibe the positive facets of their personalities, including but not limited to their styles of teaching, doing research and rendering service.

On a more personal level, I would like to acknowledge those among my family and friends who helped me and had good wishes for my progress. I should also acknowledge all my ancestors, including but not limited to Shandilya Rishi, Veere surke Dixit, Durga Shankar Dixit from my father's side and Pt. Babu Lal Tripathi and Mrs. Sushma Tripathi from my mother's side.

I would also like to thank Georgia Tech Research Corporation for filing two patent disclosures (GTRC ID 5224 and GTRC ID 5249) and a provisional patent (PCTUS1131279, International Publication No. WO 2011/127073) about the material presented in this thesis.

Finally, again I would again like to acknowledge God and through Him all the positive expressed or unexpressed forces of nature. But more than the positive forces, I would acknowledge the negative expressed and unexpressed forces of nature, for giving me an opportunity to prove my mettle. Through Him, I acknowledge all the previous researchers, named like Newton and Einstein and unnamed like the person who invented the wheel or persons who invented the prehistoric tools, without whose research and dedication, I would not have been able to make my very minor contribution.

Contents

List of Tables

List of Figures

SUMMARY

This thesis is about using structural-dynamics based methods to address the existing challenges in the field of Structural Health Monitoring (SHM). Particularly, new structural-dynamics based methods are presented, to model areas of damage, to do damage diagnosis and to estimate and predict the sensitivity of structural vibration properties like natural frequencies to the presence of damage.

Towards these objectives, a general analytical procedure, which yields n^{th}-order expressions governing mode shapes and natural frequencies and for damaged elastic structures such as rods, beams, plates and shells of any shape is presented. Features of the procedure include the following:

1. Rather than modeling the damage as a fictitious elastic element or localized or global change in constitutive properties, it is modeled in a mathematically rigorous manner as a geometric discontinuity.

2. The inertia effect (kinetic energy), which, unlike the stiffness effect (strain energy), of the damage has been neglected by researchers, is included in it.

3. The framework is generic and is applicable to wide variety of engineering structures of different shapes with arbitrary boundary conditions which constitute self adjoint systems and also to a wide variety of damage profiles and even multiple areas of damage.

To illustrate the ability of the procedure to effectively model the damage, it is applied to beams using Euler-Bernoulli and Timoshenko theories and to plates using Kirchhoff's theory, supported on different types of boundary conditions. Analytical results are compared with experiments using piezoelectric actuators and non-contact Laser-Doppler Vibrometer sensors.

Next, the step of damage diagnosis is approached. Damage diagnosis is done using two methodologies. One, the modes and natural frequencies that are determined are used to formulate analytical expressions for a strain energy based damage index. Two, a new damage detection parameter are identified.

Assuming the damaged structure to be a linear system, the response is expressed as the summation of the responses of the corresponding undamaged structure and the response (negative response) of the damage alone. If the second part of the response is isolated, it forms what can be regarded as the damage signature. The damage signature gives a clear indication of the damage. In this thesis, the existence of the damage signature is investigated when the damaged structure is excited at one of its natural frequencies and therefore it is called "partial mode contribution". The second damage detection method is based on this new physical parameter as determined using the partial mode contribution. The physical reasoning is verified analytically, thereupon it is verified using finite element models and experiments. The limits of damage size that can be determined using the method are also investigated. There is no requirement of having a baseline data with this damage detection method. Since the partial mode contribution is a local parameter, it is thus very sensitive to the presence of damage. The parameter is also shown to be not affected by noise in the detection ambience.

INTRODUCTION AND BACKGROUND

There is a significant number of reported studies that are related to fracture of solids. Some of the early works include the contributions of Inglis [30] and Griffith [24]. Griffith's [24] equation for a very high fracture strength is obtained by using lattice properties of solids. The result of Inglis [30] is of the form of the stress concentration in a plate with an elliptical hole, which becomes a crack in the limit, under a plane stress approximation of linear isotropic elastic solids. Griffith's theory to obtain an equation for fracture strength of cracked structures is $\sigma = \sqrt{2E\gamma/\pi a}$ for brittle materials. In this equation γ is the surface energy, a is the crack length, E the Young's modulus and σ is the tensile fracture stress. Then, Irwin [31] changed γ to $\gamma + \gamma_p$ where γ_p is the plastic energy at the crack tip. This modification resulted in combining the theoretical mechanics-based calculation of stress intensity factors to tests and the interpretations of fracture toughness in metals and alloys.

The studies provide an understanding of fracture mechanics in analysis and design of aerospace structures. Fracture mechanics has also found application to other branches of engineering. In these designs, it is hypothesized that a small crack in a structure has the potential to grow to a critical crack length because of crack-driving mechanisms such as large loads, repeated or cyclic loading (fatigue), and chemical reactions stemming from such phenomenon as corrosion, stress corrosion or hydrogen embrittlement.

It is also well known that aerospace structures are subjected to repeated and cyclic loading. In many cases, the structures are also exposed to corrosive environments. Thus, during the service life of aerospace vehicles, it is necessary to inspect the vehicles for cracks before they reach critical lengths and have the potential to cause a catastrophic failure of the vehicle. This has resulted in the development of many non-destructive inspection methods (NDE) to detect damage in operating aerospace vehicles and estimate the remaining

1

life of the vehicle by using various structural integrity programs. Early NDE techniques included X-ray observations, eddy current techniques, ultrasonic techniques, thermography etc. These techniques concentrate on local regions and are labor intensive. In many cases these techniques result in observations only in regions that are identified to be critical regions for potential damage growth and possible catastrophic failure regions. Thus, there is a need to develop techniques that have applications for a very rapid inspection of areas of damage and damage-like defects, without concentrating only in special regions and without a complete tear-down of the vehicle for purposes of inspection.

This has resulted in a new subject of research area that is currently known as Structural Health Monitoring (SHM), the process of implementing a damage detection and characterization strategy for engineering structures. Here, damage is defined as changes to the material and/or geometric properties of a structural system, including changes to the boundary conditions and system connectivity, which adversely affect the systems performance. The field of SHM arose from the field of fracture mechanics.

In SHM the structure of the aerospace vehicle is dynamically excited. As is believed in mechanics, the dynamic responses of the structure, with and without damage, are different because of changes in stiffness due to damage. The goals of SHM have been to use these differences in the dynamic responses to detect if a structure is damaged. If so, the goals are to identify locations of the damage, their magnitude in terms of the damage lengths, and their orientations. The third set of goals is to estimate the residual life of the structure on the basis of expected missions of the vehicle and the associated loads. Knowledge of the residual life is then used to decide if the part needs to be repaired or replaced to extend the life of the structure. Most of the current state of research in the area of SHM, however, is concentrated on the first two goals.

Restricting discussion to the first two goals of SHM, techniques are being developed to detect damage, their location and to quantify their characteristics before they reach a critical size. Very often, it is necessary to detect small and/or hidden damage in the structure of an operating vehicle. Small sized damage in a structure result in small changes in the dynamic response of the structure, as compared to the dynamic response of the structure that has

not developed damage of these sizes. The objectives of the first two goals are to:

1. Identify the specific types of dynamic response of the structure that are sensitive to these small areas of damage;

2. Employ appropriate actuators to excite the structures;

3. Use sensors that are capable of making measurements that can be used to identify the small changes in the dynamic response;

4. Formulate a measure such as a damage index and develop analytical techniques that are used in identification process;

5. Calculate the damage index and validate the identification technique.

Specifically, the objectives of this thesis are to develop supporting theoretical techniques that model the damage in structures, attempt to separate the changes in the dynamic response due to small areas of damage from the dynamic response of undamaged structures, and to ascertain the sensitivity of damage to detection in structures, by use of techniques that are known as perturbation techniques. Thus, the perturbation solution can be used to develop techniques for readily filtering and identifying small changes in the dynamic response due to the damage.

3

LITERATURE SURVEY

2.1 A Review of The Review Papers on SHM

Broadly the literature for vibration based SHM can be divided into two aspects, the first wherein models are proposed for the damage to determine the dynamic characteristics, also known as the direct problem, and the second, wherein the dynamic characteristics are used to determine damage characteristics, also known as the inverse problem.

In the literature, reviews in particular, for most cases both aspects are tackled together. Doebling et al. [21], which stems from a report submitted by the same authors to the Los Alamos National Laboratory [22], mainly addresses the inverse problem. Both the report and the review, although overlapping, are a good starting point for a researcher interested in identification of the damage using vibration based methods. The highlight of the review is that it addresses the advantages of vibration based methods over wave propagation based methods. The review also presents the advantages and disadvantages of methods based on time domain and those based on modal domain. The review is very focussed on the later, which is its strength since it addresses the nuances of modal domain based methods clearly and also its weakness since other aspects of SHM are not dealt with. The review presents few analytical models for the "forward problem" of natural frequency determination. The core of the review is devoted to methods for damage identification. The review's conclusion section, like the introduction, is very insightful.

Next, the work by Dimargonas [14] is of importance for this thesis because it deals with vibrations based SHM. The review paper primarily deals with the direct problem in the modeling of damage, but it also deals with the inverse problem of damage identification in some detail. The review is exhaustive, for pre-1996 literature, as far as enumerating methods to model cracks. The upside of the review is the amount of literature presented, the downside is that the introduction and conclusions are not given in depth, and the layout

and organization do not allow the reader to get a good holistic picture of the two aspects of SHM.

Both the above reviews can safely be recommended to any researcher intending to understand the origins of SHM for their respective merits. However, both of them are old and the field of SHM has proceeded since. The next useful review for vibration based SHM is by a team at Los Alamos research laboratory [62]. The bulky document has over 300 pages and is an exhaustive literature review of an important phase of the field of SHM, i.e. from 1996 to 2001. The document explains in detail the directions and avenues that researchers explored for damage identification, which included every conceivable physical quantity, from natural frequencies, modes and curvatures to damping, temperature and moisture. All of these various avenues taken by the researchers were explored and explained in the document. Another noticeable feature of the review is the gradual shift in the center of gravity of the research towards methodologies based on wave propagation. The document also sufficiently addresses other important aspects of SHM, such as sensing, data acquisition, data condensation and feature extraction. This high activity phase in the development of SHM resulted in no clear winners. The competing technologies as observed in the review have similar defects: lack of extensive statistical validation and lack of application to real life structures.

Staszewski et al. [63] present a collection of papers written by experts in the field. The papers are arranged randomly. This book can serve as a useful reference point if the topic of reference is established. However, it may not be useful to researchers seeking an introduction to the field.

The next review of interest for the present thesis is by Carden et al. [4]. The advantages of the review are that it is recent, concise and does a good job in listing and explaining of various methodologies used for damage diagnosis. The review is also much better organized than prior reviews. In the opinion of the author this work can serve as a good first reference for the inverse problem, that of damage diagnosis, because of its conciseness and good organization. There are two other reviews that are focussed on specific aspects of the inverse problem of SHM. The first is by Montalvo et al. [47] and deals with composites,

5

and the second is by Ciang et al. [12] and deals with wind turbine systems. Both are recommended for getting an introduction to different methodologies for damage diagnosis.

The latest review that the author came across was by Fan et al. [23]. The review is specifically focussed on modal parameter based damage diagnosis. An important facet of the review is that it gives a comparative study of different damage diagnosis based methods using modal parameters and gives recommendations and conclusions for different methods.

The reviews give exhaustive survey of status of SHM at the time they were published. A pithy review of literature dealing specifically with the objectives of the thesis is given next. First a literature survey of the models that are available for the damage in structures are given, and next a review of relevant damage diagnosis methods is given.

2.2 Damage Models

Before venturing into the literature review for this aspect of SHM, the usefulness and objectives of the methods to model damage should be understood so that the state of the art is viewed vis-à-vis the objectives. Mathematical models that provide analytical theories to model damage are useful in two ways: Firstly, they allow understanding of the physics behind the problem which allow the explanation of experimental readings. These studies are very useful in the development of new experimental techniques. Secondly and perhaps more importantly, they allow prediction of structure's response to dynamic excitation. Previously most of the modeling of damage has been done using finite element method software. The finite element method is a numerical method so it does not shed a lot of light, if any, on the physics associated with the damage in structures. Based on this observation the problem to be addressed may be described as follows:

"To develop generic methods that are applicable to various structures such as beams, plates and shells, and to different types of damage such as a 'V' notch or a rectangular notch, which provide a good understanding of the physics associated with the damage and also can be developed into methods which compete favorably with the finite element method as far as speed is concerned."

At a broad level, researchers have tried to model damage based on expected physical

6

behavior caused by the damage. After modeling the damage based on its expected physical behavior, which would provide governing differential equations, they were solved either exactly or using approximate methods. Therefore, the solutions available in literature are either exact or approximate solution to an approximate model based on expected physical behavior. It should be noted this approximation in the formulation was in addition to the approximations or assumptions already made in formulating a structural dynamics theory, e.g. for beams or plates. On account of the additional approximation made for the damage in formulating the structural dynamics theory, the quality of different solutions obtained by different approximate models is a moot point.

2.2.1 Analytical method for modes and natural frequencies of Euler-Bernoulli beam

Consider Ostachowicz [50] as an example of a model based on expected physical behavior of a crack , who modeled the crack as an elastic spring. The stiffness and flexibility of the spring are calculated based on concepts of fracture mechanics. As a result, for the solution, the beam is divided into as many elements as the number of the areas of damage, each with its own governing differential equation. The boundary conditions are given by continuity of displacement, moment and shear and discontinuity of slope given by local flexibility, determined by the elastic hinge properties as defined above. Using the boundary conditions and the governing differential equation, as many different displacement profiles are obtained as there are segments (which is one more than the number of cracks). The disadvantages of this model, which serves as an example for other similar models are given in the list below.

1. Representative disadvantages and limitations

    (a) The model represents an exact solution to an approximate model based on expected physical behavior of the crack behaving as an elastic spring.

    (b) The size of the problem increases. If there are n points of discontinuity along the beam, the total number of simultaneous equations to be solved is $4(n+1)$ in terms of $4(n+1)$ unknowns. In such a case, the difficulty in calculation increases dramatically and in general can be very complex even for $n = 2$ as pointed out

7

by Gurgoze [25].

(c) The model does not apply to other types of damage, such as a rectangular notch which is a relatively common physical occurrence.

(d) The solution procedure, although applicable to a Timoshenko beam, would require even more computational effort than for the Euler-Bernoulli beam that is solved in [50].

(e) The framework to extend the model to two and three dimensional elements such as plates and shells is not given.

(f) The inertia effects of the crack are not taken into account.

(g) The procedure to determine the elastic properties of the hinge is empirical.

(h) The physical fact that the status of the crack "breathes" (changes from open to closed) during vibrations is not considered.

(i) The neutral axis change due to the presence of the damage is not addressed.

Another similar concept that uses an extensional spring instead of an elastic hinge is also present in literature. An example using this concept is by Krawczuk [35]. The flexibility associated with damage was determined by using concept of stress intensity factors in fracture mechanics. This concept had the same disadvantages as were listed above for [50].

In an attempt to reduce the problem size, which was a big disadvantage of the model by Ostachowicz [50], Christides and Barr [11] presented a theory which models the crack by representing it by a single governing differential equation. The axial strain field was modified such that its effect was beyond the crack in the form of the equation $\gamma_{xx} = [-z + f(x,z)] S(x,t)$, where γ_{xx} is the axial strain, z the out of plane transverse coordinate, $f(x,z)$ an arbitrary function and $S(x,t)$ the strain function. The solution of the governing differential equation was done using the Rayleigh-Ritz method.

The advantage of this approximate model was that it reduced the problem size. The disadvantage was that it smeared the localized crack effect on the axial stress. Moreover, it was based on an arbitrary function $f(x,z)$ which modified the strain field and did not

8

have any physical justification. The arbitrary function $f(x, z)$ involved constants that could only be determined by experiments. The solution is semi-empirical since a factor α which governs the rate of stress decay was determined using experiments.

So the 9 disadvantages as listed in above list remain except that the item 1b is replaced by the above limitation.

Shen and Pierre [60] used the Galerkin method instead of the Rayleigh-Ritz method to solve the problem. They improved the convergence for the method by adding a function to the Galerkin expansion that accounts for the effect of the stress concentration on the continuity characteristics of the exact solution. They also used the finite element procedure instead of experiments to determine the factor α, but the essential disadvantages associated with the method proposed by Christides and Barr, as listed above, remained the same.

Qian [52] constructed a stiffness matrix for the damaged element based flexibility coefficient determined using strain energy associated with the crack. The method to determine the size of the element was not specified. The method had disadvantages from 1c to 1i in the list given above. Law et al. [36] modeled the crack as an impulse drop in the bending stiffness. The physics of the problem does reflect that the bending stiffness at the damage location changes discretely but the mathematical explanation to define the change as an impulse drop was missing. It was further assumed that the displacement modes of the damaged beam were same as undamaged beam. [67] approximated the modal displacements using Heaviside's function, which meant that modal displacements were discontinuous at the crack location.

The choice for researchers was to either have a theory which was unwieldy because of the problem size or have a theory that was semi-empirical and lacked physical justification. Both the choices had other disadvantages as given above in the list.

It is interesting to note that a model which had much lesser disadvantages was proposed long back in 1949 by Thompson [66], who modeled the damage as a concentrated couple at the location of the damage. The magnitude of moment associated with the couple is determined using the change in cross sectional dimension rather than through concepts of fracture mechanics. So, rather than modeling the beam with changed cross sectional

9

dimension, it is modeled as a beam with constant cross section but modified load (moment). The magnitude of the increase in the moment is given by a factor α which is computed based on the ratio of the moment of inertia at the damage location (I') and that for the rest of the beam (I_0). The curvature equation for the beam is therefore written as

$$\frac{d^2y}{dx^2} = -\frac{1}{EI_0}\frac{M}{\alpha} \quad \alpha = \frac{I'}{I_0} \tag{1}$$

This is an old work and has been neglected by recent researchers. However, it does not suffer from several of the shortcomings of the recent model as shown in the list of disadvantages above. The beam is tackled as a single beam, and hence the problem size does not increase depending upon the number of damage locations. Several types of damage can be tackled using this concept since computation of change in cross sectional moment of inertia is much easier to calculate as compared to calculation of stress intensity factor associated with the different types of damage. The concept can be easily applied to other beam theories such as Timoshenko theory as well as other structures such as plates and shells.

The disadvantages which remain with the model [66] are:

1. Lack of consideration of inertia effect of damage;

2. The process to apply the model as a generic procedure applicable to diverse set of structures, and diverse types of damage is not given;

3. The breathing crack problem has not been addressed;

4. It has been not shown how the change in the neutral axis due to damage would be accounted.

However, as the number of disadvantages are fewer in the model given by Thompson's [66], it is the opinion of the author that Thompson's method holds promise, and should be explored further to remove the remaining disadvantages.

The next interesting model based on expected physical behavior is by Joshi et al. [32], which tackles the a different problem that of material instead of the cracks usually addressed

10

in the literature. The problem however, is again addressed by dividing the beam into three connected beams, with the beam that contains the damage having a different (reduced) Young's modulus. Indeed an important class of problems is addressed in this work, but the approach of smearing the change in constitutive properties due to damage, which is a localized effect, through the length of the beam containing the damage has not been validated. In addition, the model suffers from all the 9 disadvantages enumerated above for the model given by [50]. Some of the variables used in the formulation are not defined before their first use, which can make reading a little confusing.

An advancement in the field of modeling of cracks can be regarded by Chondoros et al. [10] and Luo and Hanagud [41]who attempted to tackle the non-linearity of the vibration problem by using a concept of "breathing cracks." They argued that during vibrations a crack does not always remain open but the two surfaces associated with the crack move towards and away from each other, thereby making the problem non-linear. They then simplified the problem by assuming that the crack is either fully open or fully closed. They also assumed that during vibrations, when the beam reaches its undeformed state, the crack status switches from open to closed or vice versa in a discrete way. The argument for this model was that it was better than a model which assumes the crack open at all times.

The open crack condition as discussed by Chondros et al. [10] was based on another work by the same authors [9], which was a generalization of the model proposed by [11] and hence having the same disadvantages. In effect the non-linearity associated with crack is accounted by using a model that was physically not justified.

Another stream of thought that was developing was that of perturbation methods. Bayly [3] and Happawana et al. [26] studied the effects of the magnitude of perturbations (disorders) on the localization of modal shapes for non-linear vibrating systems. By applying the regular perturbation technique to the characteristic equation of the system, they obtained algebraic expressions for the eigenvalues as a power series in the small parameter or perturbation with acceptable accuracy.

11

Luo and Hanagud [41] formulated an integral equation to model a structure with notch type damage and successfully demonstrated an analytical solution technique by using perturbation methods. Next, Luo and Hanagud [42] and subsequently Lestari [37] proposed a perturbation method for mode shapes and natural frequencies to describe the behavior of damaged beams. Lestari et al. [?] used Fourier sine series expansion for the modes of damaged beams with simply-supported ends. Sharma [57, 58], discussed an "approximate solution" for the damaged plate in terms of a double Fourier sine series for a plate with simply-supported boundary conditions on all four edges.

The important development in the above methods was not the perturbation of mode shapes and natural frequencies, but the mathematical treatment of the damage. By mathematically representing the drop in the thickness at the damage location as dirac delta function, the arbitrariness of the previous models was removed. It should be noted that previous models of the damage represented the damage by elastic elements such as springs, whose elastic properties were determined based on arbitrary functions. The mathematical model of damage was not based on expected physical behavior implemented by replacing the damage with a suitable elastic element like a spring or a hinge but on actual structural layout. The two reasons together preempted the increase in the problem size since the vibrations was represented by a single governing differential equation. The perturbation allowed the tackling of the non-linearity associated with the damage.

The remaining disadvantages, however, were not addressed. No representation was given for arbitrary shaped damage. The method showed promise to be applicable to higher order beam theories or structures like plates and shells. However, the application was given to only simply-supported beam and plate. A solution applicable to a generic structure was not given. For both the cases, Lestari and Sharma had errors in the solution of the perturbed differential equation, which were corrected in [17], as they did not obtain the complementary solution but only the particular integral for the higher order equations. The treatment of inertia effects was tentative since it was present in the thesis by Lestari [37] but removed in the publication resulting from it [?].

2.2.2 Damage sensitivity: effect of shape of damage and beam shape

Damage occurs in a variety of shapes and sizes and can occur in beams of different shapes. Most of the literature, however, concentrates on either sharp cracks or rectangular notches in uniform beams of rectangular cross sections. A study of the effect of damage shape on the vibration characteristics of beams of different shapes has not been done to the best of the author's knowledge.

The objective is to ascertain the effect of the same type of damage placed on beams of different cross sections, such as a T-beam and a rectangular beam. Although a direct precedent for modeling different types of damage using vibration-based techniques was previously not found in the literature, work has been done in the area by using Lamb waves for such a characterization by Cho and Rose [7]. Experimental results for a composite T-beam are presented [49], but no theoretical model for damage is given.

2.2.3 Damaged modes and frequencies using Timoshenko beam theory and Kirchhoff plate theory

Whether it is because of the complexity of the proposed damage models or the lack of justification or availability of arbitrary functions is not known, but the literature associated with their application to higher order theories or more complex structures such as plates or shells definitely tapers off. Moreover, the methods used were on similar lines as those used for Euler-Bernoulli beams, and so the same limitations and disadvantages were applicable.

Swamidas [64] used natural frequencies to detect damage for cracked Timoshenko beams for simply-supported beams. It was assumed that there is local drop of stiffness at the damage location denoted by EI_c. This quantity was calculated based on concepts of fracture mechanics and the same limitations as listed previously were also applicable to this method. After derivation of the governing differential equation, it was solved with the Galerkin method using modes of an un-cracked beam as comparison functions.

Another attempt to model damage in Timoshenko beams is by Khaji et al. [33] who modeled the damaged beam using the same principles as were used by Ostachowicz [50] for Euler-Bernoulli beams. The closed-form solution for their approximate model is presented

13

for vibration of damaged Timoshenko beams. The damage was represented as a rotation discontinuity. The damaged Timoshenko beam with some commonly occurring boundary conditions, damage parameters and beam parameters are considered. The results showed close agreement with results from finite element models. Another attempt to determine natural frequencies of a damaged Timoshenko beam based on rotational spring model is presented by Li [39]. Loya et al. [40] showed, however, that merely assuming rotational spring at the crack location is not sufficient to model a crack. They assumed an additional extensional spring at the crack location. The extensional and the rotational spring flexibilities were determined using empirical relations cited from previous works.

In the meantime, the problem of Kirchhoff's plates with damage was tackled by Sharma et al. [59, 57], for a straight line damage oriented parallel to one of the plate coordinate axes. This was an extension of the work by Lestari [?] where the damage was modeled mathematically instead of an arbitrary elastic element. The solution was done using perturbation methods. The solution was presented only for the case of plates simply-supported on all four edges. Unfortunately, there were errors both in the perturbed differential equations and their solutions [17]. The technique had advantages over existing techniques as detailed in the previous section regarding Euler-Bernoulli beams, but they were not fully exploited.

2.3 Damage Diagnosis Methods-Vibrations

Early vibration based measures used to detect damage were based on changes in natural frequencies; see Cawley et al. [5], Man et al. [44], and Carden et al. [4]. Natural frequencies are global parameters and give a global indication of change in the structural mass and stiffness distributions. The advantage of using natural frequencies as a damage measure is that it is easy to obtain their values. The disadvantage is that, as global parameters they can be used only as indicative of the presence of damage. Also, since natural frequencies change due to environmental conditions like temperature, they cannot be considered as reliable indicators of damage.

As already mentioned earlier, the natural frequencies are functions of stiffness and mass. The change of inertia or kinetic energy effect due to damage the can be of the same order

14

of magnitude as that of the change of stiffness, but this inertia effect due to change in the mass distribution is not considered by most researchers in the literature. A damage can result in change of both the parameters, so severe damage may result in smaller change in natural frequencies than mild damage. Hence, even the severity of damage cannot be confidently adjudged using changes in natural frequencies. The change in natural frequencies is dependent on the effective change in mass and stiffness. Effective change in mass or stiffness is dependent on the location of damage and modal energy associated with the damage. So inherently the inverse problem (problem of getting the damage parameters from the vibrational characteristics) has a non-unique set of solutions.

Another vibration based measure used in damage detection is the mode shapes; see Ho and Edwins [28], West [69] and Carden et al. [4]. Use of mode shapes alleviates some of the shortcomings of using natural frequencies since it can help locate the damage. Because the response caused by damage is not erratic, the change in the mode shape can be directly related to severity of the damage. However, the change in mode shape is very small and sometimes can be of the order of the noise during measurements, making it difficult to ascertain the change; see Pandey and Biswas [51] and Qiao et al. [53] .

To improve the sensitivity of mode shapes as damage indicators, researchers proposed curvature for damage detection [51]. In the absence of any external moment acting at the damage location, the bending moment should be continuous across the damage. Bending stiffness is not continuous since the depth of beam and hence the area moment of inertia, is not continuous. Therefore, the bending stiffness, which is proportional to the area moment of inertia is not continuous. This further implies that curvature, which is the ratio of bending moment and bending stiffness, is not continuous across the damage. It was successfully shown by Chandrashekar and Ganguli [6] and Lestari [37] that curvature mode shapes can be effectively used to determine and characterize damage. Several mathematical procedures were proposed to increase their sensitivity.

However, curvature is often a secondary result [53] or it is not measured directly. It may be calculated by the numerical differentiation of the mode shapes. So, no matter how well the mathematical differentiation is done, the sensitivity of the curvature as an

15

effective damage measure depends on the accuracy of mode shapes measurements, and their sensitivity to damage.

Strain energy is a product of discontinuous curvature with discontinuous bending stiffness. Next, the researchers exploited this double discontinuity of strain energy to devise methods to identify and characterize damage. Wang et al. [68] first proposed a damage index as a function of strain energy. Kim et al. [34] formulated a damage index without requiring the knowledge of the dynamic response of the undamaged structure. She et al. [61] formulated a distributed parameter damage index, Modal Strain Energy Change Ratio (MSECR), based on the ratio of the change in strain energy of each element to the strain energy of undamaged state of that element. The stiffness of the element was kept the same for the undamaged as well as damaged structure for strain energy computations of both states of the structure. The quality of this indicator is improved by summing the contributions of multiple modes in a normalized fashion as a cumulative damage index.

Choi et al. [8] gave a different damage index based on strain energy ratios. For this they divided the beam into a number of elements. A ratio of strain energy of each element with respect to all elements in the structure is formulated for the undamaged as well as the damaged structure. Cornwell et al. [13], implement the damage index for two dimensional structures.

Damping ratios were used by Modena et al. [46], and frequency response functions by Schulz et al. [56] to determine damage in structures. Ho and Ewins [27] formulated a "Damage Index" as the quotient squared of the corresponding modal curvatures of the undamaged and damaged structure.

Wang, Xu and LLoyd [68] first proposed a damage index as a function of strain energy. Kim, Ryu, Lee, and Choi [34] formulated a Damage Index without requiring the knowledge of the dynamic response of the undamaged structure. Intrinsic Fabry-Perot optical fiber sensors were attached to a steel girder of the Sungsan Bridge which is one of the longest span bridges over the Han River in Seoul, Korea. The tests were performed as parts of safety diagnosis of the bridge. Numbers of strain gauges, acceleration sensors and a deflection gauge as well as optical fiber sensors were used. Static and dynamic loads were applied to

16

the bridge by using 30 ton trucks. The optical fiber sensor system showed good responses to the static and dynamic loading with a resolution of approximately 0.12 micro units strain. The optical fiber sensors were used as elements of the bridge monitoring system.

Chapter III

RESEARCH ISSUES AND PROBLEM ADDRESSED

3.1 Research Issues - Direct Problem

Before the research issues associated with the damage modeling aspect of SHM are high-lighted, it is helpful to reiterate the usefulness and objectives associated with that aspect. As mentioned in chapter 2 the mathematical models that give analytical theory to model damage are useful in two ways: Firstly, they allow understanding of the physics behind the problem which allow the explanation of experimental readings. These studies are very useful in the development of new experimental techniques. Secondly and perhaps more importantly, they allow prediction of response of the structure. Currently most of the modeling of damage is done using finite element software. The finite element method is a numerical method so it does not shed a lot of light on the physics associated with the damage in structures. Based on this the problem may be defined as follows:

"To develop generic methods that are applicable to various structures such as beams, plates and shells, and to different types of damage such as a 'V' notch or a rectangular notch, which provide a good understanding of the physics associated with the damage and also can be developed into methods which compete favorably with the finite element method as far as speed is concerned."

In the opinion of the author, based on the literature survey, unfortunately, this aspect of SHM has not received the emphasis it deserves. The number of elements required to model a damaged element is very high and is limited by the size of damage, at least in the vicinity of the damage. So, in a beam of length 1 m and cross sectional dimensions 0.02 m $\times$ 0.005 m, if there is a through-thickness damage of depth 0.0005 m, the elements required to model this damaged beam would be two-dimensional plane stress elements with the smallest elements being of the order of 0.0005 m. This increases the computational requirement from using a few beam elements for undamaged state to several plane stress

elements for the damaged state. This increases the time required to solve the problem by several orders of magnitude.

The damage models presented, rather than mathematically modeling the damage as a geometric discontinuity, have the physics associated with the problem already conjectured . It is already firmly established in the mind of some researchers in this field that only stiffness at the damage location is reduced. No wonder, that the physics reflected by these models reflect the conjecture rather than the actual physics. The reason why researchers followed this path was, as given in chapter 2, the origins of the field of SHM lied in the field of fracture mechanics. The field of fracture mechanics deals with fatigue and statics. At the damage location the only physical quantity affected is the only physical quantity considered, the stiffness. As far as structural dynamics is concerned, however, another physical quantity involved: inertia. This is manifested as mass per unit length for beams and mass per unit area for plates. Mass per unit length or per unit area changes due to redistribution of mass due to the damage during vibrations. Whether these inertial effects are consequential or not may only be determined using mathematical models.

One unique effort in this direction was conducted by Professor Hanagud and coworkers, by presenting a mathematical model for the damage which involved both inertial and stiffness effects. The solution of this model was attempted using a perturbation method. However, the fully utility of the method was not apparent due to errors in arriving at the perturbed differential equation and their solutions. Also, the method was applied to only simply-supported boundary condition for Euler-Bernoulli beam theory and Kirchhoff's plate theory. The damage models were presented for only very limited set of damage.

The objective of the PhD thesis is to add incremental value by addressing the research issues that arise from the state of the art. It is good to keep in mind the overall objective, as given above, to keep the perspective focussed. With regard to that incremental research issues are mentioned below.

In spite of considerable progress in the damage identification using vibration-based methods, fairly successful algorithms to model or detect damage do not exist as concluded in all the reviews since 1995. In 1995 in the review published by Dimarogonas [14], it is concluded

19

"A consistent cracked beam vibration theory is yet to be developed." In 2005, in another review about vibration based structural health monitoring, Carden et al. [4] conclude, "There is no universal agreement as to the optimum method for using measured vibration data for damage detection, location or quantification." Similarly, in 2007 Montalvao et al. [47] state as one of the conclusions, "There is no general algorithm that allows the resolution of all kinds of problems in all kinds of structures."

Let us now examine the state of the art with reference to the problem defined above. Most of the damage models in literature restrict themselves to Euler-Bernoulli beams. Even in the domain of Euler-Bernoulli beams they restrict themselves to a few boundary conditions and damage types. None of the methods given in the literature provide a framework that is applicable to all elastic structures. An important understanding regarding the research issues vis-à-vis the damage models is that the problem synthesis for damaged elastic elements invariably includes two parts, the formation and the solution of the governing differential equation(s).

There are primarily three kinds of ways by which the governing differential equation is formulated. The first is dividing the beam at the damage location and substituting it with an elastic element. The primary disadvantage with this method is the manifold increase in problem size. The order of the solution to the problem increases. If there are n discontinuity points on the beam, the total number of coefficients to be determined becomes $4(n + 1)$, which leads to a requirement to solve $4(n + 1)$ equations simultaneously . In such a case, the difficulty in calculation increases dramatically and in general can be very complex even for $n = 2$ as pointed out by Gurgoze [25].

The next method is to treat the beam as a single beam, but smearing the bending stiffness discontinuity due to the damage over the whole or part of the beam. The primary disadvantage with this model is the inaccurate representation of the physics, since the bending stiffness drops locally at the location of the damage only.

The third method assumes local drop of stiffness. The disadvantages associated with this method, which are also common to other two methods, are as follows:

1. The model represents an exact solution to an approximate model based on expected

physical behavior of the crack behaving like an elastic element.

2. No models are given for other types of damage, say a rectangular notch or a V-notch, which are a common physical occurrence.

3. The modeling of damage is based on arbitrary and empirical functions.

4. The framework to extend the model to two dimensional elements like plates and shells is not given. There are very few examples in which the method is extended to Timoshenko beam theory.

5. The inertia effects of the crack are not taken into account.

6. The physical fact that the status of the crack 'breathes' (changes from open to closed) during vibrations is not considered.

3.2 Research Issues - Inverse Problem

Two techniques in the field of SHM are wave propagation based techniques Raghavan and Cesnik [54] and vibration based techniques Carden et al. [4], Montalvao et al. [47], Fan et al. [23]. It is sometimes argued that techniques based on wave propagation are more sensitive to damage detection than those based on vibration [63]. The advantages with regard to sensitivity of wave-propagation-based techniques arise due to the selected damage detection parameters, such as the reflected wave due to the damage. The asserted shortcoming of lack of sensitivity of vibration-based techniques has several reasons. The primary among them being that the order of changes in damage detection parameters for small defects is of the order of the noise in the detection ambience. However, it is accepted that vibration-based techniques are easier to implement and the data obtained by them can be used to determine the vibration characteristic of the damaged structure Fan et al. [23]. For example, the modes determined by vibration-based techniques can be used to determine the subsequent response of the structure after the damage has been identified and defined. Vibration-based techniques are also able to examine relatively large areas of the structure as well as inaccessible areas. The natural vibrations of the structure can be used as the excitation rather than external excitation as required in wave-propagation-based techniques.

21

The viewpoint of the reviews for vibration-based structural health monitoring is similar. Regarding the sensitivity of vibration-based methods, the review by Carden [4] states "Most notably, the sensitivity and measurability of the modal parameter shifts due to localized damage is a matter of disagreement amongst the research community." Lack of sensitivity of vibration based methods is also discussed in the section 2.8.1 of a book by Staszewski et al. [63].

As can be seen in the discussion in the previous paragraph, vibration-based methods have strong advantages over wave-propagation-based methods except their lack of sensitivity towards damage detection. It is therefore proposed that a vibration-based method, that has a strong sensitivity to damage would be an open research issue.

3.3 Damage Sensitivity

Another research aspect which has not received much attention is the sensitivity of damage to the shape of the structure. For example, it would be interesting to study the shape of the beams in which the damage is more easily identifiable compared to those in which it is more difficult.

3.4 Problems Addressed

The work associated with this thesis, as probably with most research works of this nature, started with a bottom up approach.

1. The first problem is to obtain time domain analytical solutions for perturbed Euler-Bernoulli beam equations, due to notch type of damages, using superposition of modes, for boundary conditions that yield orthogonal modes. In this method the rather than assuming an elastic element at the notch location or using assumed modes or any other approximation for the crack behavior, the notch dynamics is encapsulated through perturbation methods in the change of cross-section characteristics like area and area moment of inertia. The model includes the mass change which has till now been neglected by researchers. Mass change is included as the change in cross-sectional characteristic 'area of cross-section'. The natural frequencies and mode

shapes are perturbed using principles of perturbation method. This problem addresses the correction to the problems with the solution of a damage modeling procedure presented by Lestari et al. [?] for Euler-Bernoulli beams as given by Dixit and Hanagud [17].

2. The success of a structural health monitoring technique depends on the separation of small changes in dynamic response due to structural damage from the gross dynamic response of the structure, which results from a selected excitation. To isolate the small changes of dynamic response from higher-order effects such as rotational kinetic energy and transverse shear deformation, the model developed for Euler-Bernoulli beams was extended to Timoshenko beams. It should be noted that Timoshenko beam model includes rotational kinetic and transverse shear effects. This was done by Dixit and Hanagud [15].

3. At this point it was realized that there are similarities in the derivations required to model the damage of beams using Euler-Bernoulli beam theory and Timoshenko beam theory. To exploit these similarities a generalized procedure [20] was developed. The procedure was shown to be applicable to self adjoint systems with discontinuities. It was verified for Euler-Bernoulli beams [18], Timoshenko beams [15], Kirchhoff's plates [19].

4. The damage model is applied to plate structures using Kirchhoff's plate theory [19], the following improvements were made over the work of Sharma et al. [59]. Corrections were made to both the perturbed governing differential equations and their solution. The damage model presented can account for damage oriented in any arbitrary direction. The method was extended to other boundary conditions other than simply-supported on all four ends as tackled by Sharma et al. [59].

5. The research issue associated with the inverse problem was also tackled in a similar way as for the direct problem. First, the state of the art existing in literature was improved. For an analytical expression for a damage index based on strain energy

was derived using the analytically derived mode shapes and natural frequencies for damaged beams. This damage index is given by Dixit and Hanagud [18].

6. With an eye on fulfilling an important of criteria vibration-based SHM and also its primary disadvantage as compared to wave-propagation-based SHM, that of sensitivity of damage detection, a new physical parameter is identified and is called "partial mode contribution". The physical reasoning behind the partial mode contribution was verified using the analytical derivation. This led to the next work for this thesis - that of using partial mode contribution for damage detection. This work is presented in by Dixit and Hanagud [16].

3.5   Organization of the Thesis

To make the material presented in this thesis easy to understand and to preempt redundancy the organization of the material is altered from the chronological order of work as performed. The correct chronology of development of work for the thesis entailed obtaining the corrected version of the damage model presented by Lestari [?], presented in by Dixit and Hanagud [17]. Based on the corrected modes and natural frequencies obtained, an analytical expression for a damage index based on strain energy was obtained by Dixit and Hanagud [18]. The same principles as those used to find the analytical expressions of mode shapes and natural frequencies for Euler-Bernoulli beams were used to find those for Timoshenko beams. It was discovered that the derivations for both theories were similar, which gave birth to a general framework to model areas of damage for elastic structures. Almost concurrently the physical reasoning behind a unique physical quantity for damage detection was discovered and was named partial mode contribution and the corresponding method called "Partial Mode Contribution Method." Eventually the research progressed to application to plates using Kirchhoff's plate theory and then applying to different shapes of beams to ascertain the sensitivity of damage.

The order in which material in this thesis is presented is as follows. First, the full derivation of a damage model solved using perturbation methods is given in chapter 4, since it is essentially the heart of the thesis. As mentioned earlier the thesis started with

correcting the solution presented by Lestari [?], this is presented in chapter 2. Next, the analytical derivation to determine mode shapes and natural frequencies of Euler-Bernoulli beams and also using them to formulate a damage index based on strain energy is presented in 6. Next, results for Timoshenko beam theory, and comparison with results obtained using Euler-Bernoulli beam theory, are given in chapter 7. A damage model for the damage oriented in arbitrary directions is presented to obtain analytical results for Kirchhoff's plate theory in chapter 8. Next, the interesting problem of determining the sensitivity that damage has to the beam shape is presented in chapter ??. This is done by using damage in a T beam and a rectangular beam. The first solution to the inverse problem using analytical expressions of a new damage index based on strain energy is presented in chapter 6. A new damage identification technique called the Partial Mode Contribution Method is presented in the next chapter of this thesis, chapter 9. Finally conclusions and direction for future research based on the work presented in this thesis are presented in the last chapter of this thesis, chapter 10.

Chapter IV

A GENERAL PROCEDURE TO MODEL DAMAGES SOLVED USING PERTURBATION METHOD

This chapter is to a large part a reproduction of a published work done by the author [20]. It presents a generic framework that deals with solution of the eigenvalue problem associated with vibration of elastic structures comprised of discontinuous domains, which constitute self-adjoint systems. The general representation of the eigenvalue problem is given by a homogeneous differential equation with non-constant coefficients. The damage represented mathematically by damage profile functions and a perturbation of eigenfunctions and eigenvalue is used to change the homogeneous differential equation with non constant coefficients to a series of non-homogeneous differential equations with constant coefficients. Orthogonality of modes is then used to solve those equations to obtain expressions for n^{th} order perturbed eigenfunction and eigenvalues.

4.1 General Development

The general eigenvalue problem to determine the mode shapes and natural frequencies of elastic structures such as rods, beams, plates and shells is given in [45]

$$L\phi(x_i) - \lambda M\phi(x_i) = 0 \tag{2}$$

where L is the stiffness operator, M is the inertia matrix and λ is the eigenvalue. The order of L is an even integer that is given by $2p$ (p is a natural number). The equation is valid for conservative distributed parameter structures, which represent a very large and important class of systems, namely self-adjoint systems. Here $\lambda = \omega^2$ where ω is the natural frequency and ϕ is the eigenfunction or the mode shape, and x_i the spatial independent variable, (i represents the direction). The x_i denotes the one-dimensional space in case of beams, two-dimensional space in case of plates and shells and three-dimensional space in case of three-dimensional structures. The displacements and rotations corresponding to the

spatial dimension x_i are u_i and θ_i, respectively. In case of an Euler-Bernoulli beam, the variables of Eq. (2) are given by

$$L = \frac{d^2 H_{33}(x_1)}{dx_1^2}\frac{d^2}{dx_1^2} \quad M = \rho(x_1)A(x_1) \quad \phi(x_1) = u_1(x_1) \quad H_{33}(x_1) = E(x_1)I_3(x_1) \quad (3)$$

and in the case of Timoshenko beam theory their values are

$$L = \begin{bmatrix} -\frac{dK_{22}(x_1)d}{dx_1^2} & \frac{dK_{22}(x_1)}{dx_1} \\ -\frac{K_{22}(x_1)d}{dx_1} & K_{22}(x_1) - \frac{dH_{33}(x_1)d}{dx_1^2} \end{bmatrix} \quad M = \begin{bmatrix} \rho(x_1)A(x_1) & 0 \\ 0 & \rho(x_1)I(x_1) \end{bmatrix}$$

$$\phi(x_1) = \left\{ \begin{array}{c} u_1(x_1) \\ \theta_3(x_1) \end{array} \right\} \quad K_{22}(x_1) = \kappa G(x_1)A(x_1) \quad (4)$$

where E, G, κ and I are the Young's modulus, shear modulus, shear factor and area moment of inertia, respectively, ρ is the density, A is the area, u_1 is the transverse displacement, and θ_3 is the sectional rotation. All the quantities are functions of spatial dimension x_1.

In case of plates or shells L is a partial differential operator. For Kirchhoff's plate theory the variables of equation (2) are given by [2]

$$L = \nabla^2 D \nabla^2 - (1-\nu)\left(\frac{\partial^2 D}{\partial x_2^2}\frac{\partial^2}{\partial x_1^2} - 2\frac{\partial^2 D}{\partial x_1 \partial x_2}\frac{\partial^2}{\partial x_1 \partial x_2} + \frac{\partial^2 D}{\partial x_1^2}\frac{\partial^2}{\partial x_2^2}\right) \quad \phi = u_3(x_1,x_2)$$

$$D = \frac{E(x_1,x_2)h(x_1,x_2)^3}{12(1-\nu^2)} \quad M = \rho(x_1,x_2)h(x_1,x_2) \quad (5)$$

and for Mindlin plate theory their values are given by [55]

$$L = \begin{bmatrix} -\frac{\partial D \partial}{\partial x_1^2} - \frac{\partial D/2(1-\nu)\partial}{\partial x_2^2} + F & -\frac{\partial D \nu \partial}{\partial x_1 \partial x_2} - \frac{\partial D/2(1-\nu)\partial}{\partial x_2 \partial x_1} & -F\frac{\partial}{\partial x_1} \\ -\frac{\partial D/2(1-\nu)\partial}{\partial x_1 \partial x_2} - \frac{\partial D \nu \partial}{\partial x_2 \partial x_1} & -\frac{\partial D/2(1-\nu)\partial}{\partial x_1^2} - \frac{\partial D \partial}{\partial x_2^2} + F & -F\frac{\partial}{\partial x_2} \\ \frac{\partial F}{\partial x_1} & \frac{\partial F}{\partial x_2} & -\frac{\partial F \partial}{\partial x_1^2} - \frac{\partial F \partial}{\partial x_2^2} \end{bmatrix}$$

$$M = \rho(x_1,x_2)h(x_1,x_2) \begin{bmatrix} \frac{h(x_1,x_2)^2}{12} & 0 & 0 \\ 0 & \frac{h(x_1,x_2)^2}{12} & 0 \\ 0 & 0 & 1 \end{bmatrix} \quad \phi = \left\{ \begin{array}{c} \theta_1(x_1,x_2) \\ \theta_2(x_1,x_2) \\ u_3(x_1,x_2) \end{array} \right\}$$

$$F = \kappa G(x_1,x_2)h(x_1,x_2) \quad (6)$$

In the above equations, $h(x_1,x_2)$ is the thickness of the plate, $\theta_1(x_1,x_2)$ and $\theta_2(x_1,x_2)$ are plate rotations about the x_1 and x_2 axis, respectively, and $u_3(x_1,x_2)$ is the transverse displacement.

27

The boundary conditions for equation (2) are given by

$$B_i \phi(x_j) = 0 \quad i = 1, 2 \ldots, p \tag{7}$$

where B_i is a differential operator of maximum order of $2p - 1$, where p was defined with reference to the order of the eigen value problem. Examples of clamped, pinned and free boundary conditions for Euler-Bernoulli are given by

$$B_i = \left\{ \begin{array}{c} 1 \\ \frac{d}{dx_1} \end{array} \right\} \quad @x_1 = \text{clamped} \quad B_i = \left\{ \begin{array}{c} 1 \\ EI\frac{d^2}{dx_1^2} \end{array} \right\} \quad @x_1 = \text{pinned}$$

$$B_i = EI \left\{ \begin{array}{c} \frac{d^2}{dx_1^2} \\ \frac{d^3}{dx_1^3} \end{array} \right\} \quad @x_1 = \text{free} \tag{8}$$

and for Timoshenko beam theory by

$$B_i = \begin{bmatrix} 1 & 0 \\ 0 & 1 \end{bmatrix} \quad @x_1 = \text{clamped} \quad B_i = \begin{bmatrix} 1 & 0 \\ 0 & EI\frac{d}{dx_1} \end{bmatrix} \quad @x_1 = \text{pinned}$$

$$B_i = EI \begin{bmatrix} \frac{d}{dx_1} & -1 \\ 0 & \frac{d}{dx_1} \end{bmatrix} \quad @x_1 = \text{free} \tag{9}$$

The boundary conditions for an edge parallel to x_1 for clamped, pinned and free edges of the plate, respectively, according to Kirchhoff's plate theory, are given by

$$B_i = \left\{ \begin{array}{c} 1 \\ \frac{\partial}{\partial x_1} \end{array} \right\} \quad @x_1 = \text{clamped} \quad B_i = EI \left\{ \begin{array}{c} 1 \\ \frac{\partial^2}{\partial x_1^2} \end{array} \right\} \quad @x_1 = \text{pinned}$$

$$B_i = EI \left\{ \begin{array}{c} \frac{\partial^2}{\partial x_1^2} + \nu \frac{\partial^2}{\partial x_2^2} \\ \frac{\partial D\nu}{\partial x_1}\frac{\partial^2}{\partial x_2^2} + \frac{\partial D}{\partial x_1}\frac{\partial^2}{\partial x_1^2} + 2\frac{\partial D(1-\nu)}{\partial x_2}\frac{\partial^2}{\partial x_1 \partial x_2} \end{array} \right\} \quad @x_1 = \text{free} \tag{10}$$

and for Mindlin plate theory are given by

$$B_i = \begin{bmatrix} 1 & 0 & 0 \\ 0 & 1 & 0 \\ 0 & 0 & 1 \end{bmatrix} \quad @x_1 = \text{clamped} \quad B_i = \begin{bmatrix} D\frac{\partial}{\partial x_1} & D\nu\frac{\partial}{\partial x_2} & 0 \\ 0 & 1 & 0 \\ 0 & 0 & 1 \end{bmatrix} \quad @x_1 = \text{pinned}$$

$$B_i = D \begin{bmatrix} D\frac{\partial}{\partial x_1} & D\nu\frac{\partial}{\partial x_2} & 0 \\ D\frac{\partial}{\partial x_2} & D\frac{\partial}{\partial x_1} & 0 \\ F & 0 & F\frac{\partial}{\partial x_1} \end{bmatrix} \quad @x_1 = \text{free} \tag{11}$$

28
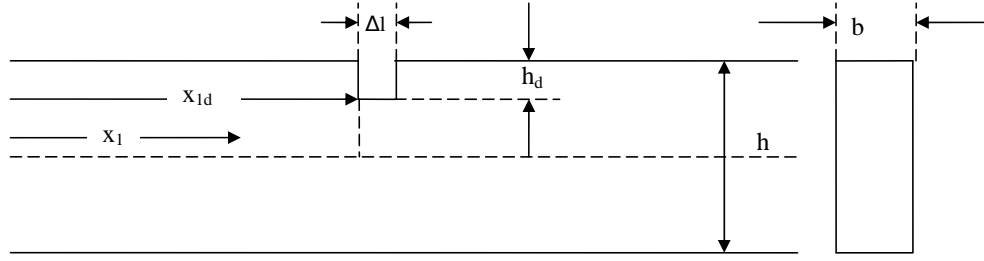
Figure 1: Rectangular notch beam
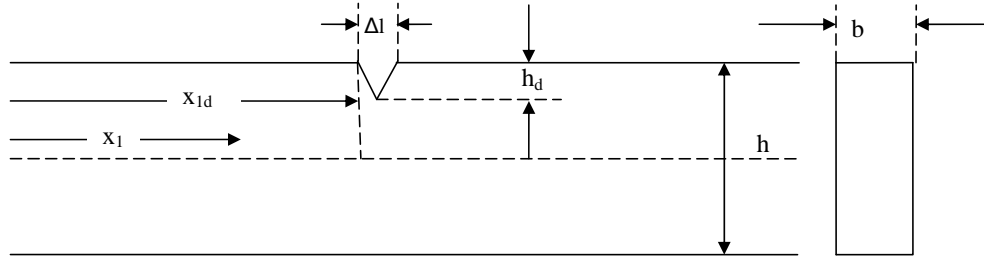
Figure 2: V-notch beam

4.1.1 Damage model

The damage model presented in this chapter models the change in cross sectional thickness at the damage location. If the damage depth is $h_d(x_i)$ then at the damage location the depth becomes $h - h_d(x_i)$, where h is the constant depth at the undamaged location. Further a quantity $\bar{h}_d$ is defined which gives the average depth of the damage given by

$$\bar{h}_d = \int\limits_\Omega h_d(x_i)dx_i \tag{12}$$

where Ω gives the domain of damage. Therefore, the depth of the structure is given by

$$h(x_i) = h - \bar{h}_d\gamma(x_i) = h\left[1 - \epsilon\gamma(x_i)\right] \quad \epsilon = \frac{\bar{h}_d}{h} \tag{13}$$

where $\gamma(x_i)$ is the damage profile function and ϵ gives ratio of the depth of damage to the depth at the undamaged location.

For example, consider a beam of uniform rectangular cross section of width b and depth h as shown in figure 1. A rectangular through-thickness notch shaped damage is located

29

at $x = x_d$ with a width of Δl and depth of h_d. Notice in this case $\bar{h}_d = h_d$. The damage profile function is given by

$$h(x_1) = h - \bar{h}_d \left[H(x_1 - x_{1d}) - H(x_1 - x_{1d} - \Delta l) \right] = h(1 - \epsilon \gamma(x_1))$$

$$\gamma(x_1) = H(x_1 - x_{1d}) - H(x_1 - x_{1d} - \Delta l) \tag{14}$$

Here $H(x - x_1)$ denotes the Heaviside function. Other representations of the crack profile functions of beams for different types of damage are given as follows:

For a V-shaped notch as given in figure 2:

$$\gamma(x_1) = < x_1 - x_{1d} > -2 < x_1 - x_{1d} - \Delta l/2 > + < x_1 - x_{1d} - \Delta l > \tag{15}$$

where $<>$ denotes ramp function. For a half V notch

$$\gamma(x_1) = < x_1 - x_{1d} > -H(x_1 - x_{1d} - \Delta l) + < x_1 - x_{1d} - \Delta l > \tag{16}$$

For a saw-cut damage the definition of differentiation is used [1]

$$\gamma(x_1) = H(x_1 - x_{1d}) - H(x_1 - x_{1d} - \Delta l) \propto \Delta l \delta(x_1 - x_{1d}) = k \Delta l \delta(x_1 - x_{1d}) \tag{17}$$

Damage does not always occur in shapes giving regular profiles. In the cases where damage cannot be represented as a regular profile as listed above, a convolution integral is used to obtain the expressions for mode shapes and natural frequencies using the crack profile function of saw cut damage as described later in the chapter.

The concept of damage profile functions may be applied to multi-dimensional structures and multi-dimensional damage. For a plate, damage profile function defined for a sharp crack is given by

$$\gamma(x_1, y_1) = \left[(x_1 - x_{1d}) - H(x_1 - x_{1d} - \Delta l_1) \right] \left[H(y_1 - y_{1d}) - H(y_1 - y_{1d} - \Delta l_2) \right]$$

$$= \Delta l_1 \Delta l_2 \delta(x_1 - x_{1d}) \delta(y_1 - y_{1d}) \tag{18}$$

where Δl_i gives the width of the damage in the ith direction.

Multiple areas of damage may be tackled by summing the different crack profile functions for individual damage, to represent a consolidated crack profile function

$$\gamma(x_j) = \sum_{i=1}^{N} \gamma_i(x_j) \tag{19}$$

where N is the number of distinct areas of damage. The change in the depth also manifests itself as changes in cross sectional properties. The change in moment of inertia and cross sectional area can be written as

$$I(x) = \sum_{j=0}^{r} \epsilon^j I_j \quad A(x) = \sum_{j=0}^{r} \epsilon^j A_j \tag{20}$$

For example, for a rectangular beam the moment of inertia is given by

$$I = \frac{bh(x)^3}{12} = \frac{bh^3}{12} \left[1 - 3\epsilon\gamma(x) + 3\epsilon^2\gamma^2(x) - \epsilon^3\gamma^3(x) \right] \tag{21}$$

Comparing with equation (20) one finds that

$$I_1 = -3I_0\gamma(x) \quad I_2 = 3I_0\epsilon^2\gamma^2(x) \quad I_3 = -\epsilon^3\gamma^3(x)I_0 \quad I_4 = 0 \tag{22}$$

Based on the above explanation, the stiffness and mass operator are thus written as

$$L = \sum_{j=0}^{r} \epsilon^j L_j \quad M = \sum_{j=0}^{q} \epsilon^j M_j \tag{23}$$

For example, the stiffness operator for Timoshenko beam theory can be written as

$$L = \begin{bmatrix} -\frac{d\kappa G(A_0+\epsilon A_1+\epsilon^2 A_2)d}{dx_1^2} & \frac{d\kappa G(A_0+\epsilon A_1+\epsilon^2 A_2)d}{dx_1} \\ -\frac{\kappa G(A_0+\epsilon A_1+\epsilon^2 A_2)d}{dx_1} & \kappa G(A_0+\epsilon A_1+\epsilon^2 A_2) - \frac{dE(I_0+\epsilon I_1+\epsilon^2 I_2+\epsilon^3 I_3+\epsilon^4 I_4)d}{dx_1^2} \end{bmatrix} \tag{24}$$

If the area moment of inertia values are taken for a beam with rectangular cross section with a rectangular notch, as given in equation (22), $I_4 = 0$. Comparing (23) and (24), $r = 3$

$$L_0 = \begin{bmatrix} -\frac{d\kappa GA_0 d}{dx_1^2} & \frac{d\kappa GA_0 d}{dx_1} \\ -\frac{\kappa GA_0 d}{dx_1} & \kappa GA_0 - \frac{dEI_0 d}{dx_1^2} \end{bmatrix} \quad L_1 = \begin{bmatrix} -\frac{d\kappa GA_1 d}{dx_1^2} & \frac{d\kappa GA_1 d}{dx_1} \\ -\frac{\kappa GA_1 d}{dx_1} & \kappa GA_1 - \frac{dEI_1 d}{dx_1^2} \end{bmatrix}$$

$$L_2 = \begin{bmatrix} -\frac{d\kappa GA_2 d}{dx_1^2} & \frac{d\kappa GA_2 d}{dx_1} \\ -\frac{\kappa GA_2 d}{dx_1} & \kappa GA_2 - \frac{dEI_2 d}{dx_1^2} \end{bmatrix} \quad L_3 = \begin{bmatrix} 0 & 0 \\ 0 & -\frac{dEI_3 d}{dx_1^2} \end{bmatrix} \tag{25}$$

In the above equations, the subscript 0 is for the nominal quantities at an undamaged location.

31

4.1.2 Perturbation

As the quantity ϵ is small, the function $\phi(x_i)$ and λ are expanded using perturbation theory [48] as the following series

$$\phi(x_i) = \phi^0(x_i) + \epsilon\phi^1(x_i) + \epsilon^2\phi^2(x_i) - \dots \qquad \lambda = \lambda^0 + \epsilon\lambda^1 + \epsilon^2\lambda^2 - \dots \qquad (26)$$

A similar equation was used in [59]. The superscripts of ϕ and λ denote the order of perturbation. It is essential to note that unlike in the equations (20) and (23) where the coefficients of ϵ^i are known, in the perturbed equations the coefficients are unknown.

4.1.3 Non-dimensionalization

The next step is non-dimensionalization, which identifies the number of parameters affecting the results. The contents of the equations are non-dimensionalized using

$$\zeta_i = \frac{x_i}{L} \quad u_{z_i} = \frac{u_i}{L} \quad \theta_{z_i} = \theta_i \quad \gamma_z(\zeta_i) = \gamma(x_i) \qquad (27)$$

The subscript z is used for the non-dimensionalized quantity.

4.1.4 Perturbed equations

Equations (23), (26) and (27) are substituted in (2) and then they are non-dimensionalized to give the equations of order 0, 1, 2 and 3 in ϵ as

$$\epsilon^0 : L_{z_0}\phi^0 - \lambda_z^0 M_{z_0}\phi^0 = 0 \qquad (28a)$$

$$\epsilon^1 : L_{z_0}\phi^1 - \lambda_z^0 M_{z_0}\phi^1 = \lambda_z^1 M_{z_0}\phi^0 + \lambda_z^0 M_{z_1}\phi^0 - L_{z_1}\phi^0 \qquad (28b)$$

$$\epsilon^2 : L_{z_0}\phi^2 - \lambda_z^0 M_{z_0}\phi^2 = \lambda_z^2 M_{z_0}\phi^0 + \lambda_z^1 M_{z_1}\phi^0 + \lambda_z^1 M_{z_0}\phi^1 + \lambda_z^0 M_{z_2}\phi^0$$
$$+ \lambda_z^0 M_{z_1}\phi^1 - L_{z_2}\phi^0 - L_{z_1}\phi^1 \qquad (28c)$$

$$\epsilon^3 : L_{z_0}\phi^3 - \lambda_z^0 M_{z_0}\phi^3 = \lambda_z^3 M_{z_0}\phi^0 + \lambda_z^2 M_{z_1}\phi^0 + \lambda_z^2 M_{z_0}\phi^1 + \lambda_z^1 M_{z_2}\phi^0$$
$$+ \lambda_z^1 M_{z_1}\phi^1 + \lambda_z^1 M_{z_0}\phi^2 + \lambda_z^0 M_{z_3}\phi^0 + \lambda_z^0 M_{z_2}\phi^1 + \lambda_z^0 M_{z_1}\phi^2 - L_{z_3}\phi^0$$
$$- L_{z_2}\phi^1 - L_{z_1}\phi^2 \qquad (28d)$$

where ϕ^k represents $\phi^k(\zeta_i)$. For the Euler-Bernoulli beam the symbols L_{z_0}, M_{z_0}, M_{z_1}, L_{z_1} and λ_z^i represent the following:

$$L_{z_0} = \frac{d^4}{d\zeta_1^4} \quad M_{z_0} = 1 \quad L_{z_1} = \frac{d^2}{d\zeta_1^2}3\gamma_z(\zeta_1)\frac{d^2}{d\zeta_1^2} \quad M_{z_1} = \gamma_z(\zeta_1) \quad \lambda_z^i = \frac{m\lambda^i L^4}{EI_3} \qquad (29)$$

32

and for Timoshenko beam theory their values are

$$
L_{z_0} = \begin{bmatrix} -\frac{d^2}{d\zeta_1^2} & \frac{d}{d\zeta_1} \\[2mm] -\frac{d}{d\zeta_1} & -\sigma^2 e \frac{d^2}{d\zeta_1^2} + 1 \end{bmatrix} \quad M_{z_0} = \begin{bmatrix} \sigma^2 e & 0 \\[2mm] 0 & \sigma^4 e \end{bmatrix}
$$

$$
L_{z_1} = \begin{bmatrix} -\frac{d\gamma_z(\zeta_1)d}{d\zeta_1^2} & \frac{d\gamma_z(\zeta_1)}{dx} \\[2mm] -\frac{\gamma_z(\zeta_1)d}{d\zeta_1} & 3\gamma_z(\zeta_1) - \frac{d\sigma^2 e\gamma_z(\zeta_1)d}{d\zeta_1^2} \end{bmatrix} \quad M_{z_1} = \begin{bmatrix} \sigma^2 e\gamma_z(\zeta_1) & 0 \\[2mm] 0 & 3\sigma^4 e\gamma_z(\zeta_1) \end{bmatrix}
$$

$$
e = \frac{E}{\kappa G} \quad \sigma^2 = \frac{I}{AL^2} \quad \lambda_z^i = \frac{\omega^2 \rho L^2}{\kappa G} \tag{30}
$$

The nth term, where $n \geq 1$ is compactly written as

$$
\epsilon^n : L_{z_0}\phi^n - \lambda_z^0 M_{z_0}\phi^n = \lambda_z^n M_{z_0}\phi^0 + \sum_{j=1}^{\min(n||q)} \lambda_z^0 M_{z_j}\phi^{n-j} + \sum_{i=1}^{n-1}\sum_{j=0}^{\min(n-i||q)} \lambda_z^i M_{z_j}\phi^{n-i-j}
$$

$$
- \sum_{j=1}^{\min(n||r)} L_{z_j}\phi^{n-j} \tag{31}
$$

To use orthogonality to solve the equation as would be evident in the solution procedure given below, M_{z_0} terms should be written separately. The above equation is rewritten as

$$
\epsilon^n : L_{z_0}\phi^n - \lambda_z^0 M_{z_0}\phi^n = \lambda_z^n M_{z_0}\phi^0 + \sum_{j=1}^{\min(n||q)} (\lambda_z^0 M_{z_j})\phi^{n-j} + \sum_{i=1}^{n-1} \lambda_z^i M_{z_0}\phi^{n-i}
$$

$$
+ \sum_{i=1}^{n-1}\sum_{j=1}^{\min(n-i||q)} \lambda_z^i M_{z_j}\phi^{n-i-j} - \sum_{j=1}^{\min(n||r)} L_{z_j}\phi^{n-j} \tag{32}
$$

The characteristics of the above development which will be used in the solution procedure given below are

1. Through the process of perturbation and by using the damage model, the homogeneous differential equation with variable coefficients is changed to a series of nonhomogeneous differential equations with constant coefficients.

2. The first differential equation of this series is the same as that representing the eigenvalue problem for the undamaged case.

3. The remaining equations in the series of differential equations have the same homogeneous parts as those of the first equation and the undamaged case.

4. The unknowns for the nth order equation are the eigenfunction ϕ^n in the left hand side of the equation and the eigenvalue λ_z^n in the right hand side of the equation.

5. The layout of the nth order equation is given in a form so that the unknowns are given separately in individual terms. The second term in the right hand side involving λ_z^0 needs to be written separately to be able to write the unknown terms involving λ_z^0 in the left hand side. The third term in right hand side involving M_{z_0} is written separately to be able to use the orthogonality condition to simplify the final expression.

4.1.5 Zeroth-order solution

Equation (84a) is same as the eigenvalue problem for the undamaged elastic element, so the solution would be the same. Let the solution be given by $S_{ud}(\zeta_i)$. For example, for an Euler-Bernoulli beam the solution is given by

$$S_{ud}(\zeta_1) = A \cos a\zeta_1 + B \sin a\zeta_1 + C \sinh a\zeta_1 + D \cosh a\zeta_1 \tag{33}$$

After applying the boundary conditions, the eigenvalue problem gives the mode shapes for the beam. Hence the solution to the zeroth-order equation is same as that for the undamaged beam given by

$$\lambda_z^0 = \lambda_{z_k}^0 \qquad \phi^0(\zeta_i) = \phi_k^0(\zeta_i), \quad k = 1, 2, 3, \ldots, \infty \tag{34}$$

4.1.6 n^{th}-order solution

Next, the equations of order higher than zero are solved. Since the solution of zeroth-order gave infinite number of modes so all the equations higher than zeroth-order will have one equation for each mode. The equation for the nth order k^{th} mode is given by

$$\epsilon^n : L_{z_0}\phi_k^n - \lambda_{z_k}^0 M_{z_0}\phi_k^n = \lambda_{z_k}^n M_{z_0}\phi_k^0 + \sum_{j=1}^{\min(n||q)} \lambda_{z_k}^0 M_{z_j}\phi_k^{n-j} + \sum_{i=1}^{n-1} \lambda_{z_k}^i M_{z_0}\phi_k^{n-i}$$

$$+ \sum_{i=1}^{n-1}\sum_{j=1}^{\min(n-i||q)} \lambda_{z_k}^i M_{z_j}\phi_k^{n-i-j} - \sum_{j=1}^{\min(n||r)} L_{z_j}\phi_k^{n-j} \tag{35}$$

where k is the mode number considered. The unknowns in the above equation are ϕ_k^n and $\lambda_{z_k}^n$. The total solution for the above equation consists of an homogeneous part and a

particular integral part ($\phi_k^n = \phi_k^n \mid_{homogeneous} + \phi_k^n \mid_{particular}$). Again the above equation, which is a representative equation of higher order equations, has the same left-hand side as (84a), so the homogeneous part of the solution would be the same, i.e. $S_{ud}(\zeta_i)$. To solve the particular integral part, the particular solution is represented as a summation of the undamaged orthogonal modes or the zeroth-order solution modes, using the expansion theorem, viz.,

$$\phi_k^n \mid_{particular} = \sum_{p=1}^{\infty} \eta_{kp}^n \phi_p^0 \tag{36}$$

where η_{kp}^n is a constant. Thus, the unknowns are now η_{kp}^n, $p = 1, 2, \ldots \infty$ and $\lambda_{z_k}^n$, and its solution for the first two orders is shown by [18]. The solution for the first-order equation is given by $\phi_k^1 = \phi_k^0 + \sum_{p=1 p \neq k}^{\infty} \eta_{kp}^1 \phi_p^0$ and solution for second-order equation is given by $\phi_k^2 = \phi_k^0 + \sum_{p=1 p \neq k}^{\infty} \eta_{kp}^2 \phi_p^0$. Using deductive reasoning, the solution for the rth-order equation with $r < n$ is $\phi_k^r = \phi_k^0 + \sum_{p=1 p \neq k}^{\infty} \eta_{kp}^r \phi_p^0$. It should be noted that $\eta_{kp}^0 = 0$. Orthogonality of the undamaged modes is used to find the values of the unknowns. Equation (35) is premultiplied by $(\phi_m^0)^T$ and integrated from $\zeta_i = 0$ to $\zeta_i = 1$ to yield

$$\epsilon^n : \int_0^1 (\phi_m^0)^T L_{z_0} \sum_{p=1}^{\infty} \eta_{kp}^n \phi_p^0 d\zeta_i - \lambda_{z_k}^0 \int_0^1 (\phi_m^0)^T M_{z_0} \sum_{p=1}^{\infty} \eta_{kp}^n \phi_p^0 d\zeta_i =$$

$$\lambda_{z_k}^n \int_0^1 (\phi_m^0)^T M_{z_0} \phi_k^0 d\zeta_i +$$

$$\sum_{j=1}^{\min(n||q)} \int_0^1 (\phi_m^0)^T \lambda_{z_k}^0 M_{z_j} (\phi_k^0 + \sum_{p=1 p \neq k}^{\infty} \eta_{kp}^{n-j} \phi_p^0) d\zeta_i +$$

$$\sum_{i=1}^{n-1} \lambda_{z_k}^i \int_0^1 (\phi_m^0)^T M_{z_0} (\phi_k^0 + \sum_{p=1 p \neq k}^{\infty} \eta_{kp}^{n-i} \phi_p^0) d\zeta_i +$$

$$\sum_{i=1}^{n-1} \sum_{j=1}^{\min(n-i||q)} \lambda_{z_k}^i \int_0^1 (\phi_m^0)^T M_{z_j} (\phi_k^0 + \sum_{p=1 p \neq k}^{\infty} \eta_{kp}^{n-i-j} \phi_p^0) d\zeta_i -$$

$$\sum_{j=1}^{\min(n||r)} \int_0^1 (\phi_m^0)^T L_{z_j} (\phi_k^0 + \sum_{p=1 p \neq k}^{\infty} \eta_{kp}^{n-j} \phi_p^0) d\zeta_i \tag{37}$$

Using orthogonality the following simplifications can be made:

$$\int_0^1 (\phi_m^0)^T M_{z_0} \phi_n^0 d\zeta_i = \delta_{mn} C_m = \delta_{mn} C_n$$

$$\int_0^1 (\phi_m^0)^T L_{z_0} \phi_n^0 d\zeta_i = \delta_{mn} \lambda_m C_m = \delta_{mn} \lambda_n C_n \tag{38}$$

35

where δ_{mn} is the Kronecker delta. Notice the orthogonality condition does not hold for M_{z_j} and L_{z_j} where $j \geq 1$. For those cases the following notations would be used to represent the equations compactly

$$\int_0^1 (\phi_m^0)^T L_{z_j} \phi_n^0 d\zeta_i = \alpha_{j_{mn}}$$
$$\int_0^1 (\phi_m^0)^T M_{z_j} \phi_n^0 d\zeta_i = \beta_{j_{mn}} \tag{39}$$

It can be shown at least for $\gamma(\zeta_i) = \Delta l_z \delta(\zeta_i - \zeta_{di})$ $\beta_{j_{mn}} = \beta_{j_{nm}}$ and $\alpha_{j_{mn}} = \alpha_{j_{nm}}$. Using the orthogonality condition of equation (38) and the compact notation of equation (130), equation (37) is now given by

$$\epsilon^n : \eta_{km}^n \left(\lambda_{z_m}^0 - \lambda_{z_k}^0\right) C_m = \lambda_{z_k}^n \delta_{mk} C_k +$$
$$\sum_{j=1}^{\min(n||q)} \left[\lambda_{z_k}^0 \left(\beta_{j_{mk}} + \sum_{p=1 p \neq k}^{\infty} \eta_{kp}^{n-j} \beta_{j_{mp}} \right) \right] + \sum_{i=1}^{n-1} \lambda_{z_k}^i \left(\delta_{mk} C_k + \sum_{p=1 p \neq k}^{\infty} \eta_{kp}^{n-i} \delta_{mp} C_p \right)$$
$$+ \sum_{i=1}^{n-1} \sum_{j=1}^{\min(n-i||q)} \lambda_{z_k}^i \left(\beta_{j_{mk}} + \sum_{p=1 p \neq k}^{\infty} \eta_{kp}^{n-i-j} \beta_{j_{mp}} \right) - \sum_{j=1}^{\min(n||r)} \left(\alpha_{j_{mk}} + \sum_{p=1 p \neq k}^{\infty} \eta_{kp}^{n-j} \alpha_{j_{mp}} \right) \tag{40}$$

The unknowns of this equation can be found by using the conditions $m = k$ and $m \neq k$. For $m = k$, the left-hand side vanishes and the following expression is obtained for the λ_k^n:

$$\lambda_{z_k}^n = \frac{1}{C_k} \left[\sum_{j=1}^{\min(n||r)} \left(\alpha_{j_{kk}} + \sum_{p=1 p \neq k}^{\infty} \eta_{kp}^{n-j} \alpha_{j_{kp}} \right) \right.$$
$$- \sum_{i=1}^{n-1} \lambda_{z_k}^i C_k - \sum_{i=1}^{n-1} \sum_{j=1}^{\min(n-i||q)} \lambda_{z_k}^i \left(\beta_{j_{kk}} - \sum_{p=1 p \neq k}^{\infty} \eta_{kp}^{n-i-j} \beta_{j_{kp}} \right)$$
$$\left. - \sum_{j=1}^{\min(n||q)} \lambda_{z_k}^0 \left(\beta_{j_{kk}} + \sum_{p=1 p \neq k}^{\infty} \eta_{kp}^{n-j} \beta_{j_{kp}} \right) \right] \tag{41}$$

36

and for $m \neq k$ the following expression is obtained for η_{km}^n

$$\eta_{km}^n = \frac{1}{(\lambda_{z_m}^0 - \lambda_{z_k}^0)C_m}\left\{ \sum_{j=1}^{\min(n||q)} \left[\lambda_{z_k}^0 \beta_{j_{mk}} + \sum_{p=1p\neq k}^{\infty} \eta_{kp}^{n-j}(\lambda_{z_k}^0 \beta_{j_{mp}}) \right] - \right.$$

$$\sum_{j=1}^{\min(n||r)} \left[\alpha_{j_{mk}} + \sum_{p=1p\neq k}^{\infty} \eta_{kp}^{n-j}(\alpha_{j_{mp}}) \right]$$

$$\left. + \sum_{i=1}^{n-1} \lambda_{z_k}^i (\eta_{km}^{n-i} C_m) + \sum_{i=1}^{n-1} \sum_{j=1}^{\min(n-i||q)} \lambda_{z_k}^i \left[\beta_{j_{mk}} + \sum_{p=1p\neq k}^{\infty} \eta_{kp}^{n-i-j} \beta_{j_{mp}} \right] \right\} \quad (42)$$

To complete the solution for mode shapes, the solution obtained till now is given by

$$\phi_k^n = S_{ud}(\zeta_i) + \sum_{p=1,p\neq k}^{\infty} \eta_{kp}^n \phi_p^0 + \eta_{kk}^n \phi_k^0 \quad (43)$$

Notice η_{kk}^n is incorrectly deduced to be zero by [61]. Instead, this constant at this stage is still undetermined. There are as many unknowns in $S_{ud}(\zeta_i)$ as there are boundary conditions as shown in the example expression given for the Euler-Bernoulli beam equation (33). The η_{kk}^n just combines with those constants. The final solution after applying the boundary conditions is given by

$$\phi_k^n = \phi_k^0 + \sum_{p=1,p\neq k}^{\infty} \eta_{kp}^n \phi_p^0 \quad (44)$$

The solution has the mode shapes of the undamaged beam as one of the parts because of the unique choice of the particular solution. The particular solution independently already satisfied the boundary conditions. The final solution for the mode shape and natural frequencies of the damaged structure is determined by using equation (26).

4.1.7 Solution to arbitrary damage profile

To determine the mode shapes and natural frequencies for an arbitrary damage profile, first the modes shapes and natural frequencies are determined using a sharp damage modeled using a delta function $\gamma_z(\zeta_i) = \delta(\zeta_i - \zeta_{di})$. Let the eigenfunction (mode shape) and the eigenvalue (which can be used to determine the natural frequency) be determined using such a damage profile be $\phi_{\delta_k}(\zeta_i)$ and λ_{δ_k}, respectively. A convolution integral in space domain is used to determine mode shapes and natural frequencies for any arbitrary damage

37

profile. The final expressions is given by

$$\phi_k(\zeta_i) = \int_\Omega \phi_{\delta_k}(\zeta_i - \zeta_{d_i})\gamma(\zeta_{d_i})d\zeta_{d_i}$$

$$\lambda_k = \int_\Omega \lambda_{\delta_k}\gamma(\zeta_{d_i})d\zeta_{d_i} \tag{45}$$

where ζ_d is the spatial location of the damage. For multiple damage locations, a damage profile function for multiple areas of damage given by equation (19) is used.

$$\phi_k(\zeta_i) = \sum_{j=1}^p \int_{\Omega_j} \phi_{\delta_k}(\zeta_i - \zeta_{d_i})\gamma(\zeta_{d_i})d\zeta_{d_i}$$

$$\lambda_k = \sum_{j=1}^p \int_{\Omega_j} \lambda_{\delta_k}\gamma(\zeta_{d_i})d\zeta_{d_i} \tag{46}$$

The subscript j denotes the damage number iterator and number, p denotes the total number of independent damage locations. Although, the natural frequency does not depend on the spatial variable ζ_i, it still can be determined in the same way.

To verify the correctness of the expression, the first-order correction is compared against the ones derived for Euler-Bernoulli beams [17] and for Timoshenko beams [15]. They were found to be the same.

$$\lambda_{z_n}^1 = \frac{\alpha_{1_{nn}} - \lambda_{z_n}^0\beta_{1_{nn}}}{C_n} \qquad \eta_{nj}^1 = \frac{\lambda_{z_k}^0\beta_{1_{nj}} - \alpha_{1_{nj}}}{(\lambda_{z_j}^0 - \lambda_{z_n}^0)C_j} \tag{47}$$

The second-order correction quantities are obtained as solution to (28c)

$$\lambda_{z_n}^2 = \frac{\alpha_{1_{nn}} - \lambda_{z_n}^1\beta_{1_{nn}} - \lambda_{z_n}^0\beta_{1_{nn}}}{C_n} \tag{48}$$

$$\eta_{nj}^2 = \frac{\lambda_{z_n}^1\beta_{1_{nj}} + \lambda_{z_n}^1\eta_{nj}^1 C_j\lambda_{z_n}^0\beta_{1_{nj}} + \lambda_{z_n}^0\sum_{l=1,l\neq n}^\infty \eta_{nj}^1\beta_{1_{nj}} - \alpha_{1_{nj}} - \sum_{l=1,l\neq n}^\infty \eta_{nj}^1\alpha_{1_{nj}}}{C_j(\lambda_{z_j}^0 - \lambda_{z_n}^0)} \tag{49}$$

4.2   Conclusions

- A general solution to damaged elastic structures is provided. The damage can have any profile, and the elastic structure can have multiple areas of damage. The elastic element can be supported on any set of boundary conditions which yield orthogonal modes.

38

- The model needs the theoretical undamaged modes. The primary advantage of the model lies in its apparent computational advantage over finite element models. The number of elements required to model a damaged element is very high and is limited by the size of damage, at least in the vicinity of the damage. So, in a beam of length 1 m and cross sectional dimensions 0.02 m × 0.005 m, if there is a through-thickness damage of depth 0.0005 m, the elements required to model this damaged beam would be two-dimensional plane stress elements with the smallest elements being of the order of 0.0005 m. This increases the computational requirement from using a few beam elements for undamaged state to several plane stress elements for the damaged state. Using the method suggested herein, however, the modes of the undamaged beam can be used to model the damaged beam, which will be computationally much less expensive.

- The inertia effects due to the damage, which has been neglected by all the prior researchers, is included in the present model. The number of terms stemming due to the inertia effects due to the damage is larger than the number of terms arising due to loss of stiffness due to the damage. Therefore, it can be concluded that the inertia effect is an important parameter for modeling damage.

- The method yields a series solution which converges to the correct value.

- Since the theory is general, it is not possible to verify it fully in one thesis, but different aspects of the theory have been verified earlier and will be tested in future publications. The first-order perturbation correction in Euler-Bernoulli beams has been verified in the work by Dixit and Hanagud [18]. The first-order correction, for Timoshenko beams the method was verified in [15].

- The framework presented in this chapter presents a mathematical model for the damage. Such mathematical models allow understanding of the physics behind the problem, which helps in the explanation of experimental readings. They also allow prediction of response of the structure. These studies are also useful for the development of new experimental techniques to address another important aspect of SHM, that of

damage diagnosis. A method based on this framework for damage diagnosis (identification and localization) in Euler-Bernoulli beams, has been proposed in [16]. Similar methods based on the framework may be developed for damage diagnosis.

Chapter V

COMMENTS ON THE SOLUTION PRESENTED BY LESTARI [38]

This chapter is reproduction of published work by Dixit and Hanagud [17]. The primary motivation for the chapter sprouts from the article [?]. The paper although very useful and informative, as it conducts a wide array of experiments on different types of damages for a beam, has some discrepancies in the solution to the perturbed ordinary differential equation. A possible solution to the equations is presented. The inconsistency should not affect the results presented in the paper enormously since it manifests itself as a higher order effect. In this chapter the process is extended and the change in mass is taken into account along with change of stiffness. Only stiffness change is modeled in the original work [?].

5.1   Discrepancy In The Paper

In the appendix of [?] the first order perturbation equation is given as

$$EI_0\frac{d^4\phi_i^1}{dx^4} - \lambda^0 m_0\phi_i^1 = \lambda^1 m_0\phi_i^0 - EI_0\frac{d^2}{dx^2}(\gamma(x,x_d)\frac{d^2\phi_i^0}{dx^2}) \tag{50}$$

where the difference of step functions $H(x-x_1) - H(x-x_2)$ is given by $\gamma(x,x_d)$. The final solution is given as

$$\phi_i^1(x) = \sum_{k=1}^{n}\beta_{ik}\phi_i^0(x) + <x-x_1>\frac{d}{dx}\phi_i^0(x_1) - <x-x_2>\frac{d}{dx}\phi_i^0(x_2)+$$

$$H(x-x_1)\phi_i^0(x_1) - H(x-x_2)\phi_i^0(x_2) - [H(x-x_1) - H(x-x_2)]\phi_i^0(x) \tag{51}$$

In the first term the subscript of ϕ^0 as i is most probably a typo, since, in that case when this quantity is multiplied by ϕ_j^0, and integrated from 0 to L, as outlined in the solution procedure, the result would be zero because of orthogonality of modes. This typo is corrected in the last equation (equation A12) of the appendix where the subscript of ϕ^0 in the first term of the first order correction is changed to j. Assuming that is indeed the

41

case the correct expression is

$$\phi_i^1(x) = \sum_{k=1}^{n} \beta_{ik}\phi_k^0(x) + <x-x_1> \frac{d}{dx}\phi_i^0(x_1) - <x-x_2> \frac{d}{dx}\phi_i^0(x_2)+$$

$$H(x-x_1)\phi_i^0(x_1) - H(x-x_2)\phi_i^0(x_2) - [H(x-x_1) - H(x-x_2)]\phi_i^0(x) \qquad (52)$$

For the case $x > x_2$ the solution becomes

$$\phi_i^1(x) = \sum_{k=1}^{n} \beta_{ik}\phi_k^0(x) + x(\frac{d}{dx}\phi_i^0(x_1) - \frac{d}{dx}\phi_i^0(x_2)) + \phi_i^0(x_1) - \phi_i^0(x_2) \qquad (53)$$

Consider a simply supported boundary condition for a beam of length L. It is known that $\phi_i^0(L) = 0$ for all i. Applying that to the above equation

$$\phi_i^1(L) = L(\frac{d}{dx}\phi_i^0(x_1) - \frac{d}{dx}\phi_i^0(x_2)) + \phi_i^0(x_1) - \phi_i^0(x_2) \qquad (54)$$

The above quantity is not zero (except for $x_1 = x_2$ which means there is no damage). Hence the solution violates the boundary condition for simply supported case. It can be similarly shown that the solution violates the boundary condition for other end conditions too.

For the case $x < x_1$ the solution becomes

$$\phi_i^1(x) = \sum_{k=1}^{n} \beta_{ik}\phi_k^0(x) \qquad (55)$$

Again consider a simply supported boundary condition with a damage at the center. It is known that for symmetric problem like simply supported boundary condition $\phi_i^0(x) = \phi_i^0(L-x)$. The problem is symmetric about the midpoint, therefore the solution should be symmetric about the midpoint hence $\phi_i^1(x) = \phi_i^1(L-x)$, putting this in (53) and (55) the following equality is obtained

$$(L-x)(\frac{d}{dx}\phi_i^0(x_1) - \frac{d}{dx}\phi_i^0(x_2)) + \phi_i^0(x_1) - \phi_i^0(x_2) = 0 \qquad (56)$$

The eigen functions for simply supported case are given by $\phi_i^0(x) = \sin(\frac{i\pi x}{L})$. Substituting in the above equation

$$(L-x)\frac{i\pi}{L}(\cos(\frac{i\pi x_2}{L}) - \cos(\frac{i\pi x_1}{L})) + \sin(\frac{i\pi x_1}{L}) - \sin(\frac{i\pi x_2}{L}) = 0 \qquad (57)$$

The above identity will hold only for $x_1 = x_2$ which means there is not damage. The solution can similarly be shown to be incorrect for other boundary conditions too by using similar arguments.

5.2 An Alternative Solution

The homogeneous part of the equation (50) is same as that obtained when solving vibration problems for Euler-Bernoulli beams after separation of variables. The solution is given by

$$\phi^1 = A\sin(ax) + B\cos ax + C\cosh ax + D\sinh ax \tag{58}$$

where $a^4 = \frac{m_0\lambda^0}{EI_0}$. In the paper [?] it is claimed that the homogenous solution is

$$\phi_i^1 \mid_{homogeneous} = \sum_{k=1}^{\infty} \eta_{ik}\phi_i^0 \tag{59}$$

In the corrected version the above is assumed as a particular solution. Similar procedure was used to obtain the particular solution for simply supported boundary condition in [37]. The particular solution is given by

$$\phi_n^1 \mid_{particular} = \sum_{k=1}^{\infty} \eta_{nk}\phi_k^0 \tag{60}$$

In the above the subscript i is changed by n. Advantage of choosing the particular solution as above is that the homogeneous solution is now simply $\phi_n^1 \mid_{homogeneous} = \phi_n^0$. The particular solution is substituted in (50) to give

$$EI_0 \sum_{k=1}^{\infty} \eta_{nk}(\phi_k^0)'''' - \lambda_n^0 m_0 \sum_{k=1}^{\infty} \eta_{nk}\phi_k^0 = \lambda_n^1 m_0 \phi_n^0 - EI_0 \frac{d^2}{dx^2}[\gamma(x,x_d)(\phi_n^0)''] \tag{61}$$

Multiplying equation (61) by $\phi_j^0(x)$, integrating from $x = 0$ to $x = L$, one gets

$$\sum_{k=1}^{\infty} \left(\eta_{nk}EI_0 \int_0^L (\phi_k^0)''''\phi_j^0 dx - \lambda_n^0 m_0 \eta_{nk} \int_0^L \phi_k^0\phi_j^0 dx\right) = \lambda_n^1 m_0 \int_0^L \phi_n^0\phi_j^0 dx$$

$$-EI_0 \int_0^L \frac{d^2}{dx^2}[\gamma(x,x_d)(\phi_n^0)'']\phi_j^0 dx \tag{62}$$

The evaluation of the integrals on the right hand side of (62) are as follows.

$$m_0 \int_0^L \phi_n^0\phi_j^0 dx = \delta_{nj}Q_{nj} \tag{63a}$$

$$\int_0^L \frac{d^2}{dx^2}[\gamma(x,x_d)(\phi_n^0)'']\phi_j^0 dx = \frac{d}{dx}[\gamma(x,x_d)(\phi_n^0)'']\phi_j^0 \mid_0^L - [\gamma(x,x_d)(\phi_n^0)''](\phi_j^0)' \mid_0^L$$

$$+ \int_0^L [\gamma(x,x_d)(\phi_n^0)''](\phi_j^0)'' dx = \int_0^L (H(x-x_1) - H(x-x_2))(\phi_n^0(x))''(\phi_j^0(x))'' dx$$

$$= \int_{x_1}^{x_2} (\phi_n^0(x))''(\phi_j^0(x))'' dx = DF_s^1 \tag{63b}$$

43

DF_s^1 denotes the damage factor due to stiffness change. The superscript 1 denotes the order of correction to which the damage factor corresponds. Notice the first two boundary terms in (63b) are zero, since, $\gamma(x, x_d) = 0$ at both $x = L$, and $x = 0$. The first integral on the left hand side of (62).

$$\sum_{k=1}^{\infty} \eta_{nk} EI_0 \int_0^L (\phi_k^0)''''\phi_j^0 dx = \sum_{k=1}^{\infty} \eta_{nk} EI_0((\phi_k^0)''' \phi_j^0 \mid_0^L - (\phi_k^0)''(\phi_j^0)' \mid_0^L +$$

$$\int_0^L (\phi_k^0)''(\phi_j^0)'' dx)) = \sum_{k=1}^{\infty} \eta_{nk} EI_0 \int_0^L (\phi_k^0)''(\phi_j^0)'' dx \qquad (64)$$

The boundary terms go to zero since the eigenfunctions should satisfy the boundary conditions. Using orthogonality condition of modes the above equation is written as

$$\sum_{k=1}^{\infty} \eta_{nk} EI_0 \int_0^L (\phi_k^0)''(\phi_j^0)'' dx = EI_0 \eta_{nj} \int_0^L ((\phi_j^0)'')^2 dx = \lambda_j^0 m_0 \eta_{nj} \int_0^L (\phi_j^0)^2 dx \qquad (65)$$

Similarly the second term of left hand side of (62) is simplified using orthogonality of modes. The left hand side of (62) is transformed as

$$\eta_{nj} m_0 \int_0^L ((\phi_j^0)'')^2 dx (\lambda_j^0 - \lambda_n^0) \qquad (66)$$

The expression $m_0 \int_0^L (\phi_j^0)^2 dx$ in the above equation is denoted by m_{0j}. Equation (62) is written as

$$\eta_{nj} m_{0j} \lambda_j^0 - \lambda_n^0 m_{0j} \eta_{nj} = \lambda_n^1 m_0 \delta_{nj} Q_{nj} - EI_0 \int_{x_1}^{x_2} (\phi_n^0(x))''(\phi_j^0(x))'' dx \qquad (67)$$

For $j = n$ the right hand side becomes zero

$$\lambda_n^1 = \frac{\lambda_n^0}{\int_0^L (\phi_n^0)^2 dx} \frac{\int_{x_1}^{x_2} ((\phi_n^0(x))'')^2 dx}{a^4} \qquad (68)$$

For $n \neq j$

$$\eta_{nj} = \frac{-1}{(\frac{\lambda_j^0}{\lambda_n^0} - 1)} \frac{\int_{x_1}^{x_2} ((\phi_n^0(x))''(\phi_j^0(x))'') dx}{a^4 \int_0^L (\phi_j^0)^2 dx} \qquad (69)$$

$$\phi_n^1 = \phi_n^0 + \sum_{j=1, j \neq n}^{\infty} \eta_{nj} \phi_j^0 \qquad (70)$$

The final mode shapes and natural frequencies for damaged beam as per the calculations can be found to be

$$\phi(x) = \phi(x)^0 - \epsilon \phi(x)^1 \qquad \lambda = \lambda^0 - \epsilon \lambda^1 \qquad (71)$$

44

5.3 Solution, Including The Decrease In Mass Effect

At the damage location not only the stiffness of the beam decreases but its mass per unit length is also reduced. Considering only the drop in stiffness will not give the complete picture of the physics of the problem. This drop in mass distribution has not considered in literature. In this section this effect is also considered along with the drop in stiffness to arrive at the expression for mode shapes and natural frequencies.

The drop in mass equation would be similar to drop in stiffness equation (4) in the appendix [?] and is given by

$$EI(x) \approx EI_0(1 - \epsilon \Delta l \delta(x - x_d))$$
$$m(x) = m_0(1 - \frac{1}{3}\epsilon \Delta l \delta(x - x_d)) \text{ where } \epsilon = \frac{3h_d}{h} \tag{72}$$

The changed perturbed equation corresponding to the first order perturbation that replaces equation (50) is

$$\epsilon^1 : EI_0 \frac{d^4\phi^1}{dx^4} - \lambda^0 m_0 \phi^1 = \lambda^1 m_0 \phi^0 + \frac{1}{3}\lambda^0 m_0 \phi^0 \gamma(x, x_d) - EI_0 \frac{d^2}{dx^2}[\gamma(x, x_d)\frac{d^2\phi^0}{dx^2}] \tag{73}$$

Due to the change in mass distribution equation (61) will have an additional term. The changed equation is given by

$$EI_0 \sum_{k=1}^{\infty} \eta_{nk}(\phi_k^0)'''' - \lambda_n^0 m_0 \sum_{k=1}^{\infty} \eta_{nk}\phi_k^0 = \lambda_n^1 m_0 \phi_n^0 + \frac{1}{3}\lambda_n^0 m_0 \gamma(x, x_d)\phi_n^0 -$$
$$EI_0 \frac{d^2}{dx^2}[\gamma(x, x_d)(\phi_n^0)''] \tag{74}$$

Following the same procedure as outlined in the previous section a factor similar to damage factor for stiffness DF_s^1, a damage factor for mass DF_m^1 is obtained. It is given by

$$\int_0^L \gamma(x, x_d)\phi_n^0 \phi_j^0 dx = \int_{x_1}^{x_2} \phi_n^0 \phi_j^0 dx = DF_m^1 \tag{75}$$

Finally the altered form of (69) and (70) is given by

$$\lambda_n^1 = \frac{\lambda_n^0}{\int_0^L (\phi_n^0)^2 dx}(\frac{DF_s^1}{a^4} - \frac{1}{3}DF_m^1) \tag{76}$$

45

$$\eta_{nj} = \frac{1}{\frac{\lambda_j^0}{\lambda_n^0} - 1} \frac{\frac{1}{3}DF_m^1 - \frac{1}{a^4}DF_s^1}{\int_0^L (\phi_j^0)^2 dx} \tag{77}$$

$$\phi_n^1 = \phi_n^0 + \sum_{j=1, j \neq n}^{\infty} \eta_{nj}\phi_j^0 \tag{78}$$

5.4   Conclusions

- The errors in the solution of perturbed differential of a damaged Euler-Bernoulli beam [?] is corrected in this chapter.

- The chapter then introduces the change in mass distribution due to damage in the perturbed differential equations. The solution for the changed perturbed differential equations is presented.

Chapter VI

SINGLE BEAM ANALYSIS OF DAMAGED BEAMS VERIFIED USING A STRAIN ENERGY BASED DAMAGE MEASURE

This chapter is to a large part a reproduction of a published work done by the author [18]. An analytical expression for a new damage measure that relates the strain energy to the damage location and magnitude is presented in this chapter. The strain energy expression is calculated using modes and natural frequencies of damaged beams that are derived based on single beam analysis considering both decrease in mass and stiffness. Decrease in mass and stiffness are a fallout of geometric discontinuity, and no assumptions regarding the physical behavior of damage are made. The method is applicable to beams with notch-like non-propagating cracks and arbitrary boundary conditions. The analytical expressions derived for mode shapes, curvature shapes, natural frequencies and an improved strain energy based damage measure, are verified using experiments. The improvement in the damage measure stems from not assuming that the bending stiffness of the damaged beam is constant and equal to that of undamaged beam when calculating the strain energy of the entire beam. It is also not assumed that the bending stiffness of the element in which the damage is located is constant.

6.1 *Natural Frequencies and Modes of a Damaged Beam*

In deriving the modes and natural frequencies of a damaged beam the following assumptions are made.

1. The damage is not located at the supports

2. Euler-Bernoulli beam theory is valid

3. The interaction effect, which is a highly non-linear phenomenon that happens when crack tips touch each other during vibrations is negligible.

47

The natural modes of vibration of Euler-Bernoulli beam are given by the equation

$$\frac{d^2}{dx^2}[E(x)I(x)\frac{d^2}{dx^2}\phi(x)] - m(x)\lambda\phi(x) = 0 \tag{79}$$

where $E(x)$ and $I(x)$ are the Young's modulus and and area moment of inertia at a section x of the beam, $m(x)$ is the mass per unit length at the same section, and λ is an unknown constant eigenvalue.

Consider a uniform rectangular cross section of width b and depth h as shown in figure 1 given in the previous chapter. A damage is located at $x = x_d$ with length of Δl and depth of h_d. Therefore at the damage location the depth of the beam is reduced to $h - h_d$. For a notch-like damage, the profile can be approximated by using Heaviside functions $H(x - x_d) - H(x - x_d - \Delta l)$. Then, the sectional bending stiffness $EI(x)$ and sectional mass $m(x)$ are given as

$$EI(x) = \frac{Ebh(x)^3}{12} = \frac{Eb\left[h - h_d(x)\right]^3}{12} =$$
$$\frac{Ebh^3}{12}\left\{1 - \frac{h_d}{h}\left[H(x - x_d) - H(x - x_d - \Delta l)\right]\right\}^3$$
$$m(x) = m_0\left\{1 - \frac{h_d}{h}\left[H(x - x_d) - H(x - x_d - \Delta l)\right]\right\} \tag{80}$$

when Δl is small, then $H(x - x_d) - H(x - x_d - \Delta l) \approx \Delta l \delta(x - x_d)$ for a sharp crack [36], where $\delta(x)$ is the Dirac delta function. Binomial expansion of these equations, retaining terms only through order one in Δl, one obtains the following expressions:

$$EI(x) \approx EI_0\left[1 - \epsilon\Delta l\delta(x - x_d)\right] \tag{81a}$$

$$m(x) \approx m_0\left[1 - \frac{1}{3}\epsilon\Delta l\delta(x - x_d)\right] \tag{81b}$$

$$\epsilon = \frac{3h_d}{h} \tag{81c}$$

In the above equation I_0 and m_0 are nominal quantities at an undamaged location. As the quantity ϵ is small, the function $\phi(x)$ and λ are expanded using perturbation theory [48] as the following series

$$\phi(x) = \phi(x)^0 - \epsilon\phi^1(x) - \epsilon^2\phi^2(x) - \ldots$$
$$\lambda = \lambda^0 - \epsilon\lambda^1 - \epsilon^2\lambda^2 - \ldots \tag{82}$$

48

The superscripts of ϕ and λ denote the order of perturbation. Equations (81a), (81b) and (82) are substituted in (79) to give

$$\frac{d^2}{dx^2}\left\{EI_0\left[1 - \epsilon\Delta l\delta(x - x_d)\right]\frac{d^2}{dx^2}\left[\phi^0(x) - \epsilon\phi^1(x) - \epsilon^2\phi^2(x)\right]\right\} -$$

$$m_0\left[1 - \frac{1}{3}\epsilon\Delta l\delta(x - x_d)\right](\lambda^0 - \epsilon\lambda^1 - \epsilon^2\lambda^2)\left[\phi^0(x) - \epsilon\phi^1(x) - \epsilon^2\phi^2(x)\right] = 0 \qquad (83)$$

The equations of order 0, 1 and 2 in ϵ are obtained as

$$\epsilon^0 : EI_0\frac{d^4\phi^0}{dx^4} - \lambda^0 m_0\phi^0 = 0 \qquad (84a)$$

$$\epsilon^1 : EI_0\frac{d^4\phi^1}{dx^4} - \lambda^0 m_0\phi^1 = \lambda^1 m_0\phi^0 + \frac{1}{3}\lambda^0 m_0\phi^0\Delta l\delta(x - x_d) -$$

$$EI_0\Delta l\frac{d^2}{dx^2}\left[\delta(x - x_d)\frac{d^2\phi^0}{dx^2}\right] \qquad (84b)$$

$$\epsilon^2 : EI_0\frac{d^4\phi^2}{dx^4} - \lambda^0 m_0\phi^2 = \lambda^2 m_0\phi^0 - \lambda^1 m_0\phi^1 - \frac{1}{3}\lambda^0 m_0\phi^1\Delta l\delta(x - x_d) -$$

$$\frac{1}{3}\lambda^1 m_0\phi^0\Delta l\delta(x - x_d) + EI_0\Delta l\frac{d^2}{dx^2}\left[\delta(x - x_d)\frac{d^2\phi^1}{dx^2}\right] \qquad (84c)$$

A quantity a is defined such that $a^4 = \frac{m_0\lambda^0}{EI_0}$. In general, the beam is supported with different boundary conditions. However, equation (84a) is the same as the equation for natural vibrations of the undamaged beam. Let the solution to the equation (84a) be given by

$$\lambda^0 = \lambda_n^0 \quad n = 1, 2, 3\ldots, \infty$$

$$\phi^0(x) = \phi_n^0(x), \quad n = 1, 2, 3, \ldots, \infty \qquad (85)$$

Using the condition of orthogonality, the following two equations are obtained

$$\int_0^L EI(\phi_m^0)''(\phi_n^0)''dx = \lambda^0\int_0^L m_0(\phi_m^0)(\phi_n^0)dx = \delta_{mn}Q_{mn} \qquad (86)$$

where δ_{mn} is the Kronecker delta and Q_{mn} is a constant. Next, equation (84b) is solved. Equation (84b) is different from (84a) as it has a RHS. Hence, the total solution consists of an homogeneous part and a particular integral part $(\phi_n^1 = \phi_n^1\mid_{homogeneous} + \phi_n^1\mid_{particular})$. The only unknown in the RHS of (84b) is λ_n^1. The homogeneous part of the equation yields $\phi_n^1\mid_{homogeneous} = \phi_n^0$ since the homogeneous parts of equations (84a) and (84b) are the same. The particular solution, $\phi_n^1\mid_{particular}$, is expanded in terms of the orthogonal modes ϕ_k^0

$$\phi_n^1\mid_{particular} = \sum_{k=1}^{\infty}\eta_{nk}\phi_k^0 \qquad (87)$$

49

From equations (84b), (87) and (85) one obtains the following:

$$EI_0 \sum_{k=1}^{\infty} \eta_{nk}(\phi_k^0)'''' - \lambda_n^0 m_0 \sum_{k=1}^{\infty} \eta_{nk}\phi_k^0 = \lambda_n^1 m_0 \phi_n^0 + \frac{1}{3}\lambda_n^0 m_0 \Delta l \delta(x - x_d)\phi_n^0 -$$

$$EI_0 \Delta l \frac{d^2}{dx^2}[\delta(x - x_d)(\phi_n^0)''] \qquad (88)$$

where there is one equation for each mode of vibration for the beam. Multiplying equation (88) by $\phi_j^0(x)$, integrating from $x = 0$ to $x = L$, one obtains

$$\sum_{k=1}^{\infty} \eta_{nk}(EI_0 \int_0^L (\phi_k^0)''''\phi_j^0 dx - \lambda_n^0 m_0 \int_0^L \phi_k^0 \phi_j^0 dx) = \lambda_n^1 m_0 \int_0^L \phi_n^0 \phi_j^0 dx +$$

$$\frac{1}{3}\lambda_n^0 m_0 \Delta l \int_0^L \delta(x - x_d)\phi_n^0 \phi_j^0 dx - EI_0 \Delta l \int_0^L \frac{d^2}{dx^2}[\delta(x - x_d)(\phi_n^0)'']\phi_j^0 dx \qquad (89)$$

The integrals in equation (89) are evaluated as follows.

$$m_0 \int_0^L \phi_n^0 \phi_j^0 dx = \delta_{nj} Q_{nj} \qquad (90a)$$

$$\int_0^L \delta(x - x_d)\phi_n^0 \phi_j^0 dx = \phi_n^0(x_d)\phi_j^0(x_d) \qquad (90b)$$

$$\int_0^L \frac{d^2}{dx^2}[\delta(x - x_d)(\phi_n^0)'']\phi_j^0 dx = \frac{d}{dx}[\delta(x - x_d)(\phi_n^0)'']\phi_j^0 \mid_0^L$$

$$-[\delta(x - x_d)(\phi_n^0)''](\phi_j^0)' \mid_0^L + \int_0^L [\delta(x - x_d)(\phi_n^0)''](\phi_j^0)'' dx = (\phi_n^0(x_d))''(\phi_j^0(x_d))'' \qquad (90c)$$

Notice the first two terms (90c) are zero because $\delta(x - x_d) = 0$ at both $x = L$, and $x = 0$. The first integral on the left hand side of equation (89) is simplified as

$$\sum_{k=1}^{\infty} \eta_{nk}EI_0 \int_0^L (\phi_k^0)''''\phi_j^0 dx = \sum_{k=1}^{\infty} \left\{ \eta_{nk}EI_0 \left[(\phi_k^0)'''\phi_j^0 \mid_0^L -(\phi_k^0)''(\phi_j^0)' \mid_0^L + \int_0^L (\phi_k^0)''(\phi_j^0)'' dx \right] \right\}$$

$$(91)$$

The boundary terms go to zero since the eigenfunction satisfies all the boundary conditions. Using equation (86) the above equation is written as

$$EI_0 \eta_{nj} \int_0^L \left[(\phi_j^0)'' \right]^2 dx = \lambda_j^0 m_0 \eta_{nj} \int_0^L (\phi_j^0)^2 dx \qquad (92)$$

Similarly, the second term on the left hand side of equation (89) can be simplified using equation (86). The left hand side of equation (89) is transformed as

$$\eta_{nj} m_0 \int_0^L (\phi_j^0)^2 dx (\lambda_j^0 - \lambda_n^0) \qquad (93)$$

50

The expression $m_0 \int_0^L (\phi_j^0)^2 dx$ in the above equation is denoted by m_{0j}. Equation (89) can now be written as

$$\eta_{nj} m_{0j} \lambda_j^0 - \lambda_n^0 m_{0j} \eta_{nj} = \lambda_n^1 m_0 \delta_{nj} Q_{nj} + \frac{1}{3} \lambda_n^0 m_0 \Delta l \phi_n^0(x_d) \phi_j^0(x_d) -$$
$$EI_0 \Delta l \left[\phi_n^0(x_d) \right]'' \left[\phi_j^0(x_d) \right]'' \tag{94}$$

For $j = n$, the left hand side becomes zero and hence

$$\lambda_n^1 = \frac{\Delta l \lambda_n^0}{\int_0^L (\phi_n^0)^2 dx} \left\{ \frac{\left[\phi_n^0(x_d)'' \right]^2}{a^4} - \frac{1}{3} \left[\phi_n^0(x_d) \right]^2 \right\} \tag{95}$$

For $n \neq j$

$$\eta_{nj} = \frac{\Delta l}{\frac{\lambda_j^0}{\lambda_n^0} - 1} \frac{\frac{1}{3} \phi_n^0(x_d) \phi_j^0(x_d) - \frac{1}{a^4} \left[\phi_n^0(x_d) \right]'' \left[\phi_j^0(x_d) \right]''}{\int_0^L (\phi_j^0)^2 dx} \tag{96}$$

$$\phi_n^1 = \phi_n^0 + \sum_{j=1, j \neq n}^{\infty} \eta_{nj} \phi_j^0 \tag{97}$$

The second order correction is required for calculation of strain energy. The same procedure is used to solve equation (84c). The second order correction quantities are obtained as

$$\lambda_n^2 = \frac{\Delta l \lambda_n^0}{\int_0^L (\phi_n^0)^2 dx} \left\{ \frac{\left[\phi_n^0(x_d)'' \right]^2}{a^4} - \frac{1}{3} \phi_n^0(x_d) \phi_n^1(x_d) - \frac{\lambda_n^1}{3 \lambda_n^0} \phi_n^1(x_d) \phi_n^0(x_d) \right\} \tag{98}$$

$$\beta_{nl} = \frac{\Delta l}{\frac{\lambda_l^0}{\lambda_n^0} - 1} \frac{\frac{1}{a^4} \left[\phi_n^0(x_d) \right]'' \left[\phi_j^0(x_d) \right]'' - \frac{1}{3} \phi_n^1(x_d) \phi_l^0(x_d) - \frac{\lambda_n^1}{3 \lambda_n^0} \phi_n^0(x_d) \phi_l^1(x_d)}{\int_0^L (\phi_l^0)^2 dx} \tag{99}$$

$$\phi_n^2 = \phi_n^0 + \sum_{l=1, l \neq n}^{\infty} \beta_{nl} \phi_l^0 \tag{100}$$

Finally, the natural frequency and mode shape correct to the second order for a damaged beam are given by

$$\phi_n = \phi_n^0 - \epsilon [\phi_n^0 + \sum_{j=1, j \neq n}^{\infty} \eta_{nj} \phi_j^0] - \epsilon^2 [\phi_n^0 + \sum_{l=1, l \neq n}^{\infty} \beta_{nl} \phi_l^0] \tag{101a}$$

$$\lambda_n = \lambda_n^0 - \epsilon \lambda_n^1 - \epsilon^2 \lambda_n^2 \tag{101b}$$

Plots of mode shapes and curvature for damaged and undamaged beams correct to first order are given in figures 3 and 4. A detailed discussion about the figures is given in the results section.

51
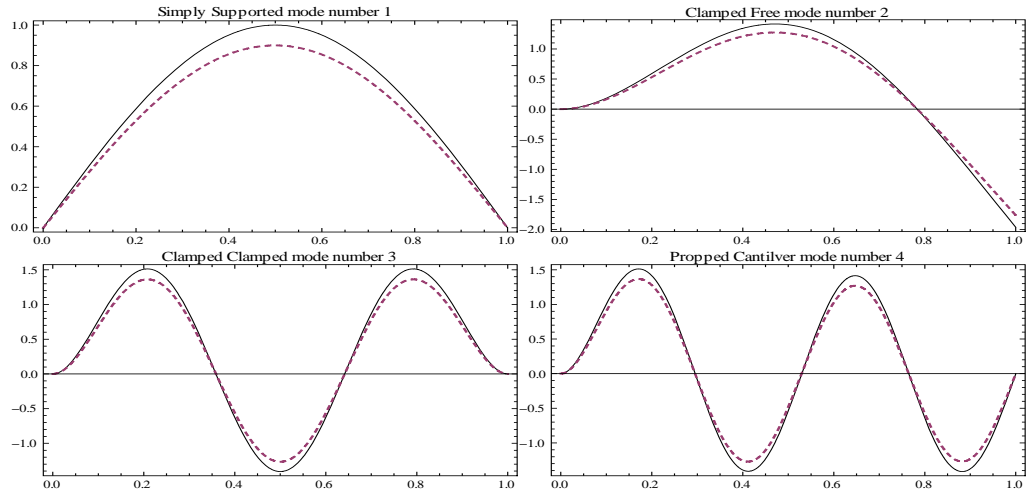
Figure 3: Damaged (dashed lines) and undamaged (continuous lines) mode shapes; $x_d = 0.35L$, $\Delta l = 0.01L$, $\epsilon = 0.1/3$
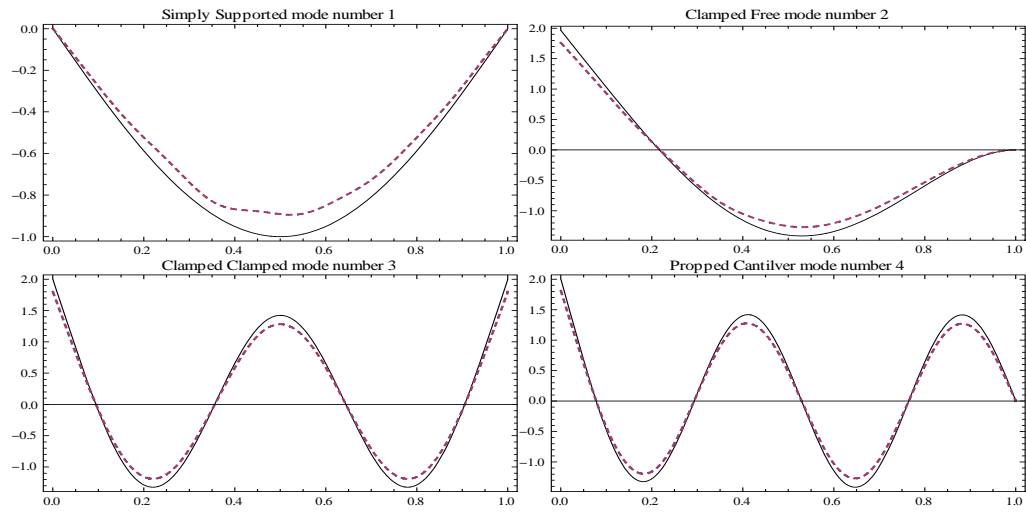
Figure 4: Damaged (dashed lines) and undamaged (continuous lines) curvature shapes; $x_d = 0.35L$, $\Delta l = 0.01L$, $\epsilon = 0.1/3$

52

6.2 Strain Energy Based Damage Measure in Terms of Damage Parameters

The strain energy due to bending for the undamaged beam, excited in its nth mode, is given as

$$U_n = \frac{1}{2}a_n^2 \int_0^L EI(x)\left[(\phi_n)''\right]^2 dx \tag{102}$$

The strain energy for the undamaged beam is given by U_{ud}

$$U_{ud} = U_n = \frac{1}{2}a_n^2 \int_0^L EI_0\left[(\phi_n)''\right]^2 dx \tag{103}$$

Similarly the strain energy due to bending, of the damaged beam U_d can be calculated by substituting (81a) and (101a) in (102). Therefore

$$U_d = \frac{1}{2}a_n^2 \int_0^L EI_0\left[1 - \epsilon\Delta l\delta(x - x_d)\right]\left\{\left[\phi_n^0 - \epsilon\left(\phi_n^0 + \sum_{j=1,j\neq n}^{\infty}\eta_{nj}\phi_j^0\right) - \right.\right.$$
$$\left.\left.\epsilon^2\left(\phi_n^0 + \sum_{l=1,l\neq n}^{\infty}\beta_{nl}\phi_l^0\right)\right]''\right\}^2 dx \tag{104}$$

Collecting terms up to the order of 2 in ϵ

$$U_d = \frac{1}{2}a_n^2 \int_0^L EI_0\left[1 - \epsilon\Delta l\delta(x - x_d)\right]\left\{\left[(\phi_n^0)''\right]^2 - 2\epsilon(\phi_n^0)''\left[(\phi_n^0)'' + \sum_{j=1,j\neq n}^{\infty}\eta_{nj}(\phi_j^0)''\right]\right.$$
$$\left. + \epsilon^2\left[(\phi_n^0)'' + \sum_{j=1,j\neq n}^{\infty}\eta_{nj}(\phi_j^0)''\right]^2 - 2\epsilon^2(\phi_n^0)''\left[(\phi_n^0)'' + \sum_{l=1,l\neq n}^{\infty}\beta_{nl}(\phi_l^0)''\right]\right\}dx \tag{105}$$

The above equation is further simplified by using the condition of orthogonality.

$$U_d = \frac{1}{2}a_n^2 \int_0^L EI_0\left\langle\left[(\phi_n^0)''\right]^2 - 2\epsilon\left[(\phi_n^0)''\right]^2 + \epsilon^2\left\{\left[(\phi_n^0)''\right]^2 + \sum_{j=1,j\neq n}^{\infty}\eta_{nj}^2\left[(\phi_j^0)''\right]^2\right\} - \right.$$
$$2\epsilon^2\left[(\phi_n^0)''\right]^2\Big\rangle dx - \frac{1}{2}a_n^2\epsilon\Delta lEI_0\left\langle\left[(\phi_n^0(x_d))''\right]^2 - 2\epsilon\left[\phi_n^0(x_d)''\right]^2 + \epsilon^2\left\{\left[(\phi_n^0(x_d))''\right]^2 + \right.\right.$$
$$\left.\left.\sum_{j=1,j\neq n}^{\infty}\eta_{nj}^2\left[(\phi_j^0(x_d)'')\right]^2\right\}\right\rangle \tag{106}$$

A way to calculate the damage measure based on strain energy is given in [13]. It is calculated as the change in flexural rigidity of a sub-region of the beam. For this, the beam

is divided into several sub-divisions. The damage measure for the kth segment is given by D_{Mk}

$$D_{Mk} = \frac{(EI)_k}{(EI)_k^*} = \left[\frac{\int_{a_k}^{a_{k+1}} \left(\frac{\partial^2 \phi_i^*}{\partial x^2} \right)^2 dx}{\int_0^L \left(\frac{\partial^2 \phi_i^*}{\partial x^2} \right)^2 dx} \right] \Big/ \left[\frac{\int_{a_k}^{a_{k+1}} \left(\frac{\partial^2 \phi_i}{\partial x^2} \right)^2 dx}{\int_0^L \left(\frac{\partial^2 \phi_i}{\partial x^2} \right)^2 dx} \right] \tag{107}$$

where the starred quantities denote the quantities with damage, and a_k denotes the starting coordinate of the kth division. An advantage of the above representation is that the modes need not be normalized, and the constant associated with displacement is canceled. However, an important assumption made in the above derivation is that the flexural rigidity of the whole beam is same for the damaged beam as for the undamaged beam, and that the flexural rigidity of the damaged beam element is reduced to a constant. In other words, the damage is assumed to extend over the whole damaged segment. Mathematically this translates in taking out the non-constant $EI(x)$ term out of the integral in equation (102) for both the segment strain energy and strain energy for the whole beam. Obviously this cannot be mathematically justified. Hence, here it is proposed that the flexural rigidity term be retained inside the integral. This is possible because we have been able to analytically obtain the expressions of mode shapes of a damaged beam as shown above. Substituting flexural rigidity from equation (81a) and formula for damaged mode shape from equation (101a), one obtains

$$U_d = EI_0 \Bigg\langle (1 - 2\epsilon - \epsilon^2) \int_0^L \left[(\phi_n^0)'' \right]^2 dx + \epsilon^2 \left\{ \int_0^L \sum_{j=1, j \neq n}^{\infty} \eta_{nj}^2 \left[(\phi_j^0)'' \right]^2 dx \right\} -$$

$$\epsilon \Delta l \left\{ \left[\phi_n^0 (x_d) \right]'' \right\}^2 - 2\epsilon \left[\phi_n^0 (x_d)'' \right]^2 \Bigg\rangle \tag{108}$$

The damage measure D_M is then be calculated by [13]

$$D_M = \frac{U_{di}}{U_d} \Big/ \frac{U_{udi}}{U_{ud}} \tag{109}$$

The subscript i denotes the strain energy for the ith segment (x_i to x_{i+1}), U_{di} and U_{udi} are

54

given by

$$U_{di} = EI_0(1 - 2\epsilon - \epsilon^2)\left\langle \int_{x_i}^{x_{i+1}} \left[(\phi_n)''\right]^2 + \sum_{j=1, j\neq n}^{\infty} \frac{\epsilon^2\eta_{nj}^2}{1 - 2\epsilon - \epsilon^2}\left[(\phi_j^0)''\right]^2 - \right.$$

$$\left. \frac{\delta(x - x_d)\Delta l\epsilon(1 - 2\epsilon)}{1 - 2\epsilon - \epsilon^2}\left\{\left[\phi_n^0(x_d)\right]''\right\}^2 \right\rangle$$

$$U_{udi} = \int_{x_i}^{x_{i+1}} EI_0 \left[(\phi_n)''\right]^2 dx \tag{110}$$

Attention is now drawn to equations (101a) and (108) which give the damaged mode shape and strain energy. The expressions are reproduced below in a changed form, only terms up to the order of ϵ are retained for mode shape.

$$U_d = EI_0(1 - 2\epsilon - \epsilon^2)\left\langle \int_0^L \left[(\phi_n)''\right]^2 dx + \int_0^L \sum_{j=1, j\neq n}^{\infty} \frac{\epsilon^2\eta_{nj}^2}{1 - 2\epsilon - \epsilon^2}\left[(\phi_j^0)''\right]^2 dx - \right.$$

$$\left. \frac{\Delta l\epsilon(1 - 2\epsilon)}{1 - 2\epsilon - \epsilon^2}\left\{\left[\phi_n^0(x_d)\right]''\right\}^2 \right\rangle$$

$$\phi_n = (1 - 2\epsilon - \epsilon^2)\left(\phi_n^0 - \sum_{j=1, j\neq n}^{\infty} \frac{\eta_{nj}\epsilon}{1 - 2\epsilon - \epsilon^2}\phi_j^0\right) \tag{111}$$

Let the expression $\sum_{j=1, j\neq n}^{\infty} \frac{\eta_{nj}\epsilon}{\sqrt{1 - 2\epsilon - \epsilon^2}}\phi_j^0$ be denoted by $\Gamma(x; x_d, \Delta l, \epsilon)$ or global damage sensitivity function and $\frac{\Delta l\epsilon(1 - 2\epsilon)}{(1 - 2\epsilon - \epsilon^2)}((\phi_n^0(x_d))'')^2$ by $\Lambda(x_d, \Delta l, \epsilon)$ or local damage sensitivity constant. Notice $x_d, \Delta l, \epsilon$ collectively represent the damage parameters. The above expressions can now be simplified to

$$U_d = U_{ud} + EI_0 \int_0^L \left\{ \left[\Gamma(x, x_d, \Delta l, \epsilon)''\right]^2 dx \right\} - EI_0\Lambda(x_d, \Delta l, \epsilon)$$

$$\phi_n = \phi_n^0 - \Gamma(x, x_d, \Delta l, \epsilon) \tag{112}$$

It can be seen that the displacements exhibit global sensitivity to damage through the function $\Gamma(x, x_d, \Delta l, \epsilon)$ only while strain energy has both global and an acute local sensitivity to damage through the function $\Gamma(x, x_d, \Delta l, \epsilon)$ and through the constant $\Lambda(x_d, \Delta l, \epsilon)$ respectively. Another important observation is that the strain energy is increased everywhere except at damage location where it is reduced due to local damage sensitivity constant.

55
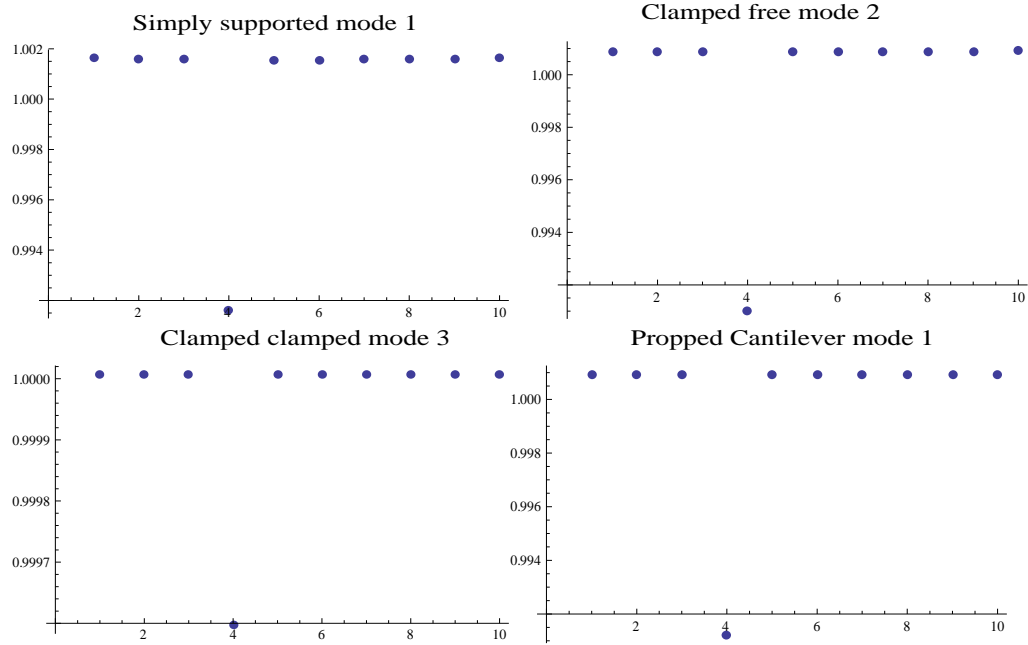
Figure 5: Damage measure, equation (109); $x_d = 0.35L$, $\Delta l = 0.01L$, $\epsilon = 0.1/3$

6.3 Results and Verification

6.3.1 Analytical results

To show the generic nature of the theory presented, four types of beams (simply-supported (SS), clamped-free (CF) clamped-clamped (CC) and propped-cantilever (PC)) are considered. First, in figure 3, the mode shape (dashed line) of the damaged beam is given. The first mode is given for the SS, second for the CF, third for the CC and fourth for the PC damaged beams. Damage parameters are taken to be $x_d = 0.35L, \Delta l = 0.01L, \epsilon = 0.1/3$. The modes of the damaged beams are given along side those of the undamaged beams (continuous line). Similarly in figure 4 the curvature shapes for the damaged beams are given along side those of the undamaged beam. The curvature plots are given in the same order and for the same beams as those for mode shapes. It is seen that mode profiles of damaged and undamaged beams are similar and the damage cannot be identified just by looking at the mode profiles.

Next in figure 5 the damage measure derived is calculated for the beams. Again the same trend is followed as previous figures as far as beams and their mode numbers are
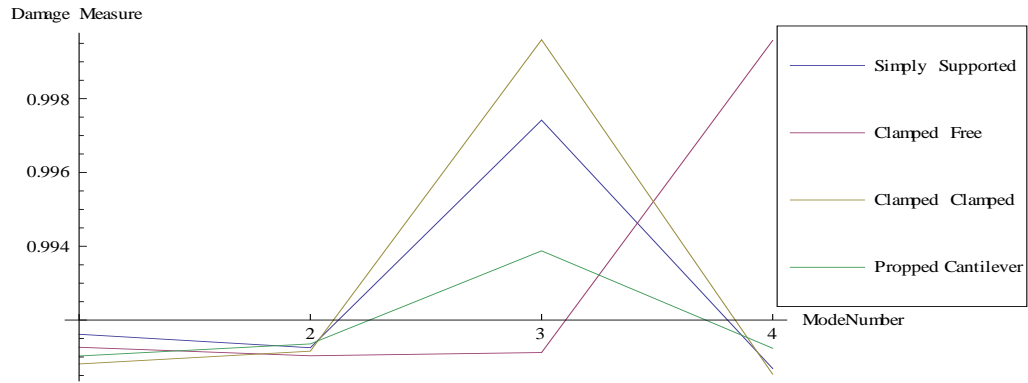
Figure 6: Damage measure modes (1-4); $x_d = 0.35L$, $\Delta l = 0.01L$, $\epsilon = 0.1/3$
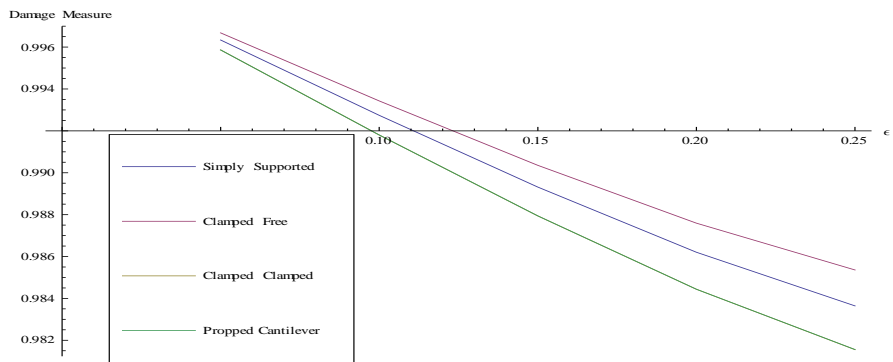
Figure 7: Effect of ϵ on the damage measure; $x_d = 0.35L$, $\Delta l = 0.01L$
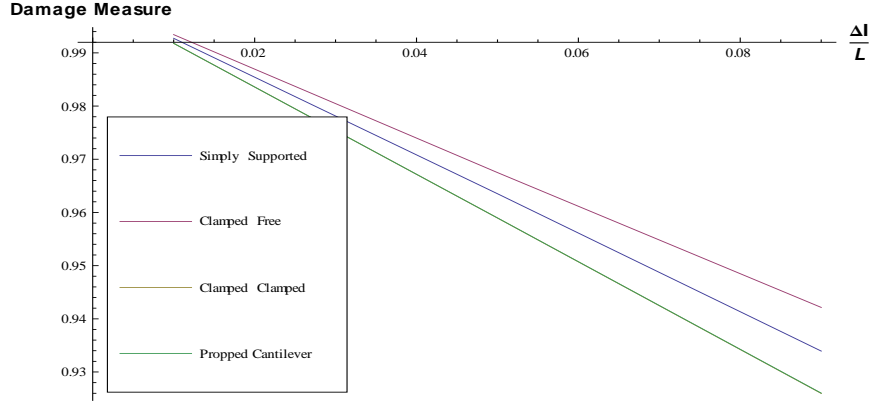
Figure 8: Effect of Δl on damage measure; $x_d = 0.35L$, $\epsilon = 0.1/3$

concerned. It is observed that the location of damage is clearly identified using the damage measure. The noticeable features of the plot are that there is a uniform global effect of damage all along the beams since the magnitude of the damage measure is greater than one. However, at the damage location there is an acute localized drop. Hence, a damage measure on strain energy gives a direct visual information regarding the location of damage. It seems likely to be able to also give damage parameters due to the localized damage effect because according to equation (112) the term $\Lambda(x_d, \Delta l, \epsilon)$ is a function of damage parameters. Once the damage location x_d is ascertained using the damage measure plots, the other damage parameters can be obtained from the local damage sensitivity function, $\Lambda(x_d, \Delta l, \epsilon)$. Similar discontinuities at the damage location were experimentally observed by Cornwell [13]. Another interesting observation regarding the plots is that the drop at the damage location is directly proportional to the increase at the locations without the damage. It would be interesting to check the area under the plots for the damage measure and to ascertain if they tend to be the same.

The next figure 6 gives the plot of damage measure versus the mode number for all four types of beams. It is observed that, the sensitivity of damage measure to damage is dependent on the mode number. Some modes are more sensitive to damage than others. To normalize this erratic behavior, a cumulative damage measure has been used by some researchers. A cumulative damage measure is an average of the damage measure over a

58
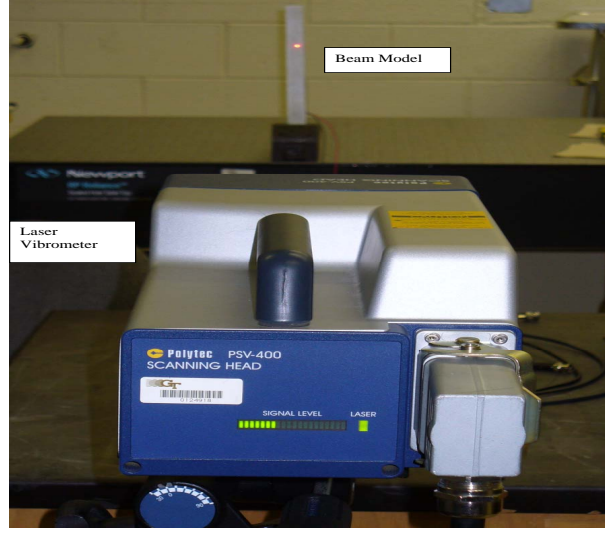
Figure 9: Experimental setup

Table 1: Frequency results comparison analytical vs experimental (Hz)

	Experimental		Analytical		
Mode	Undamaged	Damaged	Undamaged	Damaged	% error =
	$Undam_{expt}$	Dam_{expt}	$Undam_{anal}$	Dam_{anal}	$\frac{Dam_{anal}-Dam_{expt}}{Dam_{anal}}$
1	25.6	25	24.9	24.3	2.88
2	153	155	156	154.6	0.26
3	419	420	436.7	427.8	4.16
4	809	801	855.7	855.7	6.39
5	1314	1326	1414.6	1382.6	4.09

number of modes. The cumulative damage measure is used from this point on.

The cumulative damage measures for different ratios of damage depth to total depth of the beam is given in next figure, figure 7. Finally, a cumulative damage measure is given for different extent of the damage in figure 8. The results of last two figures 7 and 8 are on expected lines since the magnitude of the damage has a direct bearing on damage measure. The Δl value is more sensitive to damage than the ϵ value. However, it should be kept in mind that there is a inherent limit on the value of ϵ according to the theory: The theory neutral axis is assumed to remain unaffected by the damage. Also there is a limit on the value of Δl since the notch-shaped defect given by Heaviside function was approximated by a sharp crack given by a Dirac delta function.
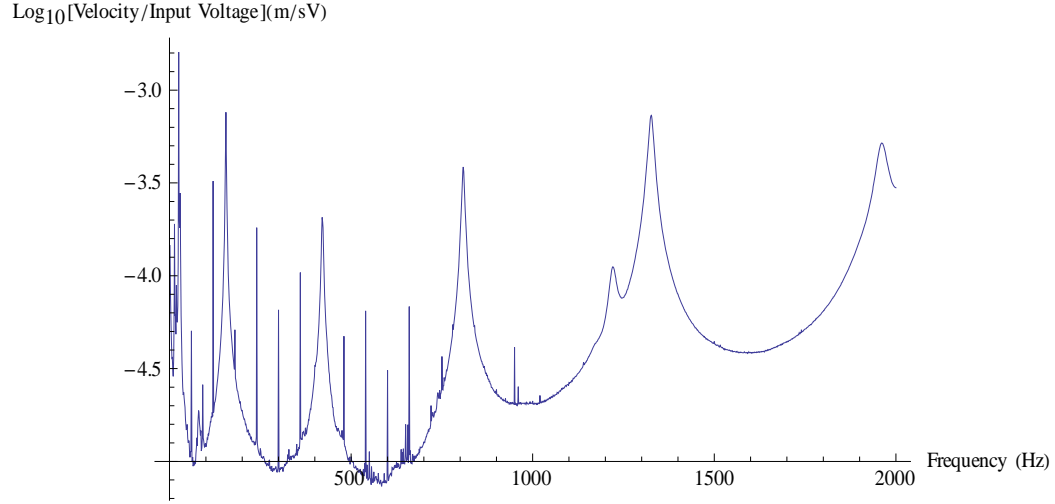
Figure 10: Frequency response function, average velocity (m/sV) against frequency (Hz)

Table 2: Frequency results comparison (Hz) between Law et al. [36] table 2 (Law) and equation (101b) of this thesis; $x_d = 0.381, \Delta l = 0.005$

	$\epsilon = 0$		$\epsilon = 0.16$		$\epsilon = 0.32$		$\epsilon = 0.48$	
Mode	Law	Dixit	Law	Dixit	Law	Dixit	Law	Dixit
2	22.86	22.43	22.80	22.43	22.77	22.42	22.77	22.42
3	62.76	62.81	62.62	62.80	62.38	62.80	62.89	62.80
4	123.05	123.08	122.56	122.85	121.70	122.62	120.0	122.40
5	203.24	203.46	202.27	202.91	201.05	202.36	198.49	201.81
6	303.45	303.93	302.49	303.45	301.51	302.97	299.5	302.49
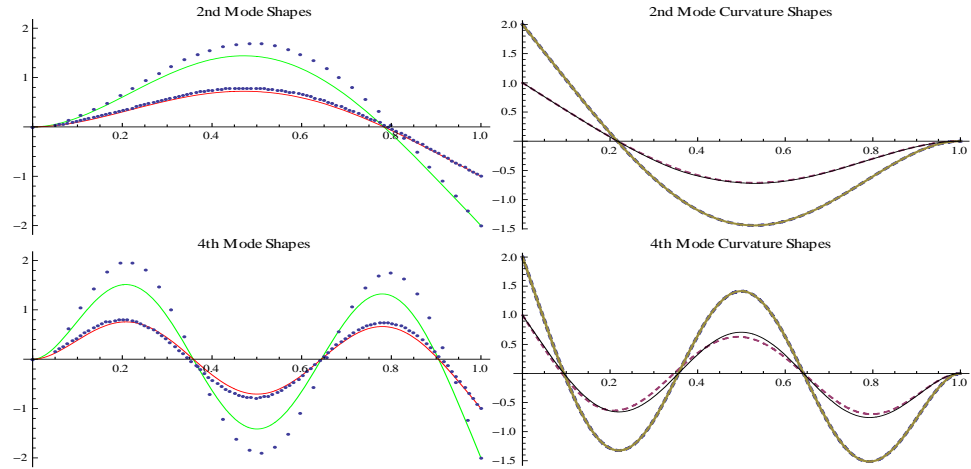
Figure 11: Modes and curvature of undamaged (normalized to 2) and damaged (normalized to 1) beam for experimental mode shapes (dots), experimental curve-fitted curvatures (dashed lines), analytical mode shapes and curvatures (continuous lines)

6.3.2 Experimental verification

Experiments were conducted to verify the theory using the experimental setup given in figure 9. Polytec^{TM} SDLV was used to generate an input voltage. The signal generated (4V) by the SDLV was amplified 100 times by an amplifier. A broadband white noise was used as the input excitation. A piezoelectric actuator was fixed towards the clamped end of the beam to provide the input excitation. Frequencies up to 2 KHz were excited. A low-pass signal filtering was used. A grid consisting of 105 points was used for an undamaged beam. For the damaged beam 505 points were used to take the readings. More points were used for the damaged case to be able to see any minute changes in mode shapes and curvature shapes at the damage location. The resonance frequencies where the frequency response function, shown in figure 10, reaches peak amplitudes and the phase change is 180°, were retained as modal frequencies. The sharp peaks other than the peaks for natural frequencies are harmonics of the power signal, which occur at multiples of 60 Hertz. 10 readings were taken with remeasure option being switched on. Data acquisition was done using Polytec data acquisition software. The obtained modal data, in universal file format, was processed using an in-house developed software. The average was taken for the points across the beam

61
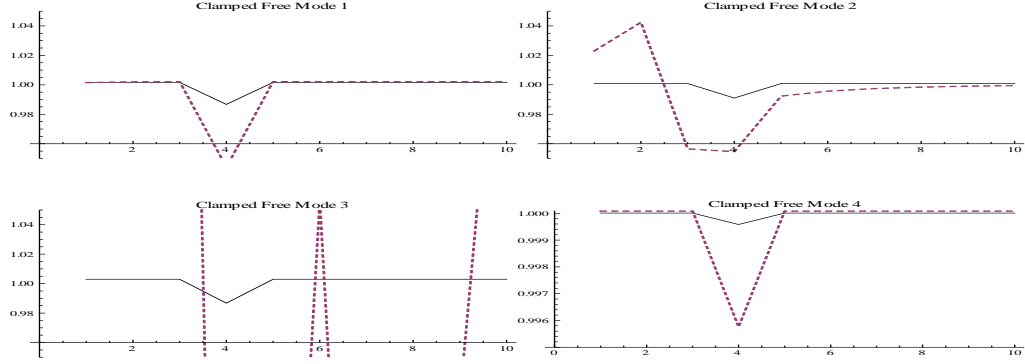
Figure 12: Damage measure for clamped-free beam, dashed (experimental), solid (analytical)

to simulate the beam neutral axis. curve-fitting was done to get a continuous curve for the operating deflected shape, which was assumed to be equivalent to the mode shape for this experiment.

The results presented in the chapter were verified by doing experiments on a cantilever beam. A fiber glass beam was used for the purpose. Modes were calculated experimentally for both damaged and undamaged beam. A rectangular notch shaped damage was made at 0.35 the length of the beam ($x_d = 0.35L$). The damage was 0.1 the depth ($\epsilon = 0.3$), and the notch length was 0.05 the length of the beam ($\Delta l = 0.05L$). The Young's modulus for the beam was 29 GPa, density of the beam 3749 kg/m^3, the length 0.267 m, the moment of inertia 1.28×10^{-10} m^4 and area 10^{-4} m^2

In Table 1 the analytical and experimental values for natural frequencies of the beam are given. The experiments show close correlation with analytical values for lower modes, for higher modes the difference in the readings increases. The experimental setup had to be dismantled for making the notch after the readings on the undamaged beam. The end conditions therefore may change and the readings may be affected. To further validate the derivation using results from published work, the natural frequency values given by Law et al. [36] in Table 2 are compared with analytical values from equations (101b), (98), (95). The Table 2 of Law et al. is reproduced for easy reference. The saw width is given to be 1.3 mm, accounting for the kerf and material loss, the extent of damage is estimated to be ($\Delta l =$

0.005) as deduced from the thickness of the blade used to make the saw cut. The position of damage was ($x_d = 0.38$). Natural frequencies for three values of $\epsilon = 0.16, 0.32, 0.48$ are given in the chapter. The Young's modulus $E = 207\text{GPa}$, mass density $\rho = 7832$ kg/m^3, area $A = 4.75 \times 10^{-4}\text{m}^2$ and area moment of inertia $I = 1.43e10^{-8}\text{m}^4$. The comparison is given in Table 2. The maximum percentage difference in the values is 2%. A point to note is that Law et al. missed the first natural frequency and the values provided are from 2nd to 6th rather than 1st to 5th as claimed. This can be easily ascertained by looking at the first undamaged frequency value which comes out to be 3.58 Hz. Looking at the values of the natural frequencies it can be said that the *presence* of damage is indicated by a change in natural frequency, but its *location and magnitude* cannot be directly ascertained this way.

In figure 11, experimental and analytical modes and curvature shapes for both the damaged and undamaged beams for modes 2 and 4 are plotted. In the mode shape results dots are the experimental data, and the continuous lines are the analytical data results. The experimental data were curve-fitted. The curve-fitted experimental curvatures are plotted as dashed lines. The analytical curvature plots are shown as continuous lines. The damaged beam mode shape and curvature shapes are normalized to unity and the undamaged beam mode shape and curvature to 2 to be able to easily distinguish them. Calculated damage measures $1 - 4$ are given in figure 12. The dashed lines gives the experimental value of the damage measure and the continuous lines give the theoretical values. Mode shape 2, which is more sensitive to damage, shows a disturbance at the place of the actuator attachment to the beam. This can be attributed to the additional mass provided by the actuator. Mode 3 has a unique phenomenon occurring, as the natural frequency value coincided with the natural harmonics of the power supply (420 Hz). As a result there was experimental noise in the measurement of the mode shape. Damage measures still indicated damage, but the correlation with analytical values was lost. figure 13 shows the third mode shape of the damaged beam along with the damage measure at a different scale from the one shown in figure 12.
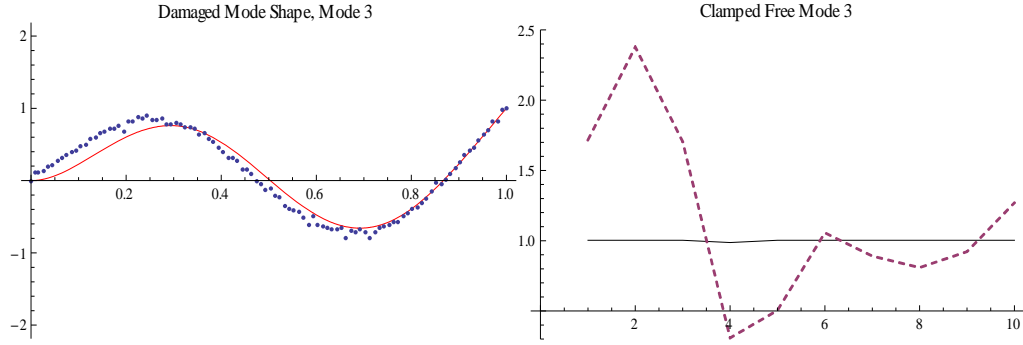
Figure 13: Mode shape, dots (experimental data), continuous line (analytical) clamped-free beam 3rd mode, damage measure, dashed (experimental), solid (analytical)

6.4 Discussion of Results and Conclusions

- A procedure is presented the mode shapes and natural frequencies of damaged beams in terms of modes and natural frequencies of the undamaged beam together with damage parameters such as location and magnitude of damage. Single beam analysis without any assumptions regarding the physical behavior of damage is used. This was verified by using natural frequencies (Table 1 and 2), mode and curvature shapes (figures 3, 4 and 11) and an improved damage measure based on strain energy (figures 5 and 12). The procedure was shown to be applicable to beams with different end conditions.

- It was seen that the modal displacement and curvature shapes for damaged and un-damaged were similar, but it was difficult to ascertain the position of the damage using them.

- Regarding the natural frequencies, although a change in their value indicates the presence of damage, they were not sufficient to directly give the location of damage nor its magnitude.

- The change in natural frequencies is given by $\epsilon \lambda_n^1$, where λ_n^1 is given by equation (95). It is seen in the equation that a decrease in mass increases the natural frequency and a decrease in stiffness decreases it. The change in the natural frequency is an aggregate

64

effect consisting of these two contradictory effects, so the natural frequency cannot serve as a robust indicator of the magnitude of the damage.

- The change in mass per unit length effect, which has been neglected by many researchers, was successfully considered in this chapter. In some types of damage, such as delamination where there is no change in the mass like delamination, the change in mass per unit length can be neglected. In other types of damage however, such as those due to corrosion and erosion, this effect should be accounted for.

- The analytical expressions derived for mode shapes, curvature shapes, natural frequencies and an improved strain energy based damage measure, are verified using experiments. The improvement in the damage measure stems from not assuming that the bending stiffness of the damaged beam is constant and equal to that of undamaged beam when calculating the strain energy of the entire beam. It is also not assumed that the bending stiffness of the element in which the damage is located is constant.The damage measure was shown to be extremely sensitive to the damage. The explanation of the sensitivity is that the damage measure is a function of strain energy, which in turn is a product of stiffness and curvature, both of which are discontinuous at the damage location.

- A limitation of the damaged measure was that it depended on accurate measurement of damaged mode shapes.

- Two damage parameters one giving global damage influence $\Gamma(x, x_d, \Delta l, \epsilon)$ and another giving acute local damage influence $\Lambda(x_d, \Delta l, \epsilon)$ were discovered. Since $\Lambda(x_d, \Delta l, \epsilon)$ is a function of damage magnitude (ϵ and Δl), the damage measure can be used to find the damage magnitude. This is a topic for further study by the author.

Chapter VII

APPLICATION TO TIMOSHENKO BEAM THEORY

The framework as described in chapter 4, which is a general formulation that is applicable to all the damaged, linear elastic structures , is applied to Timoshenko beam theory in this chapter. Timoshenko beam theory is taken as an example, and its results are compared with results using Euler-Bernoulli beam theory and finite element models. The range of applicability for damage characteristics, such as depth and extent of damage and beam characteristics like slenderness ratio and Poisson's ratio, are ascertained for Timoshenko and Euler-Bernoulli beam theories. Unlike most methods for analysis of damaged structures, the mass reduction along with the stiffness reduction where applicable are considered. A rectangular notch-like non-propagating damage are taken as examples of the damage.

7.1 Results And Verification

Equations (41) gives the solution to the nth order correction to the eigenvalue. The first order correction is given by the equation (47). In this chapter the first order correction to eigenvalue is used to obtain corrected eigenvalue of the damaged beams for both Euler-Bernoulli and Timoshenko beam theories using the following equation

$$\lambda_z = \lambda_z^0 + \epsilon \lambda_z^1 \tag{113}$$

where λ_z is the non-dimensionalized eigenvalue and the superscripts represent the order of perturbation and ϵ represent the ratio of the depth at the damage location to the total depth of the beam. The corrected eigenvalues are then used to calculate the natural frequencies of the damaged beams for both the theories. The natural frequencies are calculated using the following expressions.

$$\omega = \frac{1}{2\pi}\sqrt{\frac{EI_3\lambda_z}{\rho A L^4}} \quad \omega = \frac{1}{2\pi}\sqrt{\frac{\lambda_z \kappa G}{\rho L^2}} \tag{114}$$

66

Table 3: Frequency comparison (Hz): simply-supported beam; $\sigma = 3.70 \times 10^{-4}$, $e = 3.2$, $\epsilon = 0.2$, $\Delta L_z = 0.04/3$; values that vary more than 5% are given in bold. D-Damaged, U-Undamaged

Mode	FE-Model		Analytical, EB		Analytical, TB	
	U	D	U	D	U	D
1	47.97	46.58	48.33	46.78	47.96	46.45
2	187.88	181.29	193.30	184.72	187.69	179.85
3	409.13	406.53	**434.93**	**432.94**	408.23	406.48
4	697.77	687.66	**773.22**	**760.29**	695.27	685.69
5	1039.7	1009.1	**1208.4**	**1148.7**	1034.4	997.87
6	1422.3	1404.8	**1739.7**	**1710.6**	1412.9	1396.7
7	1835.6	1822.5	**2368.0**	**2357.1**	1820.7	1812.1

where ω represents the natural frequency, E the Young's modulus, I_3 the area moment of inertia, ρ the material density, κ the shear factor, A the area, L the length , and G the shear modulus of the beam, respectively.

7.1.1   Analytical results

To test the ability of the procedure presented in the previous chapter to correctly predict the results for a damaged beam using Euler-Bernoulli and Timoshenko beam theories, a finite element model of the beam was constructed in $Abaqus^{TM}$ [29] with both simply-supported and clamped-free end conditions. The constants involved were $E = 62.1$GPa, $G = 23.3$GPa, $\kappa = 5/6$, $L = 3$m, $h = 0.2$m, $b = 0.1$m, $x_d = 0.3L$, $k = 9$, $\Delta L_z = 0.04/3$, $\rho = 2700$Kg/m^3, $\epsilon = 0.2h$. The beam was modeled with plane stress elements of size 0.02m, the material constant poisson's ratio was $\nu = 0.33$. Results for simply-supported end condition are presented in Table 3, and those for clamped-free end condition in Table 4. The two end conditions collectively simulated the symmetric and asymmetric cases.

The maximum percentage difference between the values of the finite element model results and those using the analytical derivation presented using first order correction to natural frequencies for Timoshenko beam theory was about 1% for both clamped-free and simply-supported beams. Euler-Bernoulli beam theory results were accurate for only the first two natural frequencies

The next objective is to demonstrate that the inertia effects due to the damage are

67

Table 4: Frequency comparison (Hz): clamped-free beam; $\sigma = 3.70 \times 10^{-4}$, $e = 3.2$, $\epsilon = 0.2$, $\Delta L_z = 0.04/3$; values that vary more than 5% are given in bold. D-Damaged, U-Undamaged

	FE-Model		Analytical, EB		Analytical, TB	
Mode	U	D	U	D	U	D
1	17.17	16.61	17.21	16.34	17.15	16.29
2	105.43	104.24	107.89	107.76	105.28	105.13
3	286.29	277.20	**302.10**	291.4	285.61	277.07
4	538.50	532.23	**591.99**	583.82	536.60	532.05
5	848.93	840.96	**978.60**	**973.51**	844.82	838.67
6	1204.4	1169.9	**1461.9**	**1395.8**	1196.9	1157.05
7	1594.2	1569.5	**2041.8**	**1976.1**	1582.1	1557.38

Table 5: Comparison of mass defect vs stiffness defect (non-dimensionalized); $\sigma = 3.70 \times 10^{-4}$, $e = 3.2$, $\epsilon = 0.2$, $\Delta L_z = 0.04/3$

	simply-supported (SS)		clamped-free(CF)		Ratio	
Mode	Mass	Stiffness	Mass	Stiffness	SS	CF
i	$E_{m_{ii}}$	$E_{s_{ii}}$	$E_{m_{ii}}$	$E_{s_{ii}}$	$E_{m_{ii}}/E_{s_{ii}}$	$E_{m_{ii}}/E_{s_{ii}}$
1	-0.09	-0.26	-0.00048	-0.0258	0.35	0.02
2	-7.49	-21.73	-1.724	-1.901	0.35	0.91
3	-14.84	-30.87	-75.115	-157.46	0.48	0.48
4	-193.90	-462.93	-198.031	-379.543	0.42	0.52
5	-1566.03	-3956.01	-625.56	-1357.3	0.40	0.46
6	-2020.82	-4214.04	-7578.37	-19245.9	0.48	0.39
7	-2928.52	-4928.94	-13525.6	-29794.0	0.59	0.45

not higher-order effects. The inertia effects for the two cases is given in Table 5. The observations from Table 5 are that it is not reasonable to neglect the inertia effect where it occurs, since it has an important bearing on the overall behavior of the damaged beam. The ratio is as high as 91%. Theoretically, there is a possibility of the inertia effect being greater in magnitude than the stiffness effect. The frequency of the damaged beam in that case would increase.

The next objective is to test the domain of validity of the theory. The four variables that influence the results are the depth of damage, which is measured by ϵ giving the ratio of the depth of the damage to the overall depth of the beam; ΔL_z, giving the extent of the damage; e, giving the ratio of the Young's modulus to the shear modulus of the material; and σ, which is the slenderness ratio, i.e., the ratio of the area moment of inertia and the area times the length squared of the beam. The first two are damage parameters and the

last two are beam parameters. The results are assumed to be reasonable if the theory gives values within 5% of those given by $Abaqus^{TM}$ results. If the results are not within the reasonable range then they are written in bold.

The depth of damage effect is investigated by considering widths where $\epsilon = 0.025$, 0.1, 0.4 in Tables 6 and 7. For $\epsilon = 0.2$ and for undamaged case, the results are already given in Table 3 and 4. It is seen that the classical beam theory gives reasonable results for only first two natural frequencies while Timoshenko beam theory gives reasonable results with natural frequencies within 5% up till $\epsilon = 0.4$ for the first seven natural frequencies.

The extent of damage effect is investigated by considering depths where $\Delta L_z = 0.01/3$, 0.05/3, 0.1/3 in the Tables 8 and 9. For $\Delta L_z = 0.04/3$ and for undamaged case, the results are already given in Table 3 and 4. It is seen that the Euler-Bernoulli theory gives reasonable results only for first two natural frequencies while Timoshenko beam theory gives reasonable results with natural frequencies within 5% until $\Delta L_z = 0.1/3$ for the first seven natural frequencies. The range may be further improved by using the damage profile function to be a step function instead of the approximation of a delta function as done by Dixit and Hanagud [17] for Euler-Bernoulli beams. The effect of the ratio of Young's modulus to the shear factor times shear modulus given by e forms the next part of study. Reasonable values of Poisson's ratio ν for engineering materials are between 0.2 and 0.4. The results are presented for $\nu = 0.417, 0.167$ ($e = 3.4, 2.8$) in Tables 10 and 11. Since this is a material property, the values for the undamaged beam frequencies also change and are given in the tables. It is noted, however that the ν values do not affect the Euler-Bernoulli beam frequencies. This result is on expected lines since ν affects the torsional frequency of classical beam theory (Euler-Bernoulli for bending and St. Venant theory for torsion).It is seen that the Timoshenko theory is able to give values within 1% for both simply-supported and clamped-free beams for both the limiting values of e. The Euler-Bernoulli beam theory is able to predict correct values for the first two natural frequencies. Next, the last beam factor σ, a measure of the slenderness ratio, is investigated and results presented in Tables 12 - 17. The slenderness ratio can be altered by either changing the length or by changing the depth. If two beams has the same slenderness ratio but different dimensions, the beam with

69

Table 6: Variation of ϵ frequency (Hz): simply-supported beam; $\sigma = 3.70 \times 10^{-4}$, $E = 3.2$, $\Delta L_z = 0.04/3$; values that vary more than 5% are given in bold.

Mode	$\epsilon = 0.025$			$\epsilon = 0.1$			$\epsilon = 0.4$		
	FE-Model	TB	EB	FE-Model	TB	EB	FE-Model	TB	EB
1	47.72	47.77	48.25	47.37	47.21	47.56	43.20	44.90	45.19
2	186.87	186.72	192.25	185.09	183.81	189.06	167.63	171.66	**175.72**
3	407.48	408.01	**434.69**	406.93	407.35	**433.94**	405.71	404.73	**430.93**
4	694.90	694.07	**771.61**	692.37	690.50	**766.78**	673.33	675.97	**747.13**
5	1034.8	1029.8	**1200.9**	1025.9	1016.3	**1178.8**	967.00	959.97	**1086.0**
6	1417.1	1410.8	**1736.1**	1412.6	1404.6	**1725.3**	1382.3	1379.4	**1681.0**
7	1829.7	1819.6	**2366.6**	1827.3	1816.39	**2362.5**	1795.4	1803.53	**2346.2**

Table 7: Variation of ϵ frequency (Hz): clamped-free beam; $\sigma = 3.70 \times 10^{-4}$, $e = 3.2$, $\Delta L_z = 0.04/3$; values that vary more than 5% are given in bold.

Mode	$\epsilon = 0.025$			$\epsilon = 0.1$			$\epsilon = 0.4$		
	FE-Model	TB	EB	FE-Model	TB	EB	FE-Model	TB	EB
1	17.14	17.05	17.11	16.93	16.73	16.79	15.31	15.37	15.42
2	105.37	105.26	107.88	104.71	105.20	107.83	102.26	104.98	**107.63**
3	285.89	284.56	**300.78**	282.41	281.37	**296.8**	257.52	268.25	**280.29**
4	538.15	536.04	**590.98**	534.72	534.33	**587.92**	525.80	527.46	**575.54**
5	848.49	844.06	**977.97**	843.90	841.75	**976.06**	830.50	832.47	**968.38**
6	1202.7	1192.0	**1453.8**	1188.9	1177.2	**1429.2**	1120.2	1115.74	**1326.54**
7	1592.9	1579.0	**2033.7**	1581.3	1569.8	**2009.2**	1537.2	1532.27	**1908.13**

70

71

Table 8: Variation of ΔL_z frequency (Hz): simply-supported beam; $\sigma = 3.70 \times 10^{-4}$, $e = 3.2$, $\epsilon = 0.2$; values that vary more than 5% are given in bold.

| Mode | $\Delta L_z = 0.01/3$ | | | $\Delta L_z = 0.05/3$ | | | $\Delta L_z = 0.1/3$ | | |
	FE-Model	TB	EB	FE-Model	TB	EB	FE-Model	TB	EB
1	46.80	47.59	47.95	46.51	46.07	46.39	46.18	44.10	44.37
2	182.28	185.76	191.19	180.99	177.84	182.51	179.58	**167.41**	171.04
3	406.62	407.79	**434.44**	406.49	406.04	**432.44**	406.24	403.85	**429.92**
4	688.77	692.89	**770.00**	687.31	683.27	**757.02**	685.64	671.06	**740.47**
5	1012.5	1025.4	**1193.6**	1008.2	988.53	**1133.3**	1004.8	**940.45**	**1053.2**
6	1406.6	1408.8	**1732.5**	1404.2	1392.1	**1703.3**	1401.0	1370.9	**1666.1**
7	1824.3	1818.5	**2365.3**	1821.7	1810.0	**2354.4**	1816.5	1799.22	**2340.7**

Table 9: Variation of ΔL_z frequency (Hz): clamped-free beam; $\sigma = 3.70 \times 10^{-4}$, $e = 3.2$, $\epsilon = 0.2$; values that vary more than 5% are given in bold.

| Mode | $\Delta L_z = 0.01/3$ | | | $\Delta L_z = 0.05/3$ | | | $\Delta L_z = 0.1/3$ | | |
	FE-Model	TB	EB	FE-Model	TB	EB	FE-Model	TB	EB
1	16.83	16.94	17.00	16.70	16.06	16.12	16.48	15.90	**14.94**
2	104.77	105.24	107.86	104.70	105.09	107.73	104.22	104.91	107.57
3	280.23	283.5	**299.46**	278.81	274.89	288.66	276.20	263.73	274.57
4	534.95	535.47	**584.96**	534.31	530.91	**581.76**	531.69	525.15	**571.35**
5	844.92	843.29	**977.33**	843.89	837.13	**972.23**	839.66	829.36	**965.81**
6	1180.4	1187.1	**1445.6**	1175.7	1146.9	**1378.8**	1167.9	**1094.5**	**1290.5**
7	1578.6	1576.0	**2025.6**	1575.6	1551.1	**1959.3**	1567.1	**1803.53**	**1873.23**

Table 10: Variation of ν, e frequency (Hz): simply-supported beam; $\sigma = 3.70 \times 10^{-4}$, $\epsilon = 0.2$, $\Delta L_z = 0.04/3$; values that vary more than 5% are given in bold. D-Damaged, U-Undamaged

| | $e = 3.4, \nu = 0.417$ | | | | $e = 2.8, \nu = 0.167$ | | | | $e = 3.4$ or 2.8 | |
| | FE-Model | | Analytical, TB | | FE-Model | | Analytical, TB | | Analytical, EB | |
Mode	U	D	U	D	U	D	U	D	U	D
1	47.96	46.57	47.94	46.44	48.00	46.61	48.00	46.48	48.33	46.78
2	187.66	181.09	187.43	179.64	188.30	181.67	188.20	180.28	193.30	184.72
3	408.13	405.61	407.08	405.30	411.01	408.30	410.55	408.87	**434.94**	**432.94**
4	695.04	685.04	692.13	682.63	702.96	692.63	701.66	691.93	**773.22**	**760.29**
5	1034.0	1004.0	1027.9	992.42	1050.5	1019.0	1047.7	1009.0	**1208.2**	**1148.7**
6	1412.4	1395.2	1401.6	1385.1	1441.4	1423.2	1436.4	1419.4	**1739.7**	**1710.6**
7	1820.1	1807.3	1803.01	1793.8	1865.4	1851.7	1857.4	1850.2	**2368.0**	**2357.1**

Table 11: Variation of ν, e frequency (Hz): clamped-free beam; $\sigma = 3.70 \times 10^{-4}$, $\epsilon = 0.2$, $\Delta L_z = 0.04/3$; values that vary more than 5% are given in bold.

| | $e = 3.4, \nu = 0.417$ | | | | $e = 2.8, \nu = 0.167$ | | | | $e = 3.4$ or 2.8 | |
| | FE-Model | | Analytical, TB | | FE-Model | | Analytical, TB | | Analytical, EB | |
Mode	U	D	U	D	U	D	U	D	U	D
1	17.17	16.65	17.15	16.29	17.16	16.29	17.17	16.64	17.22	16.34
2	105.37	104.24	105.16	105.01	105.52	105.37	105.57	104.44	107.89	107.76
3	285.76	277.38	284.89	276.46	287.06	278.28	287.35	278.82	**302.10**	**291.40**
4	536.68	530.87	534.35	529.91	541.20	536.41	542.08	536.03	**591.99**	**583.82**
5	844.69	836.86	839.77	833.38	855.20	849.57	857.23	849.43	**978.60**	**973.51**
6	1196.5	1164.8	1187.7	1149.0	1216.1	1173.8	1216.1	1186.1	**1461.9**	**1395.8**
7	1581.4	1559.3	1567.3	1543.6	1613.0	1585.9	1619.4	1595.0	**2041.8**	**1976.1**

72

greater length and corresponding greater depth is more accurately represented by the beam theories that the one with lower length and corresponding lower depth. This deduction as evident from the tables, holds for both of damaged and undamaged case. First the slenderness ratio of $\frac{1}{30}$ is used in Tables 12 and 13. The length is changed (increased) and the depth remains the same as the base beam given in Tables 3 and 4, and the depth is changed but the length remains the same as the base beam. Even Euler-Bernoulli beam theory gives accurate frequency estimation for this beam.

The next case is for slenderness ratio of $\frac{1}{10}$ in Tables 14 and 15. All frequencies using Euler-Bernoulli beam theory fall outside the 5% range. On the other hand Timoshenko beam theory results are within an average difference of less than 1% for the first seven natural frequencies. The next slenderness ratio considered is $\frac{1}{5}$ in Tables 16 and 17. The analytical derivation using Timoshenko beam theory gives frequency values that are within 2% for the first seven natural frequencies. An important thing to note is that the last row of the Table gives frequencies values belonging to the so-called second frequency branch. The frequencies even for this branch are predicted to an accuracy of within 2% in the example given.

The theory needs the width of damage as an input, none of the four papers [64, 33, 39, 65], in the same area and preceding the work presented in this thesis has this value as input. Therefore, only qualitative comparison is done. In an excellent work by Khaji et al. [33], a closed-form solution for a damaged Timoshenko beam using an approximate formulation is given. The results as calculated using the theory presented is given in Table 16. Both the works give comparable results.

7.1.2 Experimental verification

In the previous chapter, experimental validation was done for an Euler-Bernoulli beam. The validation is extended to a Timoshenko beam using the same setup as shown in figure 9.

In Table 18 the analytical and experimental values for natural frequencies of the beam are given. The analytical values show close correlation to experiments for lower modes using

73

Table 12: Variation of σ frequency (Hz): simply-supported beam; $\sigma = \frac{1}{10800}$ or $\frac{h}{L} = \frac{1}{30}$, $\epsilon = 0.2$, $\Delta L_z = 0.04/3$, $e = 3.2$; values that vary more than 5% are given in bold.

| | $h = 0.2, L = 6$ | | | | | | $h = 0.1, L = 3$ | | | | | |
| | FE-Model | | Analytical, TB | | Analytical, EB | | FE-Model | | Analytical, TB | | Analytical, EB | |
Mode	U	D	U	D	U	D	U	D	U	D	U	D
1	12.06	11.81	12.06	11.68	12.08	11.70	24.12	23.25	24.12	23.35	24.16	23.39
2	47.97	46.77	47.96	45.86	48.33	46.18	95.95	92.10	95.92	91.73	96.65	92.36
3	106.98	106.22	106.91	106.43	108.73	108.23	213.95	209.47	213.83	212.87	217.47	216.47
4	187.87	185.36	187.69	184.72	193.30	190.07	375.75	365.52	375.37	369.44	386.61	380.14
5	289.15	282.40	288.71	275.79	302.04	287.17	578.31	556.57	577.43	551.59	604.08	574.35
6	409.09	404.63	408.23	402.17	434.93	427.66	818.19	798.32	816.45	804.34	**869.87**	**855.32**
7	545.87	542.26	544.36	542.06	591.99	589.27	1091.8	1070.7	1088.7	1084.1	**1184.0**	**1178.6**

Table 13: Variation of σ frequency (Hz): clamped-free beam; $\sigma = \frac{1}{10800}$ or $\frac{h}{L} = \frac{1}{30}$, $\epsilon = 0.2$, $\Delta L_z = 0.04/3$, $e = 3.2$; values that vary more than 5% are given in bold.

| | $h = 0.2, L = 6$ | | | | | | $h = 0.1, L = 3$ | | | | | |
| | FE-Model | | Analytical, TB | | Analytical, EB | | FE-Model | | Analytical, TB | | Analytical, EB | |
Mode	U	D	U	D	U	D	U	D	U	D	U	D
1	4.30	4.20	4.3	4.08	4.30	4.09	8.61	8.30	8.60	8.17	8.61	8.17
2	26.82	26.59	26.80	26.77	26.97	26.94	53.64	52.43	53.61	53.54	53.95	52.88
3	74.48	72.77	74.42	71.89	75.52	72.85	148.97	143.34	148.84	143.79	151.05	145.70
4	144.25	142.64	144.07	142.32	148.00	146.00	288.51	281.22	288.15	284.64	296.00	291.91
5	234.97	233.27	234.58	233.23	244.65	243.38	469.96	460.15	469.16	466.45	489.30	**486.75**
6	344.95	337.30	344.20	329.97	**365.47**	348.96	689.95	664.87	688.40	659.95	**730.93**	**697.92**
7	472.41	465.25	471.10	483.60	**510.44**	494.62	944.89	917.59	942.21	907.19	**1020.9**	**988.04**

Table 14: Variation of σ frequency (Hz): simply-supported beam; $\sigma = \frac{1}{1200}$ or $\frac{h}{L} = \frac{1}{10}$, $\epsilon = 0.2$, $\Delta L_z = 0.04/3$, $e = 3.2$; values that vary more than 5% are given in bold.

| | $h = 0.3, L = 3$ | | | | | | $h = 0.2, L = 2$ | | | | | |
| | FE-Model | | Analytical, TB | | Analytical, EB | | FE-Model | | Analytical, TB | | Analytical, EB | |
Mode	U	D	U	D	U	D	U	D	U	D	U	D
1	71.32	68.89	71.28	69.08	72.49	70.18	106.98	103.03	106.91	103.62	108.73	105.26
2	272.77	261.57	272.15	261.57	**289.96**	**277.08**	409.16	391.19	408.23	392.35	**434.93**	**415.62**
3	575.35	572.08	572.77	570.36	**652.40**	**649.40**	863.03	856.01	859.16	855.54	**978.60**	**974.11**
4	948.43	935.20	941.94	930.84	**1159.8**	**1140.4**	1422.7	1399.5	1412.9	1396.3	**1739.7**	**1710.6**
5	1367.8	1326.6	1355.3	1320.5	**1812.2**	**1723.0**	2051.8	1985.0	2033.0	1980.8	**2718.3**	**2584.6**
6	1816.8	1794.8	1796.3	1778.9	**2609.6**	**2566.0**	2725.2	2686.2	2694.4	2668.4	**3914.4**	**3848.9**
7	2284.2	2270.8	2254.0	2239.8	**3552.0**	**3535.6**	3426.3	3398.7	3381.0	3359.7	**5327.9**	**5303.5**

Table 15: Variation of σ frequency (Hz): clamped-free beam; $\sigma = \frac{1}{1200}$ or $\frac{h}{L} = \frac{1}{10}$, $\epsilon = 0.2$, $\Delta L_z = 0.04/3$, $e = 3.2$; values that vary more than 5% are given in bold.

| | $h = 0.3, L = 3$ | | | | | | $h = 0.2, L = 2$ | | | | | |
| | FE-Model | | Analytical, TB | | Analytical, EB | | FE-Model | | Analytical, TB | | Analytical, EB | |
Mode	U	D	U	D	U	D	U	D	U	D	U	D
1	25.65	24.66	25.62	24.33	25.82	24.52	38.48	36.90	38.43	36.50	38.74	36.77
2	153.79	152.04	153.41	153.15	**161.84**	**161.64**	230.71	227.52	230.11	229.73	**242.75**	**242.47**
3	404.77	382.35	403.07	393.22	**453.15**	**437.10**	607.19	572.61	604.61	589.82	**679.72**	**655.65**
4	734.92	728.25	730.36	726.87	**887.98**	**875.73**	1102.4	1090.1	1095.5	1090.3	**1332.0**	**1313.6**
5	1119.9	1107.9	1110.7	1100.7	**1467.9**	**1460.3**	1680.0	1658.6	1666.1	1651.0	**2201.9**	**2190.4**
6	1540.8	1494.1	1525.2	1487.0	**2192.8**	**2093.8**	2311.4	2236.2	2287.7	2230.4	**3289.2**	**3140.7**
7	1985.2	1946.9	1961.4	1940.3	**3062.7**	**2964.1**	2977.9	2915.1	2942.1	2910.4	**4594.0**	**4446.2**

75

www.manaraa.com

Table 16: Variation of σ frequency (Hz): simply-supported beam; $\sigma = \frac{1}{300}$ or $\frac{h}{L} = \frac{1}{5}$, $\epsilon = 0.2$, $\Delta L_z = 0.04/3$, $e = 3.2$; values that vary more than 5% are given in bold, the seventh frequency is from second frequency branch, Khaji et al. [33] Eq. (10a)

| Mode | h = 0.6, L = 3 Case C-1 | | | | | h = 0.2, L = 1 Case C-2 | | | | | % diff | |
| | FE-Model | | Analytical, TB | | Khaji | FE-Model | | Analytical, TB | | Khaji | C-1 | C-2 |
	U	D	U	D		U	D	U	D			
1	136.42	129.11	136.08	132.26	129.77	409.26	385.37	408.23	396.77	389.30	2.4	3.0
2	474.54	454.36	470.97	457.57	448.72	1423.7	1357.8	1412.9	1372.7	1346.2	0.7	1.1
3	909.33	903.22	898.12	893.16	894.61	2728.1	2700.4	2694.4	2679.5	2683.8	0.1	0.8
4	1383.3	1359.8	1360.8	1349.3	1344.3	4150.1	4062.3	4082.5	4048.0	4033.0	0.8	0.4
5	1871.5	1793.8	1835.5	1825.9	1786.5	5614.9	5349.6	5506.5	5477.8	5359.4	1.8	2.4
6	2362.9	2327.5	2312.7	2295.4	2295.1	7089.2	6918.1	6938.1	6886.2	6918.1	1.4	0.5
7	2622.5	2591.5	2624.6	2591.7	2612.3	7868.2	7733.3	7873.9	7775.2	7733.3	0.0	0.5

Table 17: Variation of σ frequency (Hz): clamped-free beam; $\sigma = \frac{1}{300}$ or $\frac{h}{L} = \frac{1}{5}$, $\epsilon = 0.1$, $\Delta L_z = 0.05/0.267$, $e = 3.2$; values that vary more than 5% are given in bold.

| Mode | h = 0.6, L = 3 Case C-1 | | | | h = 0.2, L = 1 Case C-2 | | | | % diff | |
| | FE-Model | | Analytical, TB | | FE-Model | | Analytical, TB | | C-1 | C-2 |
	U	D	U	D	U	D	U	D		
1	50.21	47.20	50.06	47.62	150.65	141.49	150.18	142.86	0.8	0.7
2	270.70	265.79	268.95	268.11	812.19	796.86	806.85	804.33	0.9	0.9
3	645.49	624.00	639.01	634.22	1936.8	1870.8	1917.0	1902.7	1.6	1.7
4	1073.9	1069.0	1059.4	1059.7	3222.3	3204.6	3178.3	3179.0	0.9	0.8
5	1529.8	1495.7	1505.0	1490.3	4589.9	4482.9	4515.1	4470.8	0.4	0.3
6	1986.7	1886.1	1951.3	1937.3	5960.6	5652.6	5853.8	5811.9	2.7	2.8
7	2417.2	2378.9	2378.1	2350.6	7252.1	7127.1	7134.4	7051.7	1.2	1.1

76

Table 18: Frequency results (damaged beams): comparison analytical vs experimental (Hz), Timoshenko and Euler-Bernoulli beam theory; $\sigma = 1.81 \times 10^{-5}$, $\epsilon = 0.1$, $\Delta L_z = 0.05$, $e = 3.12$

Mode	Expt	EB	% error(EB)	TB	% error(TB)
1	25	24.7	1.20	23.8	4.80
2	155	157.3	1.48	154.4	0.39
3	420	435.9	3.79	415.5	1.07
4	801	870.3	8.66	865.7	8.07
5	1326	1406.3	6.06	1328.6	0.20

Euler-Bernoulli beam theory. For higher modes the differences increase. When Timoshenko beam theory results is used, the percentage error decreases substantially for all natural frequencies except the first. White noise was used as an excitation but for the first mode the mode shape obtained using white noise was not smooth therefore sinusoidal excitation was used at the peak for the first mode for the frequency response function as shown in figure 10. Therefore, there was decrease in the accuracy for measurements for the first mode. It can be concluded that the formulation presented is able to predict natural frequencies with fair accuracy.

7.2 Conclusions And Suggestions For Further Study

- An analytical framework to tackle problems of damaged elastic structures is used to compare results of Euler-Bernoulli and Timoshenko beam theories for damaged beams.

- The effect of rotational kinetic energy and shear deformation energy on natural frequencies is investigated for the two damage parameters ϵ and ΔL_z, which give the ratio of depth of damage to total depth of the beam and the ratio of the length of damage to total length of beam, respectively.

- As far as damage parameters are concerned, the theory is able to give values within 5% of those predicted by finite element models, for damage with depths 40% of the total depth of the beam and extent of damage $\Delta L = 0.1L$.

- The beam parameters σ and e, which denote slenderness ratio and ratio of the Young's

77

modulus to shear factor times shear modulus, respectively, are also studied. It was found that for the range of e between 2.8 and 3.4 ($\nu = 0.167, 0.417$) and for σ values that correspond to slenderness ratio up through $\frac{1}{3}$, the difference between the frequencies as given analytically and finite element models, was within 5%. The First seven natural frequencies are considered for comparison. Euler-Bernoulli beam theory is able to give a reasonable estimation for the first few frequencies.

- The changes in mass distribution (mass per unit length) due to damage, which has been neglected by most researchers until now has been incorporated. Its importance is demonstrated by showing that the effect is of the same order as the reduction in bending stiffness. This result is based on the consideration of first order effects in both mass and stiffness.

- A direct fallout of the study would be to study the accuracy of results for plate and shell structures. An interesting parameter that arises in the derivation is η_{nj}, which is the coefficient of eigenfunctions for the undamaged beam when used to find the particular solution for perturbed differential equations. The ability of the parameter to predict areas of damage should be investigated.

- The method presented used perturbation method, which led to discretization of the change due to the damage, as per the orders of perturbation. This discretization can be used to evaluate the desired accuracy and the required orders of perturbation for that accuracy.

Chapter VIII

MODEL DAMAGES TO KIRCHHOFF'S PLATE THEORY

In this chapter the model for damaged structures as presented in chapter 4 is used to obtain their vibration characteristics, is applied to plates. There are two inputs to the model, the damage model and the modes and natural frequencies of the undamaged structure. The damage model is presented for a damage of arbitrary shape and size. Examples of for four different types of damage are presented: a point damage, a line damage, a curvilinear damage and a two dimensional rectangular shaped area of damage. Although, the method is applicable to any arbitrary set of boundary conditions of a self-adjoint system, for plates only sets of boundary conditions that have at least two opposite edges simply-supported have been solved in the literature.

Modeling of damage in plate structures is mathematically more challenging than modeling it in beams. The first challenge, which is applicable to all the theories that have been used to model damage in beam structures, is the mathematical representation of the damage in two dimensions. The second challenge is particularly applicable to the method presented in this thesis. The method uses the modes of the undamaged structure to determine the modes and natural frequencies of the damaged structure. The modes of the undamaged plate structures for some boundary conditions is a challenging problem in itself, which may restrict the applicability of the theory presented.

8.1 Improvements to damage model

The problem of modeling of damage in two dimensional structures has been addressed in the paper by Sharma et al. [59]. However, there were some missing terms in the perturbed differential equations. The eigenvalue problem for the Kirchhoff's plate theory is given by equation (14) in the paper, which is reproduced below.

$$\nabla^2 D \nabla^2 \phi - (1-\nu)\left(\frac{\partial^2 D}{\partial x_2^2}\frac{\partial^2 \phi}{\partial x_1^2} - 2\frac{\partial^2 D}{\partial x_1 \partial x_2}\frac{\partial^2 \phi}{\partial x_1 \partial x_2} + \frac{\partial^2 D}{\partial x_1^2}\frac{\partial^2 \phi}{\partial x_2^2}\right) - m\lambda\phi = 0 \qquad (115)$$

The following substitutions are made using equations (11), (12), (15), and (16) as given in the paper, which are reproduced below.

$$\phi = \phi^0 - \epsilon\phi^1 \quad \lambda = \lambda^0 - \epsilon\lambda^1 \quad m = m_0(1 - \frac{\epsilon\gamma_D}{3}) \quad D = D_0(1 - \epsilon\gamma_d) \tag{116}$$

Upon substitution the first order perturbed differential equation is calculated to be

$$\nabla^2 D_0 \nabla^2 \phi^1 - (1-\nu)\left(\frac{\partial^2 D_0}{\partial x_2^2}\frac{\partial^2 \phi^1}{\partial x_1^2} - 2\frac{\partial^2 D_0}{\partial x_1 \partial x_2}\frac{\partial^2 \phi^1}{\partial x_1 \partial x_2} + \frac{\partial^2 D_0}{\partial x_1^2}\frac{\partial^2 \phi^1}{\partial x_2^2}\right) - m_0\lambda^0\phi^1 =$$
$$\nabla^2 D_0 \gamma_D \nabla^2 \phi^0 - (1-\nu)\left(\frac{\partial^2 D_0\gamma_D}{\partial x_2^2}\frac{\partial^2 \phi^0}{\partial x_1^2} - 2\frac{\partial^2 D_0\gamma_D}{\partial x_1 \partial x_2}\frac{\partial^2 \phi^0}{\partial x_1 \partial x_2} + \frac{\partial^2 D_0\gamma_D}{\partial x_1^2}\frac{\partial^2 \phi^0}{\partial x_2^2}\right)$$
$$- \frac{m_0\lambda^0\phi^0\gamma_D}{3} - m_0\lambda^1\phi^0 \tag{117}$$

The second term in the left hand side of the above equation is missing in the paper [59]. This error is corrected as shown in the derivation below. Other improvements are that frequency results are

1. Instead of only first order perturbed differential equation, n-th order perturbed differential equation are given.

2. Instead of a damage parallel to x and y axes only, analytical representation of a randomly oriented curvilinear damage is given.

3. The complementary solution not given in [59]. This is part of the solution is provided in this theory presented in this chapter.

4. The theory presented in this chapter is presented as an application to the the theory presented in chapter 4 rather than a stand alone theory as in [59].

5. The results obtained are compared with finite element based model. This has not been done in [59].

8.2   Application to plates

The general framework, to model damages in elastic structures which are self adjoint, to obtain eigenfunctions and eigenvalues correct through the nth order is presented in an earlier chapter 4. In the chapter, first the general eigenvalue problem to determine the mode shapes
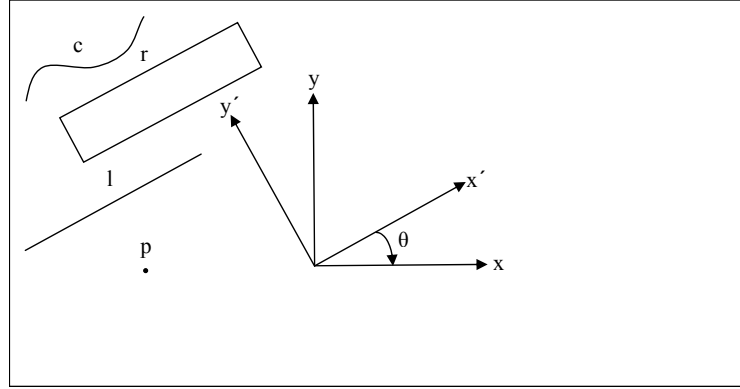
Figure 14: Different types of damage on a plate, p-point damage, l-line damage, c-curve shaped damage and r-a two dimensional rectangular shaped damage. The prime denotes the axes oriented in damage (damage axes) and x, y denote axes oriented in the plate along the sides of the plate.

and natural frequencies of elastic structures like rods, beams, plates and shells is given by equation (2). The equation consists of L as the stiffness operator, M as the mass operator, ϕ as the eigen function, and λ as the eigenvalue which may be used to find natural frequencies. For the Kirchhoff's plate theory L is a partial differential operator. The expressions for the eigenvalue equation are given in equation (5). Next, the general representation for boundary conditions is given by equation (7). The specific boundary conditions for Kirchhoff's plate theory for the three support conditions: clamped, simply-supported and free edges are given by equation (10)

8.2.1 Damage model

The next objective is to develop an accurate damage model to represent the damage mathematically. The purpose of these damage models is to obtain the damage profile functions; see equation (13). Several damage models for beams are given in the chapter in equations (14) to (17).

Four distinct types commonly occurring types of damage in plates are shown in figure 14. The damage profile functions for these types of damage are given next. The representation

81

for a rectangular cut and a point damage on the surface are given by

$$\gamma(x_1, y_1) = [H(x_1 - x_{1d}) - H(x_1 - x_{1d} - \Delta l_1)] [H(y_1 - y_{1d}) - H(y_1 - y_{1d} - \Delta l_2)]$$

$$\gamma(x_1, y_1) = \Delta l_1 \Delta l_2 \delta(x_1 - x_{1d}) \delta(y_1 - y_{1d}) \tag{118}$$

where Δl_i gives the width of the damage in the ith direction. Physically the most common type of damage is a crack. A straight line crack is mathematically represented by a pair of delta and Heaviside functions.

$$\gamma(x_1, y_1) = \Delta l_1 \delta(x_1 - x_{1d}) [H(y_1 - y_{1d}) - H(y_1 - y_{1d} - \Delta l_2)] \tag{119}$$

Alternatively a 2-dimensional crack is given by defining it vectorially as

$$\gamma(s)\hat{n} = f_1(s)\hat{i} + f_2(s)\hat{j} \quad \gamma(s)\hat{n} = s\hat{i} + (ms + c)\hat{j} \tag{120}$$

where $f_k(x_1, x_2)$, $k = 1, 2$ are arbitrary functions along the direction of unit vectors $\hat{i}$ and $\hat{j}$, and $\hat{n}$ is a unit vector along the curve. The second equation is an example for a straight line crack where m and c are the slope and y-intercept constants, associated with the straight line, respectively.

Once the damage profile functions are determined, the different geometric quantities such as area and area moment of inertia are determined to obtain different orders of stiffness and mass operators. These operators for plates are given as

$$L_{z_0} = \nabla^2\nabla^2 \quad M_{z_0} = 1 \quad M_{z_1} = \gamma_z(\zeta_1) \quad \lambda_z^i = \frac{\rho\lambda^i 12(1 - \nu^2)}{Eh^2} \quad \phi^i(x_1, x_2) = \frac{u_3(x_1, x_2)}{h}$$

$$L_{z_1} = \frac{\partial^2 M_2}{\partial x_1^2} - 2\frac{\partial^2 M_{12}}{\partial x_1 \partial x_2} - \frac{\partial^2 M_1}{\partial x_2^2} \quad M_1 = -3\gamma\left(\frac{\partial^2}{\partial x_2^2} + \nu\frac{\partial^2}{\partial x_1^2}\right)$$

$$M_{12} = -3\gamma(1 - \nu)\left(\frac{\partial^2}{\partial x_2 \partial x_1}\right) \quad M_2 = 3\gamma\left(\frac{\partial^2}{\partial x_1^2} + \nu\frac{\partial^2}{\partial x_2^2}\right) \tag{121}$$

In the above equations, M_{z_0}, M_{z_1}, L_{z_0}, L_{z_1} represent stiffness and mass operators and λ_{z_i} the non-dimensionalized eigenvalue. It should be noted that there are other representations possible, especially for L_{z_1}, however, the above representation was found to be well suited to represent the equations in weak form, since the boundary terms are easily visible and separated. Also, x_1 and x_2 are retained and are not non dimensionalized for ease of algebraic manipulation.

The next step is to perturb the eigenfunctions and eigenvalues as shown in equation. (26). This together with the damage model results in obtaining the perturbed differential equations as given by equations (28a) to (28d).

8.2.2 Perturbed equations and their solution

The characteristics of the perturbed differential equations are reproduced below.

1. Through the process of perturbation and by using the damage model, the homogeneous differential equation with variable coefficients is changed to a series of non-homogeneous differential equations with constant coefficients.

2. The first differential equation of this series is the same as that representing the eigenvalue problem for the undamaged case.

3. The remaining equations in the series of differential equations have the same homogeneous parts as those of the first equation and the undamaged case.

4. The unknowns for the nth order equation are the eigenfunction ϕ^n in the left hand side of the equation and the eigenvalue λ_z^n in the right hand side of the equation.

5. The layout of the nth order equation is given in a form so that the unknowns are given separately in individual terms. The second term in the right hand side involving λ_z^0 needs to be written separately to be able to write the unknown terms involving λ_z^0 in the left hand side. The third term in right hand side involving M_{z_0} is written separately to be able to use the orthogonality condition to simplify the final expression.

The next objective in the process is to solve the perturbed differential equations. The zeroth-order equation, which is the same as the equation for the undamaged case is solved using the procedure given by Magrab [43]. The same procedure is followed to solve the zeroth order equation which is also constitutes the homogeneous part of the higher order equations. If the plate is simply-supported in the x_1 direction and clamped in the x_2 direction, then the zeroth-order equation may be solved by using separation of variables.

83

Therefore, the eigenfunction is represented as

$$\phi^0(x_1, x_2) = X(x_1)Y(x_2) \quad X(x_1) = \sin(\gamma_m x_1) \quad 0 < x_1 < L_x \tag{122}$$

where L_x is the length of the plate in the x_1 direction and $\gamma_m = \frac{m\pi}{L_x}$. Then, the solution for $Y_m(x_2)$ is given by

$$Y_m(x_2) = C_{1_m} \cosh(\delta_m x_2) + C_{2_m} \sinh(\delta_m x_2) + C_{3_m} \cos(\epsilon_m x_2) + C_{4_m} \sin(\epsilon_m x_2)$$
$$\delta_m^2 = \Omega_m^2 + \gamma_m^2 \quad \epsilon_m^2 = \Omega_m^2 - \gamma_m^2 \quad \Omega_m^4 = \lambda_z^0 \tag{123}$$

The constants C_{i_m} are determined by applying the boundary conditions given by

$$Y(0) = Y'(0) = Y(L_y) = Y'(L_y) = 0 \tag{124}$$

Applying the boundary condition, $Y(x_2)$ is determined to be

$$Y(x_2) = C_{1_m} \left[\cosh(\delta_m x_2) + \frac{C_{2_m}}{C_{1_m}} \sinh(\delta_m x_2) - \cos(\epsilon_m x_2) + \frac{\delta_m C_{2_m}}{\epsilon_m C_{1_m}} \sin(\epsilon_m x_2) \right]$$
$$\frac{\delta_m C_{2_m}}{\epsilon_m C_{1_m}} = -\frac{\delta_m \sinh(\delta_m) + \epsilon_m \sin(\epsilon_m)}{\delta_m [\cosh(\delta_m) - \cos(\epsilon_m)]} = -\frac{\epsilon_m [\cosh(\delta_m) - \cos(\epsilon_m)]}{\epsilon_m \sinh(\delta_m) + \delta_m \sin(\epsilon_m)} \tag{125}$$

The characteristic equation is given by

$$2\epsilon_m \delta_m = (\epsilon_m^2 - \delta_m^2) \sinh(\delta_m) \sin(\epsilon_m) + 2\epsilon_m \delta_m \cosh(\delta_m) \cos(\epsilon_m) \tag{126}$$

A useful representation of the characteristic equation which makes finding the roots easier compared to the above equation is

$$\epsilon_m = n\pi + (-1)^n \zeta_{2_m} - \zeta_{1_m} \quad \sin(\zeta_{1_m}) = \frac{2\epsilon_m \delta_m \cosh(\delta_m)}{R} \quad \cos(\zeta_{1_m}) = \frac{(\epsilon_m^2 - \delta_m^2) \sinh(\delta_m)}{R}$$
$$\sin(\zeta_{2_m}) = \frac{2\epsilon_m \delta_m}{R} \quad R = \sqrt{4\epsilon_m^2 \delta_m^2 \cosh^2(\delta_m) + (\epsilon_m^2 - \delta_m^2)^2 \sinh^2(\delta_m)} \tag{127}$$

For the nth order equation the unknowns are ϕ^n and λ_z^n. $\phi^n = \phi^n|_{complementary} + \phi^n|_{particular}$. The particular part of the solution is expanded in terms of the modes of the undamaged structure using expansion theorem $\phi_k^n|_{particular} = \sum_{p=1}^{\infty} \eta_{kp}^n \phi_p^0$. This implies $\phi^n|_{complementary} = \phi^0$. The solution procedure to the nth equation is given in the chapter 4. In the same chapter the first order correction to natural frequencies is given by

$$\lambda_{z_n}^1 = \frac{\alpha_{1_{nn}} - \lambda_{z_n}^0 \beta_{1_{nn}}}{C_n} \tag{128}$$

84

where

$$\int_0^1 (\phi_m^0)^T M_{z_0} \phi_n^0 d\zeta_i = \delta_{mn} C_m = \delta_{mn} C_n \quad \int_0^1 (\phi_m^0)^T L_{z_0} \phi_n^0 d\zeta_i \;\; = \delta_{mn} \lambda_m C_m = \delta_{mn} \lambda_n C_n$$

(129)

where δ_{mn} is the Kronecker delta. Notice the orthogonality condition does not hold for M_{z_j} and L_{z_j} where $j \geq 1$. For those cases the following notations would be used to represent the equations compactly

$$\int_0^1 (\phi_m^0)^T L_{z_1} \phi_n^0 dx_i = \alpha_{1mn} \quad \int_0^1 (\phi_m^0)^T M_{z_1} \phi_n^0 dx_i = \beta_{1mn}$$

(130)

As detailed in the solution procedure of undamaged plates, in the above equations $m = rs$ and $n = pq$ where r, s, p, and q are integers. Computation of the energy equivalent inertia loss due to damage is straight forward, however energy equivalent stiffness loss due to damage involves representation of equation (130) using L_{z_1} from equation (121) and converting it into weak form to give

$$\alpha_{1mn} = \int_0^{L_{x_i}} (\phi_{m,x_1 x_1}^0)^T 3\gamma \phi_{n,x_1 x_1} + \nu (\phi_{m,x_1 x_1}^0)^T 3\gamma \phi_{n,x_2 x_2} + 2(1-\nu)(\phi_{m,x_1 x_2}^0)^T 3\gamma \phi_{n,x_1 x_2} +$$

$$(\phi_{m,x_2 x_2}^0)^T 3\gamma \phi_{n,x_2 x_2} + \nu (\phi_{m,x_2 x_2}^0)^T 3\gamma \phi_{n,x_1 x_1} dx_i \quad \beta_{1mn} = \int_0^1 (\phi_m^0)^T \gamma \phi_n^0 d\zeta_i$$

(131)

8.2.3 Coordinate axes difference effects

The integrals in the above equations are be written as $\int \gamma(x_1', x_2') f(x_1, x_2)$. As given in the section 8.2.1 about damage model, the axes in which the damage is defined and those in which the plate is defined may be different. There are two options for calculation of energy equivalent inertia and energy equivalent stiffness loss due to damage, one, change the damage coordinates in which the function γ is defined to plate coordinates or vice versa. Both will yield the same results since integrals are independent of the coordinates. The authors are of the opinion changing the plates coordinates of the function f will yield simpler computations, since the function γ consists of discontinuous functions like Heaviside functions or delta function. For curvilinear thin cracks this problem does not happen as long as the curve is defined as in equations (120). The integral can then be computed using $\int_{s_i}^{s_f} f[x_1(s), x_2(s)] \,|\, \frac{d\gamma}{ds} \,|\, ds$, s_i and s_f are the start and end points on the damage curve.

85

Table 19: Natural frequencies (Hz): plates pinned at all boundaries, with damage along x axis. $L_x = 1.5$m, $L_y = 1.0$m, $E = 71$Gpa, $\rho = 2700$kg/m^3, $\nu = 0.3$, $\epsilon = 0.1$, $h = 0.01$m

Mode(i,j)	FEA (U)	Anal(U)	FEA (D)	Anal (D)	% Diff (U)	% Diff (D)
1,1	35.093	35.210	34.511	35.070	0.33	1.62
1,2	67.453	67.710	66.430	67.430	0.38	1.51
1,3	121.49	121.88	119.66	121.52	0.32	1.55
1,4	197.13	197.71	194.00	197.33	0.29	1.72
2,1	108.11	108.34	106.42	106.88	0.21	0.43
2,2	140.26	140.84	138.08	136.31	0.41	-1.28
2,3	194.03	195.00	191.09	187.63	0.50	-1.81
2,4	269.42	270.84	265.42	261.42	0.53	-1.51
3,1	229.69	230.21	225.50	229.13	0.23	1.60
3,2	261.70	262.72	257.65	258.89	0.39	0.48

8.3   Results

Analytical (Anal) and Finite Element (FEA) results using Kirchhoff's plate theory in Table 19. In the table $L_x = 1.5$ m, $L_y = 1.5$ m, $E = 71$ Gpa, $\rho = 2700$ kg/m^3, $\nu = 0.3$, $\epsilon = 0.1$, $h = 0.01$ m. The damage is along x axis, located at 0.25 m either side of the center of plate. The plate was pinned at all boundaries. Two layers of $3 - D$ tetrahedral elements were used with in plane size about 0.02 and transverse size 0.005 to keep the aspect ratio below $1 : 4$. For the damaged plate, the depth of damage was kept to be 0.001m so that $\epsilon = 0.1$. Boundary along the damage was meshed at 0.004 m in plane, to again keep the aspect ratio below $1 : 4$. The damage had to be given a breath too (along y axis). This was kept to be at a minimum of 0.002 m.

8.4   Conclusions

- The results given in Table 19 show that the frequencies predicted by the theory are within an accuracy of 2% for the damaged case.

- The theory yields an analytical model with potential to be able model arbitrary shaped areas of damage on plates.

- The veracity of the framework presented in chapter 4 is shown for Kirchhoff's plate theory.

86

PARTIAL MODE CONTRIBUTION METHOD

A new physical parameter is presented and it is applied to damage detection. It addresses the two main challenges in the field of vibration based structural health monitoring, the sensitivity of detection and the requirement of data from baseline state. The parameter is also shown to be not affected by noise in the the detection ambience. Assuming the damaged structure to be a linear system the response can be expressed as the summation of the responses of the corresponding undamaged structure and the response (negative response) of the damage alone. If the second part of the response is isolated, it forms what can be regarded as the damage signature. Damage signature gives a clear indication of the damage. In this chapter the occurrence of damage signature is investigated when the damaged structure is excited at one of its natural frequencies, and is called partial mode contribution. The existence of damage signature as partial mode contribution is first ascertained using analytical derivation, thereupon it is ascertained using finite element models and experiments. The limits of damage size that can be determined using the method are also investigated.

9.1   Introduction

With that background, the main contribution of this portion of the thesis is; alleviating the of the lack of sensitivity of vibration based techniques by presenting a new physical quantity, which gives accurate estimation of areas of damage by making the damage detection parameter solely dependent on the damage. This is achieved by first expressing the response of the damaged structure as a linear combination of the sum of the responses of the undamaged part of the damage structure and the response due to damaged part of the damaged structure. Subsequently, the part of the response due to the damage of the structure alone 'damage signature' is isolated to give information regarding the location of damage. The technique is applied to the free vibration modes (the term vibration modes

87

is used to signify the displacement mode, sectional rotation mode or any of sectional strain modes (bending and shear)) of the damaged structure. The free vibrations modes of the damaged structure are expanded, using the undamaged modes of the structure, as the basis functions as shown below,

$$\mu_d^i = \chi\mu_{ud}^i + \sum_{j=1,j\neq i}^{\infty} \xi_{ij}\mu_{ud}^j = R_1(x) + R_2(x) \quad \chi < 1, \quad \chi >> \eta_{ij} \tag{132}$$

where μ is the mode shape, the subscript d denotes damaged and ud denotes undamaged, χ and ξ are numerical factors. Then, the second part of the response ($R_2(x)$) gives the "damage signature". Damage signature has a definitive spike at the damage location as it exist entirely due to the damage. In this case, the damage signature arises due to partial mode contribution of the damaged structure and hence the method is called 'Partial Mode Contribution Method'. In this chapter partial mode contribution is used to identify the damage.

An important word of caution is that $R_2(x)$ is not the difference between the mode shape of the undamaged and damaged structure. Mathematically the difference between the two is given by

$$(1-\chi)\mu_{ud}^i - \sum_{j=1,j\neq i}^{\infty} \xi_{ij}\mu_{ud}^j \quad (1-\chi) >> \xi_{ij} \tag{133}$$

Such a difference would be composed of a constituent of the main undamaged mode $(1-\chi)\mu_{ud}^i$, which is sometimes large enough to mute out any damage indication expressed by $R_2(x)$. This explains the lack of sensitivity of vibration based damage detection methods, which were based on the difference between normalized modes of damaged and undamaged structures. Not requiring the response of the undamaged structure also removes the limitation of current damage identification techniques that require it.

9.2 Verification

The equation (44) in chapter 4, which gives the solution of the nth order mode shape, and equation (82), which gives the perturbation equation of mode shape, can be combined to

obtain the mode shape for the damaged beam.

$$\phi_k = \phi_k^0 + \sum_{n=1}^{\infty} \epsilon^n \left(\phi_k^0 + \sum_{p=1,p\neq k}^{\infty} \eta_{kp}^n \phi_p^0 \right) \tag{134}$$

$$\phi_k = \frac{1}{1-\epsilon}\phi_k^0 + \sum_{n=1}^{\infty} \epsilon^n \left(\sum_{p=1,p\neq k}^{\infty} \eta_{kp}^n \phi_p^0 \right) \tag{135}$$

The analytically derived equation (134) and theoretically reasoned equation (132) are of the same form. Comparing equations (134) and (132) one gets $\mu_d^i = \phi_k$, $\mu_{ud}^i = \phi_k^0$ the values obtained for χ and ξ are

$$\chi = \frac{1}{1-\epsilon} \qquad \xi_{kp} = \left(\sum_{n=1}^{\infty} \epsilon^n \eta_{kp}^n \right) \tag{136}$$

Hence, the theoretical assertion of the introduction section is verified by the rigorous analytical derivation presented in chapter 4.

9.3   Results

9.3.1   Experimental results

In the chapter 6 experimental validation was done for mode shapes and natural frequencies of damaged beams using Euler-Bernoulli beam theory. The same experimental setup and readings are used here to verify the existence of 'damage signature' as partial mode contribution and its ability to identify the damage. It is also verified that partial mode contribution is more sensitive to damage identification than the displacement or curvature mode shapes for the damaged beam, or the difference between normalized displacement or curvature mode shapes of the damaged and the undamaged beams. The effect of noise on detection of damage is also studied.

The experimental process can be referenced in chapter 6. First four modes are used to detect the damage for this beam. The noise in the measurement ambience is different for different modes as can be seen from the experimental data plots of mode shapes in figure 15. The modes shapes in order of increasing noise are 4th, 2nd, 1st and 3rd. As found by other researchers [53], the first mode is found to contain high ambient noise. The third mode natural frequency coincides with one of the harmonics of the power supply ($420Hz$)

and hence has high amount of ambient noise. These modes are not neglected because the actual measurements in the field may have data with high ambient noise.

In the figure 15, the experimental data for mode shapes of damaged beam, curve-fitted experimental data using the modes of undamaged beam, and analytical modes of the damaged and undamaged beams are shown for mode numbers 1 to 4. In figure 16, the experimental curvature shape for undamaged beam, experimental curvature for damaged beam and analytically derived curvature for damaged and undamaged beam, is shown. All the mode shapes and curvature shapes are normalized such that the maximum value is one. It is seen that both the displacement mode shapes given in figure 15 and curvature mode shapes given in figure 16, are similar and damage cannot be ascertained by looking at the mode shapes.

Next in figure 17, the damage is ascertained using the difference between the normalized displacement and curvature mode shapes for the damaged and undamaged cases . Difference between normalized modes is plotted for: the experimental displacement of damaged beam and the analytical displacement of undamaged beam, the experimental displacement of damaged beam and the experimental displacement of undamaged beam, the analytical displacement of damaged beam and the analytical displacement of undamaged beams, the experimental curvature of damaged and the analytical curvature of undamaged beam, the experimental curvature of damaged and the experimental curvature of undamaged beam and the analytical curvature of damaged and the analytical analytical curvature of undamaged beams.

The resulting curves are normalized such that the maximum value is one. The peaks are used to determine the position of damage. The difference between the displacement and curvature mode for the damaged and undamaged beams for the analytical case give the damage location correctly. Among other curves the difference between experimentally observed curvature of the damaged beam and analytically obtained curvature of the undamaged beam is able to predict the damage location correctly for the first three mode shapes. The difference between experimentally observed displacement modes and curvature modes of the damaged and undamaged cases is not able to give correct location of damage.

90

The difference between experimental displacement mode and analytical displacement mode is able to give the location of damage only for the third mode shape. Based on the above observations, it is concluded that although difference between analytical mode shape give the location of damage but this observation is not corroborated experimentally. The reason for that is that the change in mode shapes due to small defects is extremely small, even slight amount of numerical errors or experimental noise can compensate this change, and hence not give the damage information. It is also seen that among the cases considered the best results are for difference between experimental curvature for the damaged beam and analytical curvature for the undamaged beam.

Next, the partial mode contribution is shown in figure 18. Four cases are considered: partial mode contribution for displacement and curvature modes of damaged beams for the experimental data and those for the analytical plots. The partial mode contribution for the analytical displacement and the curvature mode shapes of damaged beams give a sharp peak at the damage location. Similarly, the partial mode contribution for the experimental data give sharp peaks at the damage location for all the curvature shapes. For the case of displacement mode shapes, modes one, three and four are able to correctly identify the damage. Therefore, it can be concluded that the partial mode contribution can be effectively used to detect the position of damage. It is especially sensitive in the curvature mode shapes of damaged beams. The noise in the case of mode shapes 1 and 3 did not have an effect on determining the damage position. This was because mode shapes do not have a magnitude. In the case of random and unbiased noise for every deviation on one side there would be a corresponding compensating deviation on the other side such that the partial mode contribution integrity was maintained. In case of random biased noise, the mode shape would be shifted uniformly up or down, again maintaining the integrity of the shape. However, in the case of a damage there is local deviation that is neither compensated nor globally uniform, and hence a parameter which can detect this local change in mode shape would be able to identify the damage. This is true in the case of partial mode contribution.
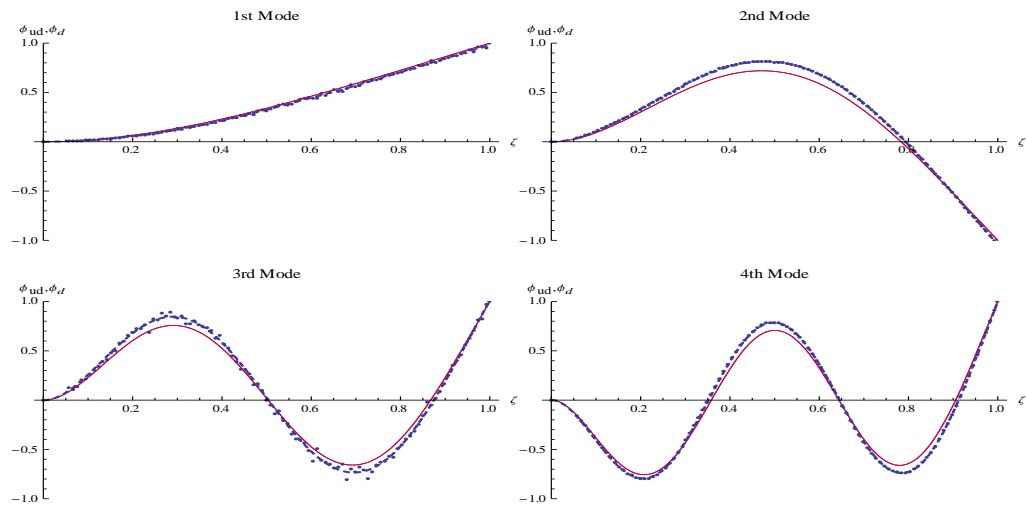
91

Figure 15: Displacement mode shapes (normalized): experimental damaged mode (dots), experimental data curve-fitted using undamaged modes (dashed), analytical undamaged mode (red), analytical damaged mode (blue)
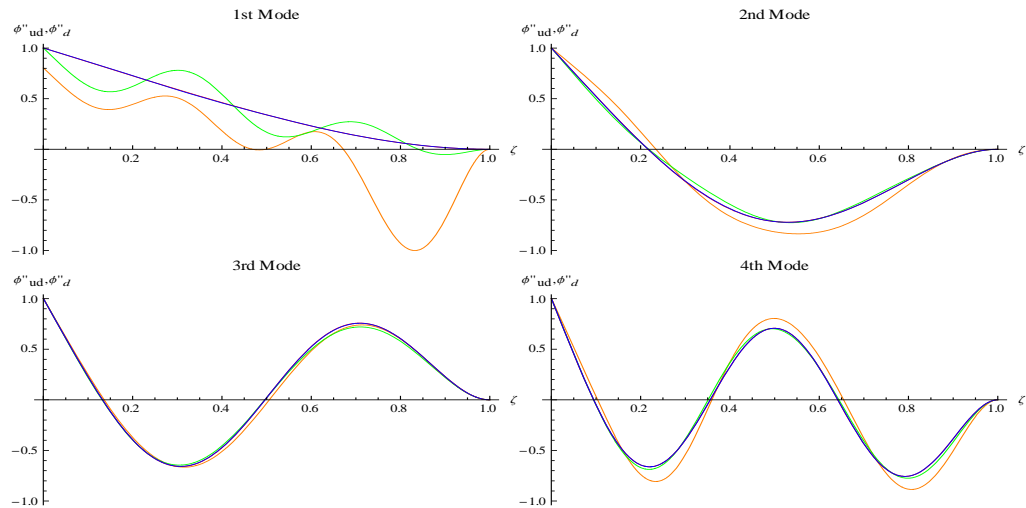

Figure 16: Curvature shapes (normalized): experimental undamaged curvature (orange), experimental damaged curvature (green), analytical undamaged curvature (red), analytical damaged curvature (blue)
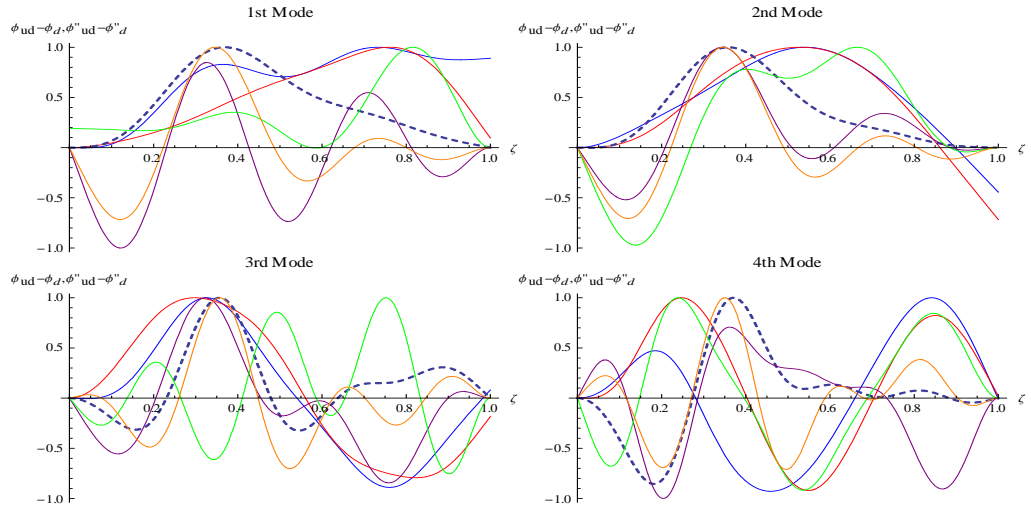
92

Figure 17: Normalized difference between normalized damaged and undamaged, mode shapes and curvature shapes: experimental-analytical mode (blue), experimental-experimental mode (red), analytical-analytical mode (dashed), experimental-analytical curvature (purple), experimental-experimental curvature (green), analytical-analytical curvature (orange)
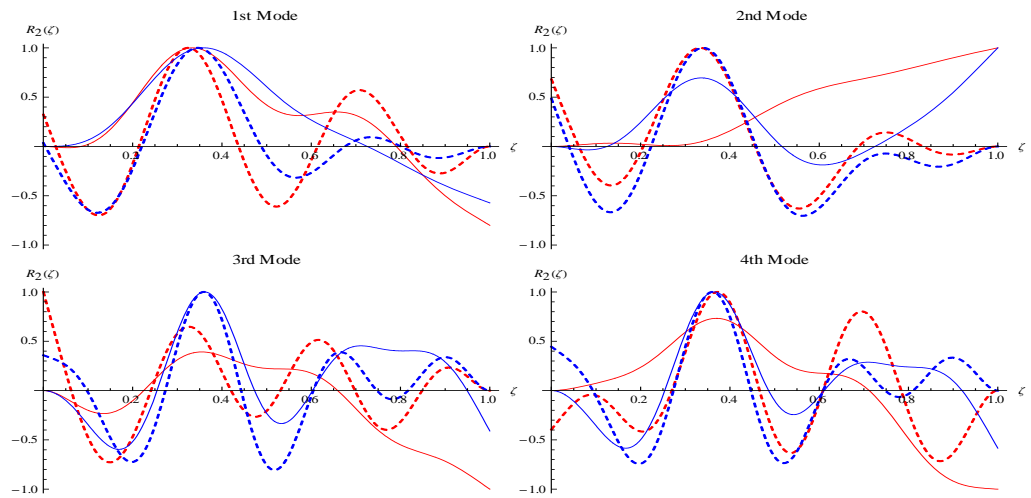
Figure 18: damage signature (normalized partial mode contribution): experimental (red), analytical (blue), displacement mode (solid line), curvature mode (dashed line)

9.3.2 Finite element model results

The validity of the method is illustrated for different boundary conditions and also the relative sensitivity of the displacement mode shapes versus curvature mode shapes is assessed using finite element method. A beam with three different boundary conditions modeled in abaqus using two dimensional plane stress elements is used for the purpose. The beams were modeled using Abaqus software. The length of the beam was 1 m, the cross sectional dimensions were 0.02 m and 0.0201 m, respectively, the density was 7890 kg/m^3, Young's modulus $E = 210GPa$ and poisson's ratio $\nu = 0.3$. The slight change in the cross sectional dimensions was necessitated to remove the coupling of modes in the two bending directions.

The curves of the damaged beam displacement and curvature mode shapes were normalized such that the maximum value is one. The curves were subsequently curve-fitted using modes of the undamaged beam for the same boundary condition. The effect of the main mode (the mode which contributed the most to the curve-fitted data) was zeroed out. The plots for the contribution of rest of the undamaged modes to the curve-fitted damaged mode is given in figure 19. Since the modes shapes have been normalized, the sensitivity of different modes can be determined. It is seen that curvature shapes are more sensitive by an order of magnitude compared to displacement mode shapes, but they also have a higher number of oscillations. The same sensitivity is shown for mode shapes 1 and 2 when comparing displacement mode shapes with displacement mode shapes and curvature mode shapes with curvature mode shapes for different boundary conditions.

9.3.3 Analytical results

The range of valid values for different damage parameters like location of damage ζ_d, depth of damage ϵ and width of damage ΔL_z is explored in this section. The modes used are derived using the analytical derivation, developed in the previous chapter. Beams with four different boundary conditions, simply-supported, clamped-free, clamped-clamped and propped-cantilever are considered. For all the plots the damage parameters are $\zeta_d = 0.35L$, $\epsilon = 0.1$, $\Delta L_z = 0.01$. First, in figure 20, the normalized modes of damaged beam using the analytical expressions correct up to first order are given along side the normalized
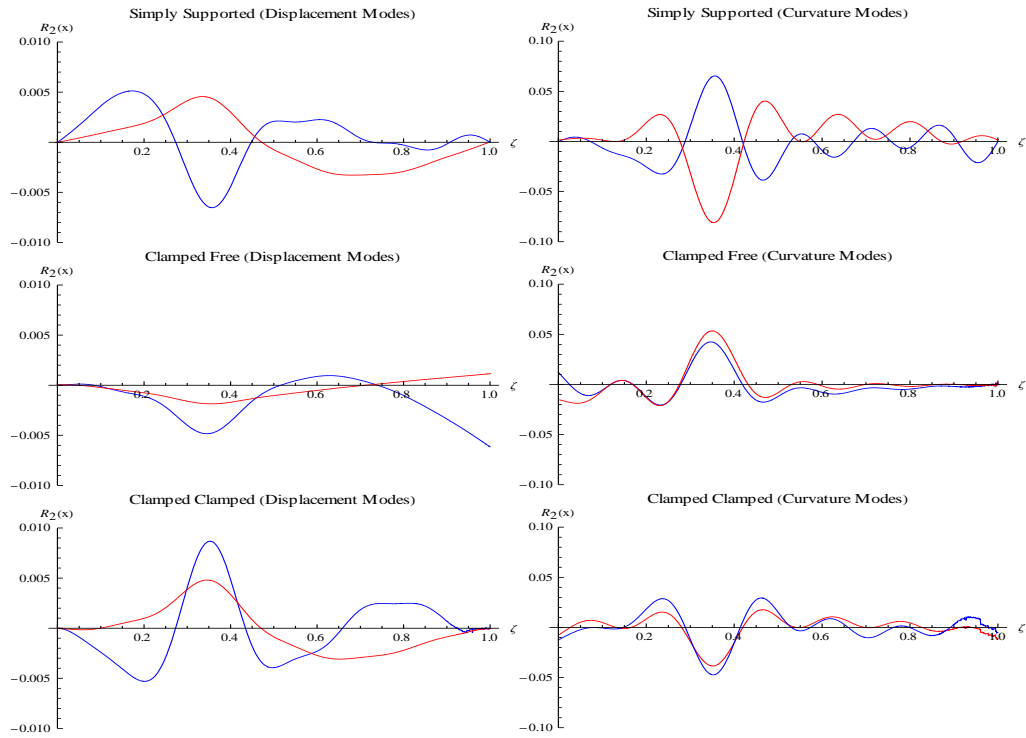
94

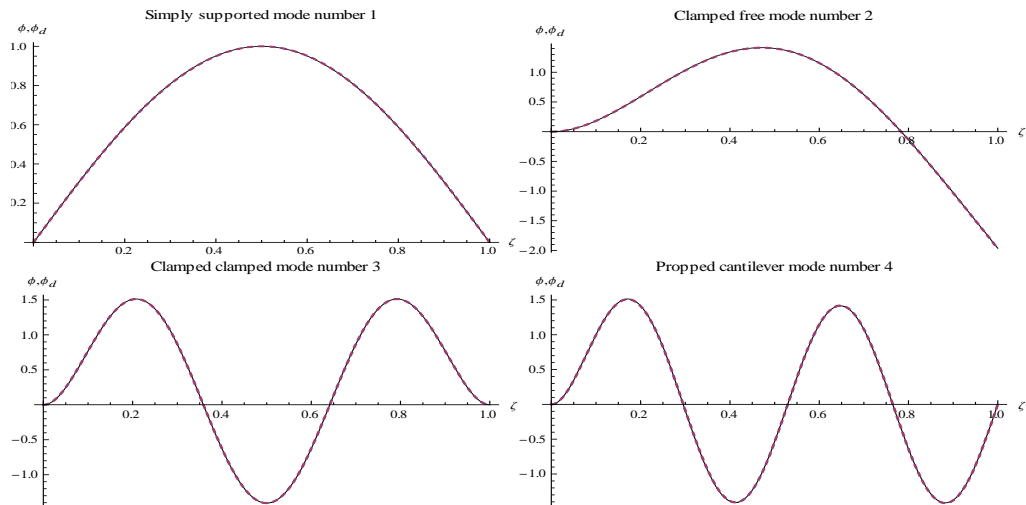**Figure 19:** Damage signature of normalized modes and curvatures, mode 1 (red), mode 2 (blue)

Figure 20: Damaged (dashed lines) and undamaged (continuous lines) beam mode shapes; $\zeta_d = 0.35$, $\epsilon = 0.1$, $\Delta L_z = 0.01$
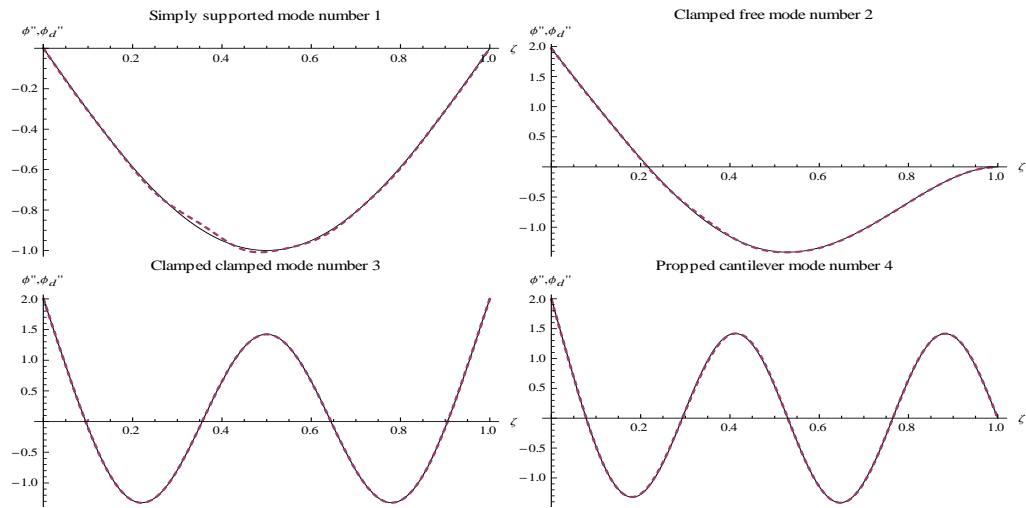
95

Figure 21: Damaged (dashed lines) and undamaged (continuous lines) beam curvature shapes; $\zeta_d = 0.35$, $\epsilon = 0.1$, $\Delta L_z = 0.01$
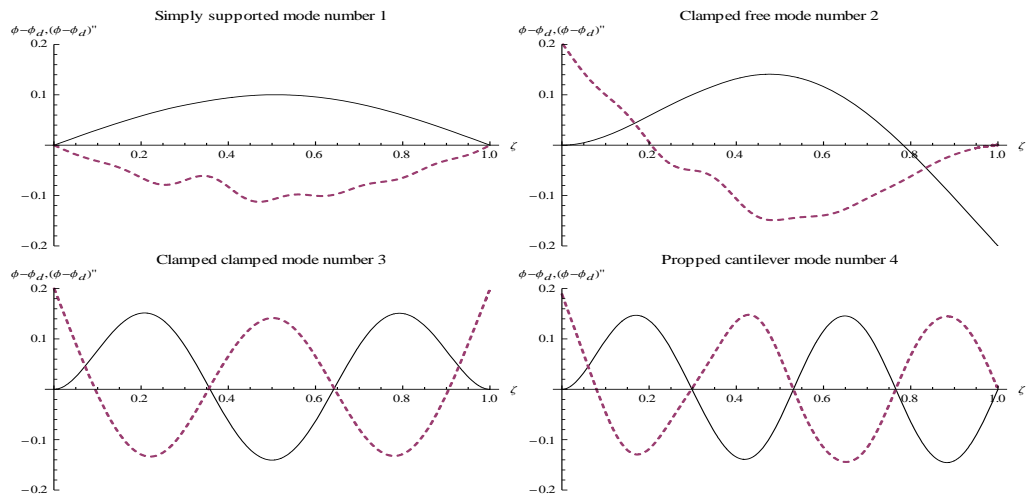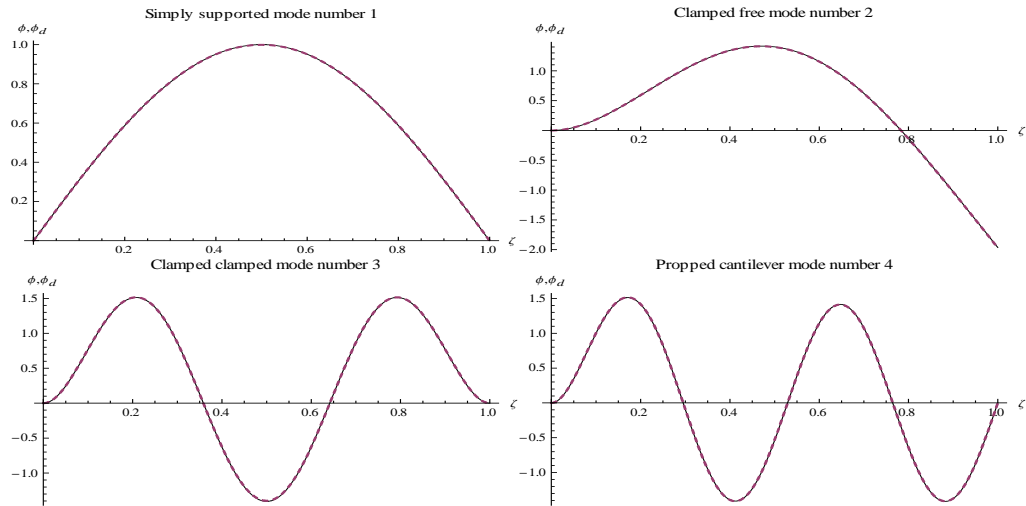

Figure 22: Difference between damaged and undamaged beam, normalized, mode shape (continuous lines) and curvature shape (dashed lines); $\zeta_d = 0.35$, $\epsilon = 0.1$, $\Delta L_z = 0.01$

96
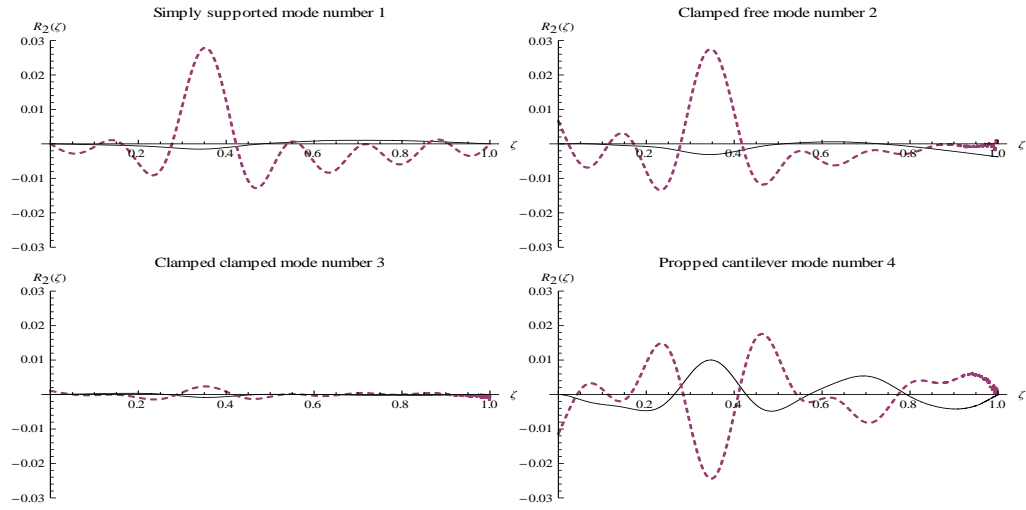
Figure 23: Partial mode contribution, mode shape (continuous lines) and curvature shape (dashed lines); $\zeta_d = 0.35$, $\epsilon = 0.1$, $\Delta L_z = 0.01$; first twelve modes considered

Figure 24: Damaged (dashed lines) and undamaged (continuous lines) beam mode shapes; $\zeta_d = 0.5$, $\epsilon = 0.1$, $\Delta L_z = 0.01$

97
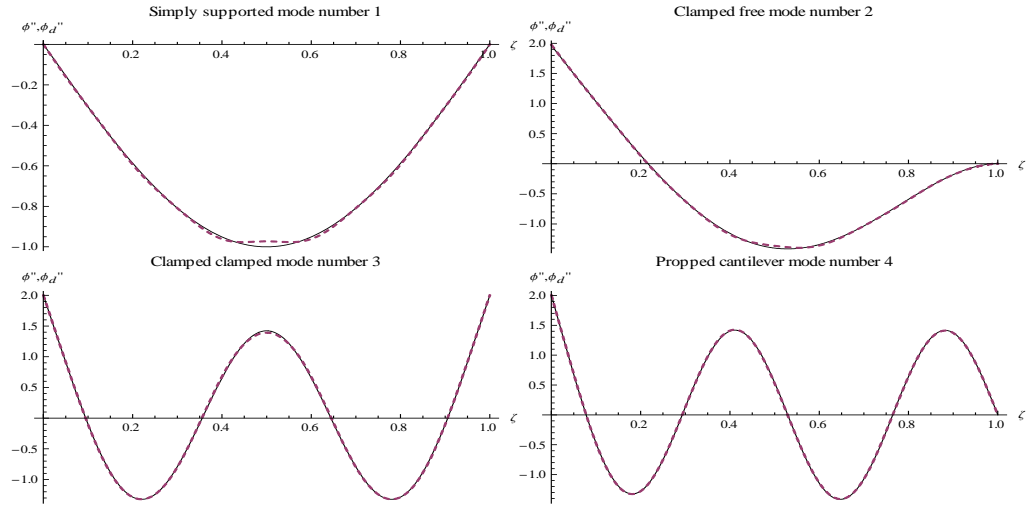
Figure 25: Damaged (dashed lines) and undamaged (continuous lines) beam curvature shapes; $\zeta_d = 0.5$, $\epsilon = 0.1$, $\Delta L_z = 0.01$

modes of undamaged beams. The first set of modes is given for simply-supported, second set for clamped-free, third set for clamped-clamped, and fourth set for propped-cantilever boundary conditions, respectively. Similarly in figure 21, the normalized curvature shapes are given (same modes and same beams) for damaged and undamaged beams. Since Euler-Bernoulli beam theory is considered, hence the plots are the same for any material or geometric characteristics of the beam. However, that would not be the case if Timoshenko beam theory is used. It is seen that mode profiles of damaged and undamaged beams are similar and the damage cannot be identified just by looking at the mode profiles. Only the first curvature mode of damaged case for simply-supported boundary condition, shows a deviation from curvature mode shape of the undamaged case at the damage location.

Next, in figure 22 the difference of the normalized mode and the curvature shapes of damaged and undamaged beam is given. The damage location can be identified only for mode number one for simply-supported, and mode number two for clamped-free boundary conditions, respectively. Damage cannot be identified for mode three and mode four for clamped-clamped and propped-cantilever case, respectively. Figure 23 gives the plot of $R_2(x)$ as defined in equation (132) for the mode shape and curvature shape. For example, for the 2nd mode of damaged beam it gives the contribution of all the modes of undamaged

beam other than the 2nd mode when using them to curve-fit the 2nd mode of the damaged beam. Mode shapes up to the 12th mode are considered. Damage is identified for all the mode shapes for all the different boundary conditions. The spike at the damage location is muted in case of displacement modes but pronounced in case of curvatures. It is seen that, different modes (curvature and displacement) for different beams are excited to varying amounts at the damage location, but all modes show clear indication of damage.

To study the phenomenon further, parametric studies are performed on different damage parameters. Since Euler-Bernoulli beam is considered, the only parameters effecting the mode shapes are the three damage parameters, the location of damage ζ_d, the depth of damage ϵ and the extent of damage ΔL_z. First set of plots are given for the location of damage at $\zeta_d = 0.5$ and $\zeta_d = 0.7$. The case of $\zeta_d = 0.35$ has already been considered in the plots given in figures 20-23. The rest of the parameters remain the same as earlier i.e. $\epsilon = 0.1$ and $\Delta L_z = 0.01$. The mode shapes for the first case are given in figure 24, curvature shapes in figure 25, difference of normalized modes in figure 26 and partial mode contribution ($R_2(x)$) in figure 27. Similarly for the second case $\zeta_d = 0.7$, the plots are given in figure 28 for mode shapes, figure 29 for curvature shapes, figure 30 for the difference between normalized modes and figure 31 for the partial mode contribution. The observations from the figures are on similar lines as from the first set of figures 20, 21, 22 and 23, i.e., none of the three quantities the mode shapes, or the curvature shapes or the difference between normalized modes and curvature shapes are able to identify the damage for the four kinds of beams considered. However, the 'damage signature' in the form of partial mode contribution is able to identify the damage for all the twelve cases considered.

The next damage parameter considered is ϵ that gives the ratio of the depth of damage to the total depth of the beam. Two cases are considered $\epsilon = 0.01$ and $\epsilon = 0.4$ along with the one already considered before that of $\epsilon = 0.1$. The plots for the mode shapes are similar to those for the figure 20 so they are not given again. The curvature shapes for the case $\epsilon = 0.01$ are again similar to that for figure 21. However, when the damage depth increases to $\epsilon = 0.4$, there is more clear indication of damage location in the curvature mode shape for the mode one of simply-supported, and mode two of clamped-free beams. The damage

was still not identified using the curvature shapes for clamped-clamped case and propped-cantilever case. The plots for curvature shapes for $\epsilon = 0.4$ is given in figure 34. The modal difference for the normalized modes is given in figures 32 and 35 for the cases $\epsilon = 0.01$ and $\epsilon = 0.4$, respectively. In the former, the damage location is less marked for the simply-supported and clamped-free boundary condition cases but it is still distinguishable. The damage location is again not identified for both clamped-clamped and propped-cantilever cases for both the ϵ values considered. The damage signature plots are presented in figures 33 and 36. The damage location is clearly identified for all the cases.

The change in the scale of both the modal difference and damage signature plots for the case of $\epsilon = 0.4$ should be noted. It changes from 0.2 to 0.7 for the modal difference plots because the modal difference increases between the modes of damaged and undamaged beams. However, there was no corresponding positive effect on the damage identification. It changed from 0.03 to 0.1 for the damage signature plots. There was positive effect on damage identification in these cases, since the peaks became of higher magnitude.

The last damage parameter i.e. the extent of damage is investigated next. The two cases considered are for $\Delta L_z = 0.001$ and $\Delta L_z = 0.1$ along with the case $\Delta L_z = 0.01$ considered earlier. The mode shapes are similar in characteristics to the plots in the figure 20 for both the cases. The curvature shape too has same characteristics for the case of $\Delta L_z = 0.001$. However, for the case of $\Delta L_z = 0.1$ the damage is more prominently identified. The curvature shapes for $\Delta L_z = 0.1$ are given in figure 39. The modal difference plots are given in figures 37 and 40. None of the four modes are identified the damage for the first case $\Delta L_z = 0.001$. For the second case $\Delta L_z = 0.1$, the peaks becomes sharper for the first mode of the simply-supported case, and the second mode of the clamped-free case. The third mode with clamped-clamped boundary condition still does not give any indication of damage. An important feature is that the propped-cantilever mode 4 gives an incorrect indication for the location of damage.

The plots giving the damage signature are given in figures 38 and 41. The y-axis range for the plots is increased from 0.03 to 0.3 to be able to see the peaks clearly for the case when $\Delta L_z = 0.1$. Unlike the normalized modal difference plots, the damage can still be
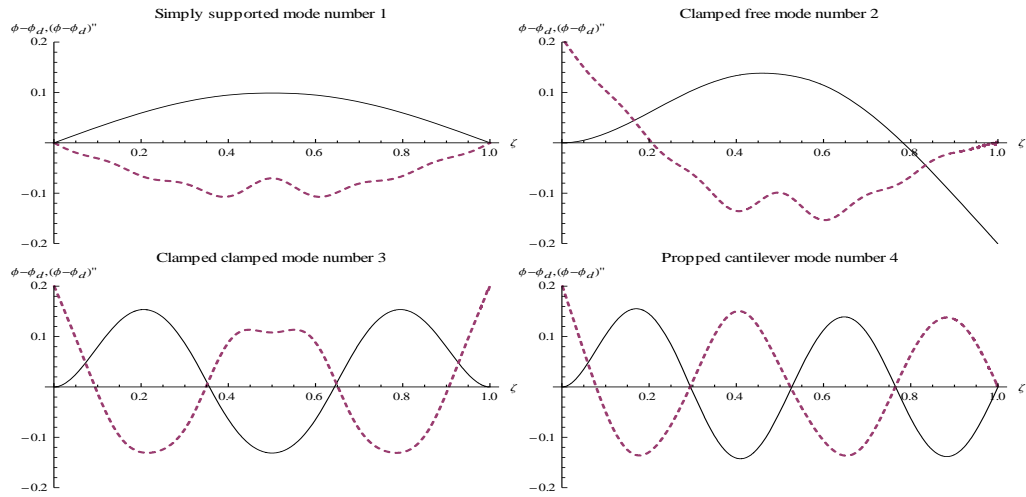
100

Figure 26: Difference between damaged and undamaged beam, normalized, mode shape (continuous lines) and curvature shape (dashed lines); $\zeta_d = 0.5$, $\epsilon = 0.1$, $\Delta L_z = 0.01$

identified for the case of $\Delta L_z = 0.001$, although the peaks are diminished. Also, unlike the normalized modal difference plots, there are no false damage locations identified.

9.4 Conclusions

- A new physical quantity, damage signature expressed as 'partial mode contribution' is physically explained in the introduction, equation (132), and verified by the analytical derivation, as given by equation (136). An application of partial mode contribution, to damage identification in the field of SHM is presented.

- The method outlined was able to address the two challenges in the field of vibration based SHM, that of

  1. sensitivity, since the presented quantity, partial mode contribution was shown to be more sensitive than existing physical quantities like displacement mode shapes, curvature mode shapes and difference of normalized displacement or curvature shape between damaged and undamaged states of the beam. The sensitivity was maintained even for mode shapes which had experimental noise. Also the sensitivity was uniform when mode shapes were compared for different boundary conditions.
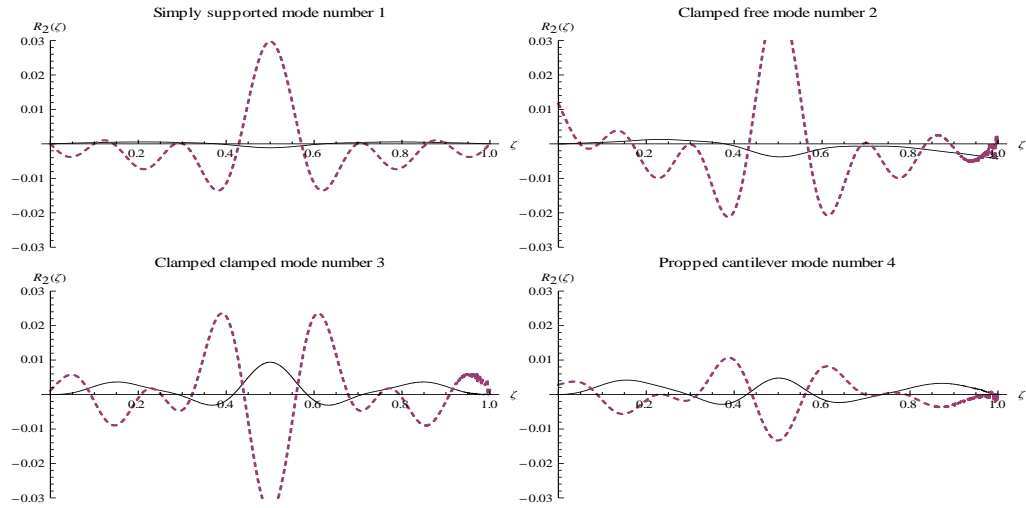
101

Figure 27: Partial mode contribution, mode shape (continuous lines) and curvature shape (dashed lines); $\zeta_d = 0.5$, $\epsilon = 0.1$, $\Delta L_z = 0.01$; first twelve modes considered
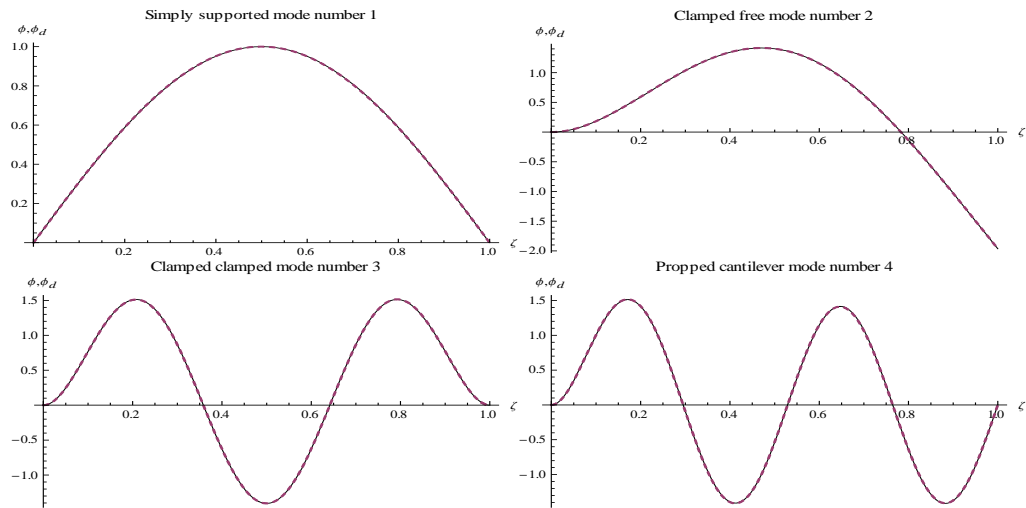

Figure 28: Damaged (dashed lines) and undamaged (continuous lines) beam mode shapes; $\zeta_d = 0.7$, $\epsilon = 0.1$, $\Delta L_z = 0.01$
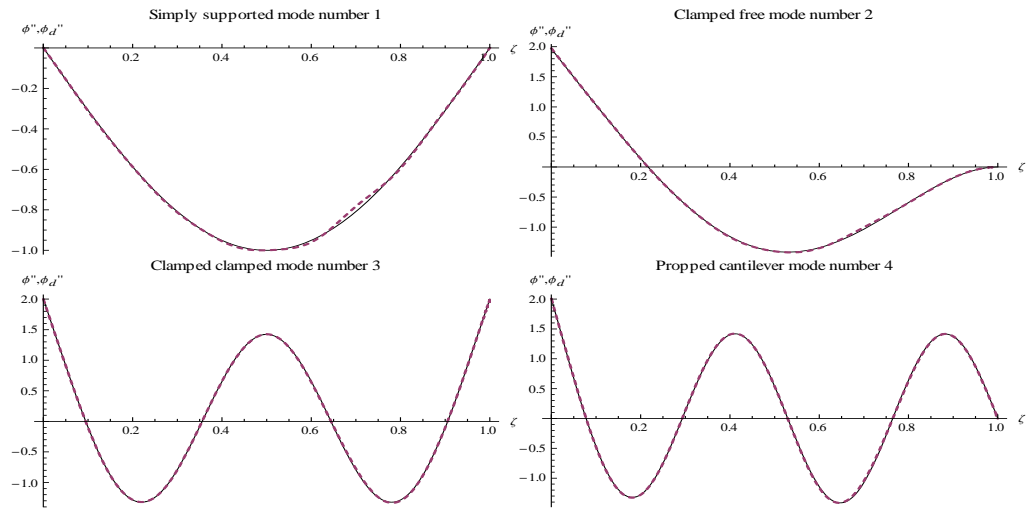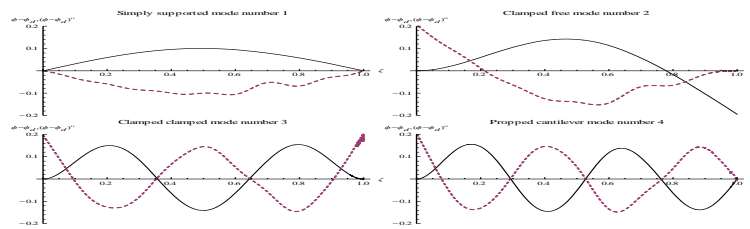
Figure 29: Damaged (dashed lines) and undamaged (continuous lines) beam curvature shapes; $\zeta_d = 0.7$, $\epsilon = 0.1$, $\Delta L_z = 0.01$

Figure 30: Difference between damaged and undamaged beam, normalized, mode shape (continuous lines) and curvature shape (dashed lines); $\zeta_d = 0.7$, $\epsilon = 0.1$, $\Delta L_z = 0.01$
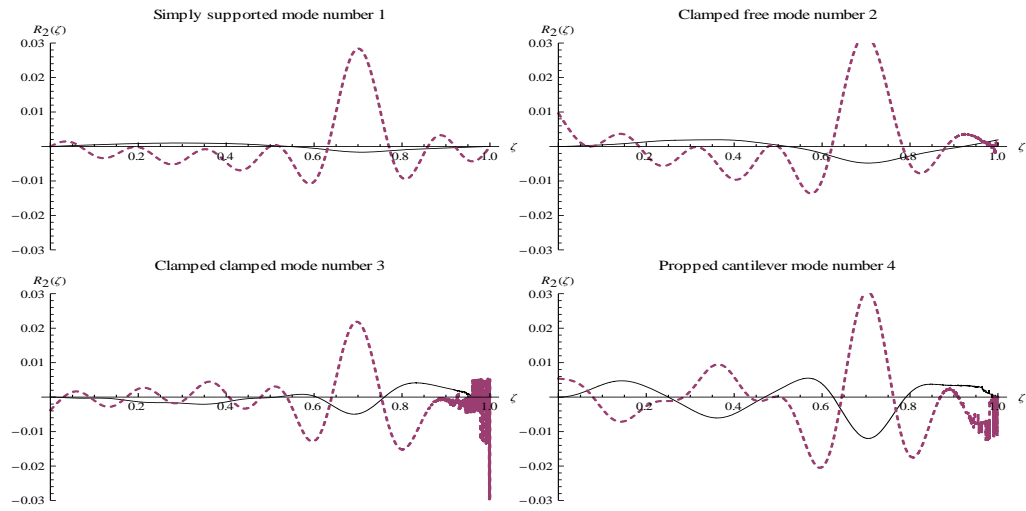
103

Figure 31: Partial mode contribution, mode shape(continuous lines) and curvature shape(dashed lines); $\zeta_d = 0.7$, $\epsilon = 0.1$, $\Delta L_z = 0.01$; first twelve modes considered
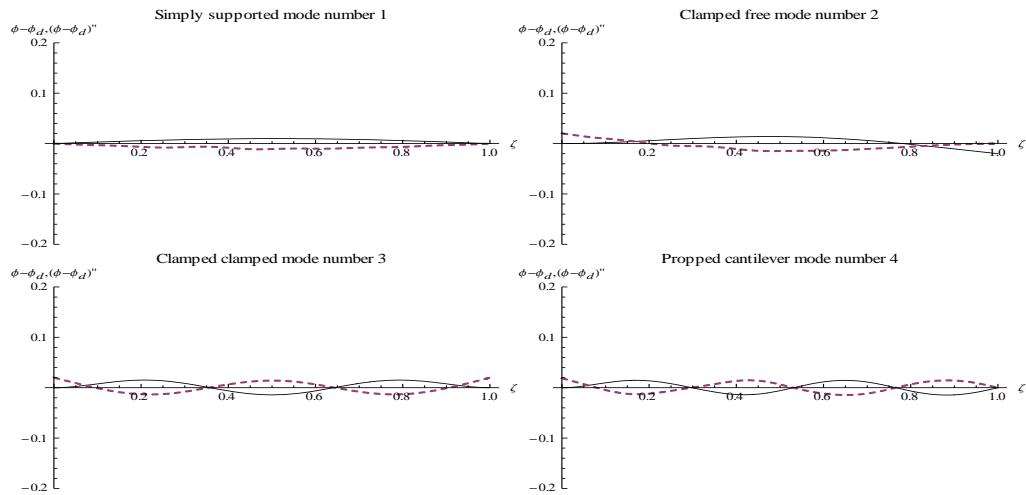

Figure 32: Difference between damaged and undamaged beam, normalized, mode shape (continuous lines) and curvature shape (dashed lines); $\zeta_d = 0.35$, $\epsilon = 0.01$, $\Delta L_z = 0.01$
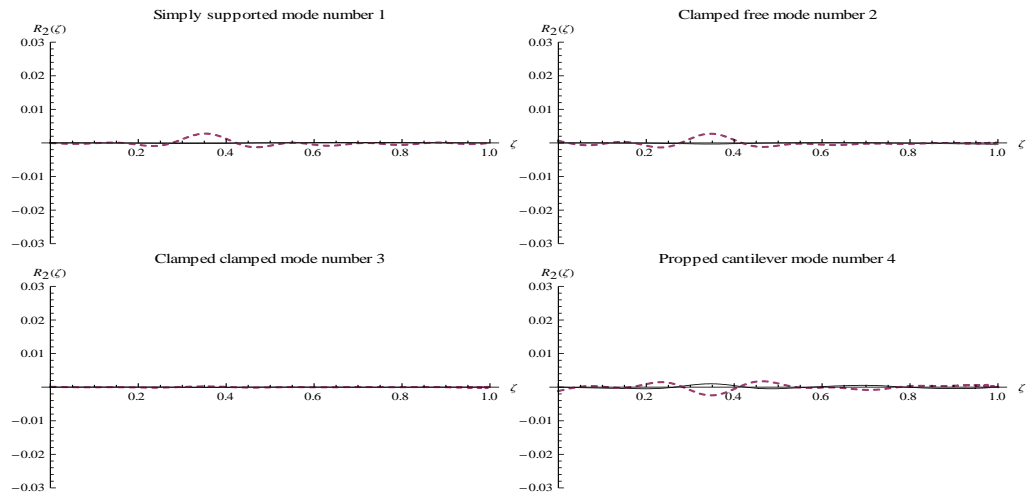
104

Figure 33: Partial mode contribution, mode shape (continuous lines) and curvature shape (dashed lines); $\zeta_d = 0.35$, $\epsilon = 0.01$, $\Delta L_z = 0.01$; first twelve modes considered
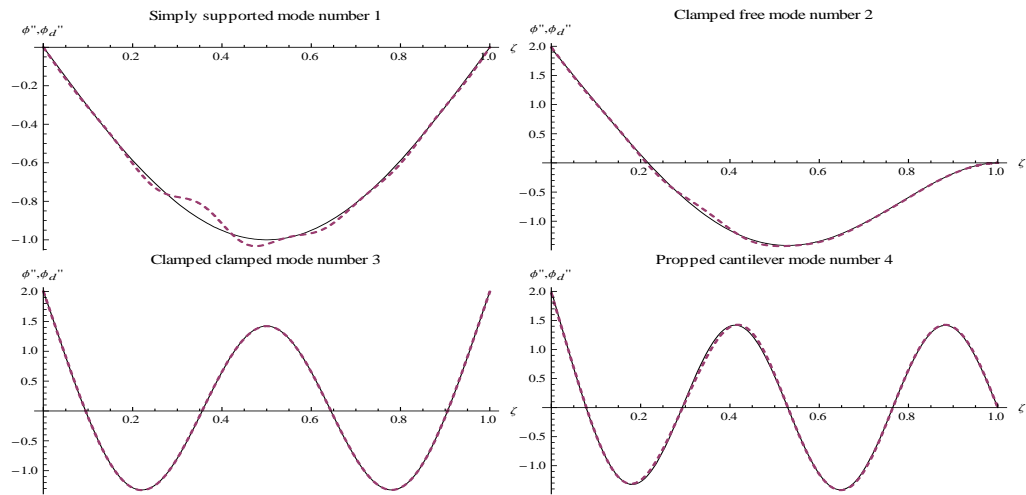

Figure 34: Damaged (dashed lines) and undamaged (continuous lines) beam curvature shapes; $\zeta_d = 0.35$, $\epsilon = 0.4$, $\Delta L_z = 0.01$
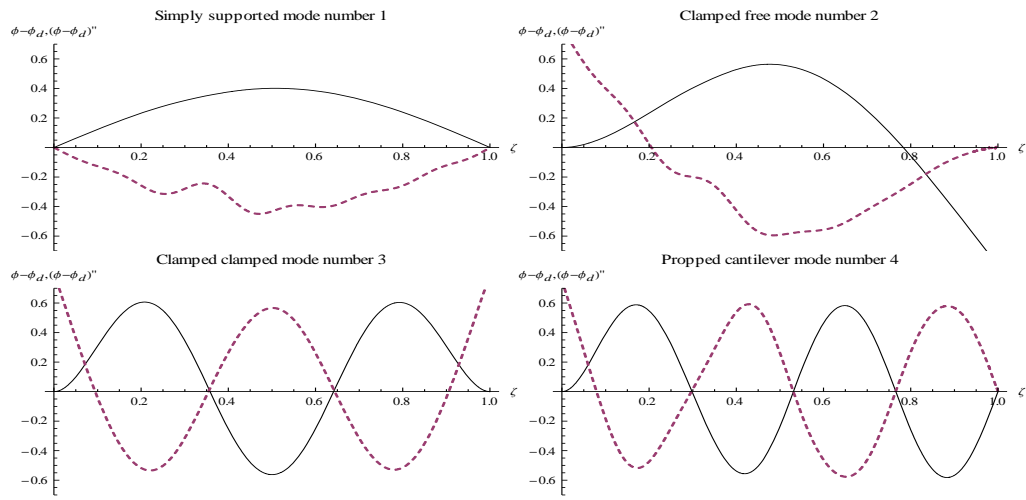
Figure 35: Difference between damaged and undamaged beam, normalized, mode shape (continuous lines) and curvature shape (dashed lines); $\zeta_d = 0.35$, $\epsilon = 0.4$, $\Delta L_z = 0.01$

Figure 36: Partial mode contribution, mode shape (continuous lines) and curvature shape (dashed lines); $\zeta_d = 0.35$, $\epsilon = 0.4$, $\Delta L_z = 0.01$; first twelve modes considered

106

Figure 37: Difference between damaged and undamaged beam, normalized, mode shape (continuous lines) and curvature shape (dashed lines); $\zeta_d = 0.35$, $\epsilon = 0.1$, $\Delta L_z = 0.001$
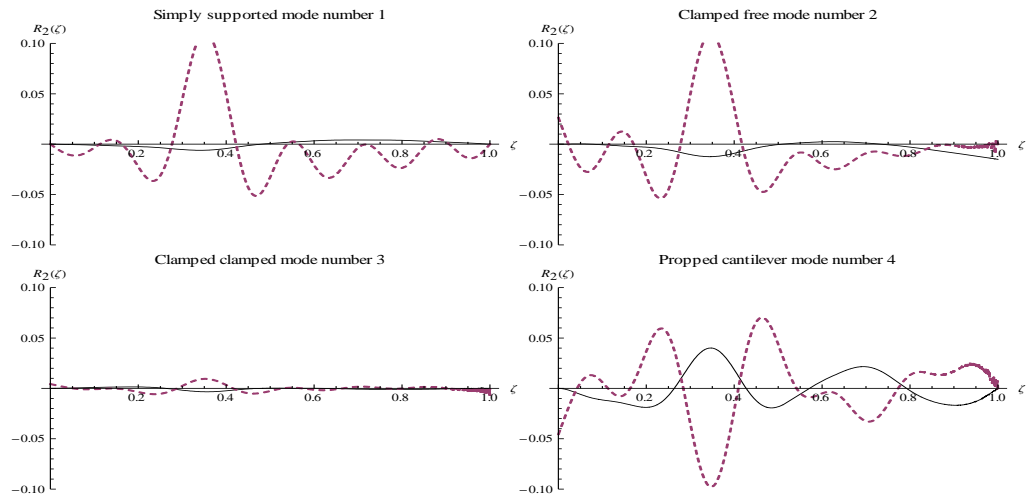

Figure 38: Partial mode contribution, mode shape (continuous lines) and curvature shape (dashed lines); $\zeta_d = 0.35$, $\epsilon = 0.1$, $\Delta L_z = 0.001$; first twelve modes considered
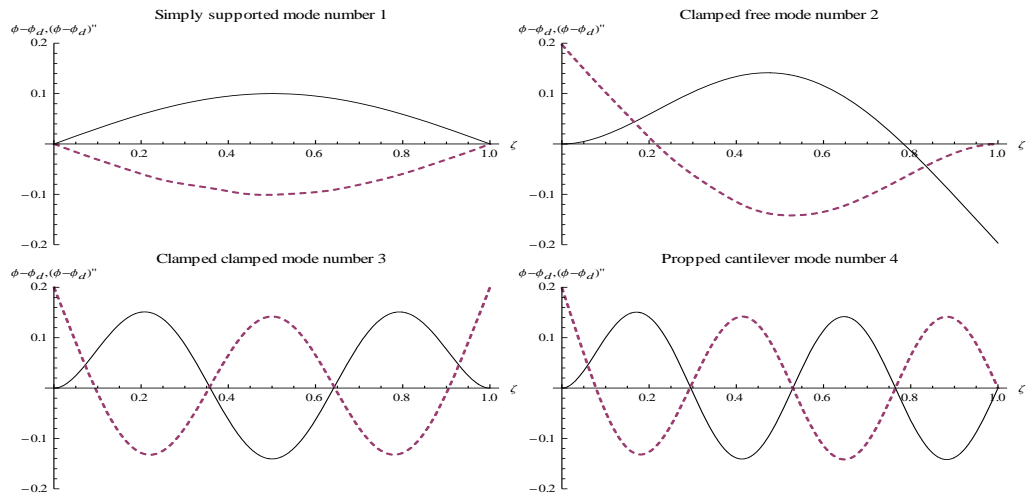
107

Figure 39: Damaged (dashed lines) and undamaged (continuous lines) beam curvature shapes; $\zeta_d = 0.35$, $\epsilon = 0.1$, $\Delta L_z = 0.1$

Figure 40: Difference between damaged and undamaged beam, normalized, mode shape (continuous lines) and curvature shape(dashed lines); $\zeta_d = 0.35$, $\epsilon = 0.1$, $\Delta L_z = 0.1$

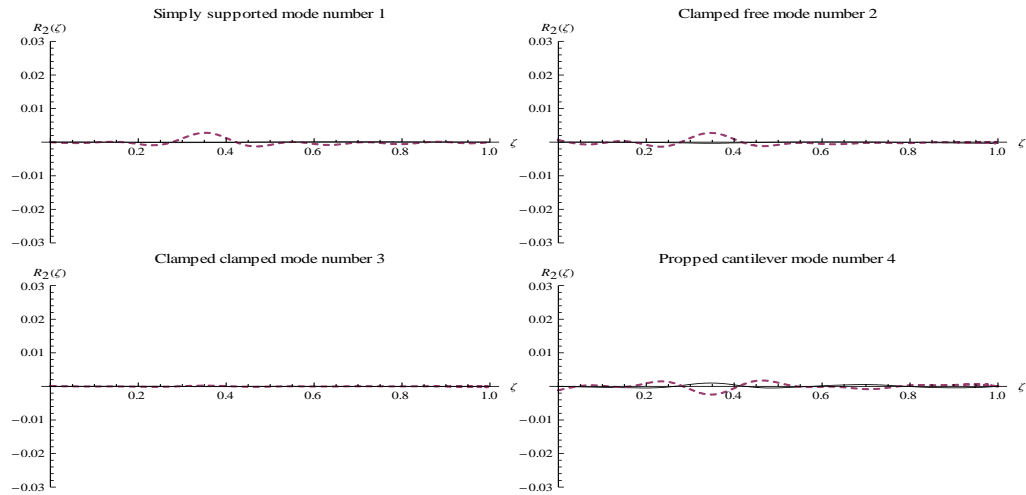**Figure 41:** Partial mode contribution, mode shape (continuous lines) and curvature shape (dashed lines); $\zeta_d = 0.35$, $\epsilon = 0.1$, $\Delta L_z = 0.1$; first twelve modes considered
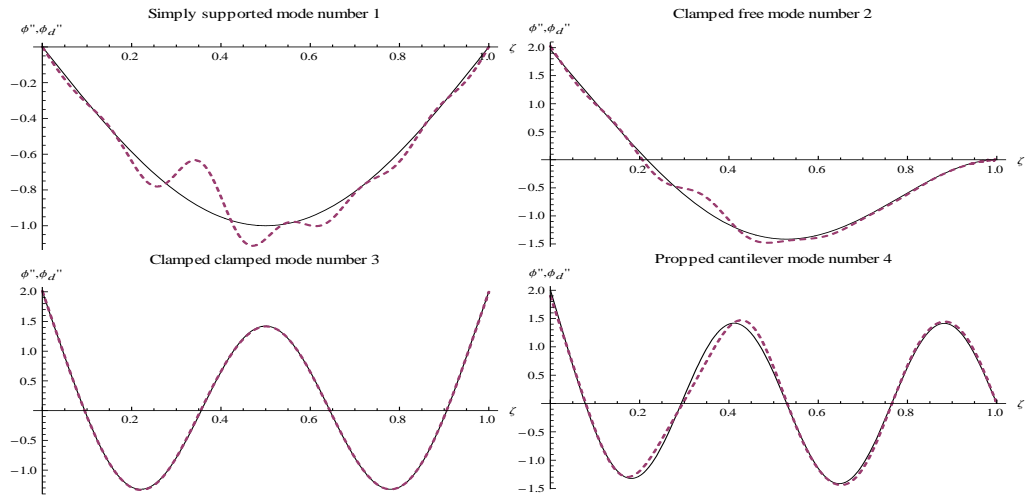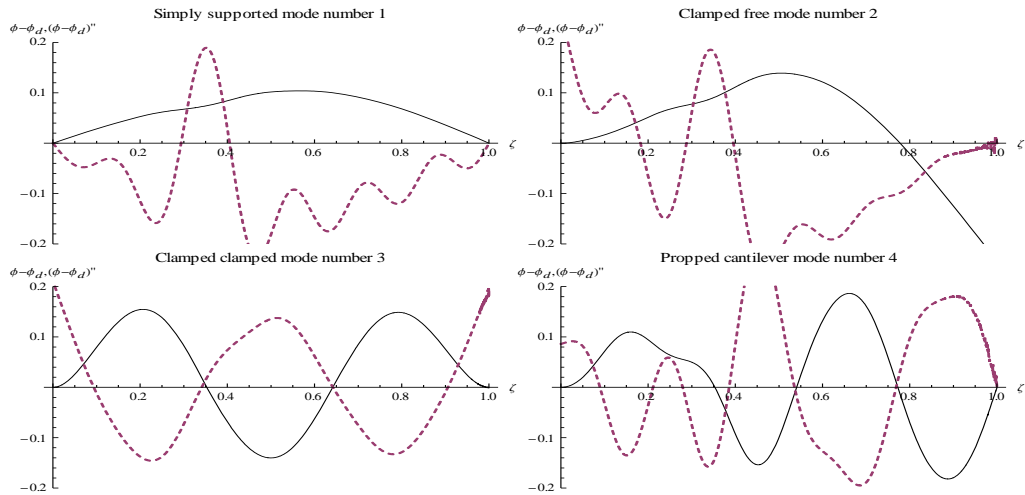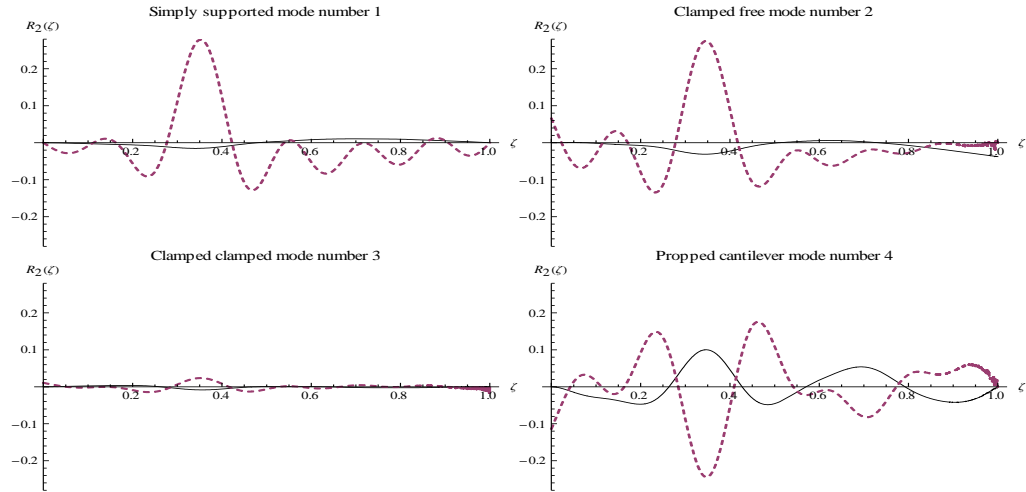
  2. requirement of baseline data from undamaged structural state, since presented physical quantity did not require a baseline to identify the damage.

- The difference between normalized mode shapes and curvature shapes gives a false indication of damage for the propped-cantilever case as shown in figure 40.

- Partial mode contribution is a primary physical quantity and does not require derivative numerical processes as required by natural frequencies and strain energy based damage identification procedures for damage identification.

- Similar to the derivative procedures for displacement and curvature mode shapes such as calculation of strain energy, derivative procedures for partial mode contribution can be investigated for damage characterization and quantification.

- The method was applied to structures using Euler-Bernoulli beam theory. It was seen that the order of sensitivity was same for different boundary conditions. The sensitivity however was greater for curvature mode shapes as compared to displacement mode shape as were the number of oscillations.

- The ability of these two parameters to detect damage can be studied for different

109

levels of noise in the measured data.

- The lack of dependence of partial mode contribution to environmental conditions like temperature is also a matter for further investigation by the author.

Chapter X

CONTRIBUTIONS AND RECOMMENDATION FOR FUTURE STUDIES

10.1 Contributions

The thesis has the following contributions:

1. The thesis provides a generic framework to model damage in elastic structures which are self adjoint systems. Specifically the framework was applied to Euler-Bernoulli beam theory, Timoshenko beam theory and Kirchhoff's plate theory. The framework was applied to beams with different shapes. The framework was applied to an exhaustive set of boundary conditions. Damage models for different shapes of damage in beams and different orientation of damage in plates were presented.

2. The framework is applicable to eigenvalue problems with discontinuities for self adjoint systems.

3. The inertia effects (kinetic energy) due to damage were included in modeling, and it was shown that they are not negligible as compared to stiffness effects (strain energy).

4. An analytical expression for a damage index based on strain energy was presented and experimentally verified.

5. Physical reasoning was provided for a new damage identification quantity called the "Partial Mode Contribution" and it was verified using rigorous mathematical procedure. The quantity was shown to be more sensitive than existing damage detection quantities such as displacement mode shapes, curvature mode shapes and difference of normalized displacement or curvature shape between damaged and undamaged states of the beam. Partial mode contribution was able to give accurate estimations of the location of damage in spite of noise in the detection ambience. The quantity was shown to not require baseline state data.

111

10.2   Recommendation For Future Studies

1. The perturbed differential equations that were developed are in the same form as those that are used to develop finite elements. The displacement in finite element procedure is replace with perturbed eigenfunction and the forcing function with the right hand side of the perturbed differential equation. Therefore, it is proposed to develop a finite element formulation based on the method presented in this thesis. Such a formulation would reduce significantly the computation time associated to determine mode shapes and natural frequencies of a damaged structure. Consider a simple beam, initially when no damage is there the dynamic response is computed accurately using few beam elements, however, if there is a small damage introduced, several plate finite elements of a high density mesh, at least in the vicinity of the damage are needed. Using the framework, the same mesh as used for undamaged case would be used with the beam element at the location of damage substituted with damaged beam element.

2. The method presented in this thesis is essentially a solution to an eigenvalue problem with discontinuous domains for systems which are self adjoint systems. Self adjoint systems form a very large class of physical problem set. It is therefore proposed to apply to see the validity of the framework to other self-adjoint systems such as computing the buckling load of damaged beams, getting the mode shapes of tapered beams and Mindlin plate theory.

3. In the presentation of the damage measure based on the strain energy, two damage parameters were discovered one giving global damage influence $\Gamma(x, x_d, \Delta l, \epsilon)$ and another giving acute local damage influence $\Lambda(x_d, \Delta l, \epsilon)$, where x_d, Δl and ϵ give the location, extent and ratio of depth to total depth of the damage, respectively. Since $\Lambda(x_d, \Delta l, \epsilon)$ is a function of damage magnitude (ϵ and Δl), the damage measure can be used to find the damage magnitude. This is a topic for further study.

4. It has been found by previous researchers that derivative quantities such as curvature shapes, strains and strain energy are more sensitive to damage than mode shapes

112

themselves. It is therefore recommended to explore the derivative quantities associated with the partial mode contribution for damage detection and characterization.

5. The lack of dependence of partial mode contribution to environmental conditions like temperature is also a matter for further investigation by the author.

6. An interesting parameter that arose in the derivation was η_{nj}, which is the coefficient of eigenfunctions for the undamaged beam when used to find the particular solution for perturbed differential equations. The physical significance of this parameter and its ability to identify and characterize damage can be investigated.

REFERENCES

[1] APETRE, N., RUZZENE, M., HANAGUD, S., and GOPALKRISHNAN, S., "Spectral and perturbation analysis of first-order beams with notch damage," *Journal of Applied Mechanics*, vol. 75, pp. 1–10, 2008.

[2] BAUCHAU, O. and CRAIG, J., *Structural Analysis with Applications to Aerospace Structures*. New York: Springer, 2009.

[3] BAYLY, P. V., "On the spectral signature of weakly bilinear oscillators," *ASME Journal of Vibrations and Acoustics*, vol. 118, pp. 252–261, 1996.

[4] CARDEN, E. and FANNING, P., "Vibration based condition monitoring: a review," *Structural Health Monitoring*, vol. 3, no. 4, pp. 355–377, 2004.

[5] CAWLEY, P. and ADAMS, R., "The location of defects in structures from measurements of natural frequencies," *Journal of Strain Analysis*, vol. 14, no. 2, pp. 49–57, 1979.

[6] CHANDRASHEKAR, M. and GANGULI, R., "Structural damage detection using modal curvature and fuzzy logic," *Structural Health Monitoring*, vol. 19A, pp. 153–160, 2009.

[7] CHO, Y. and ROSE, J. L., "An elastodynamic hybrid boundary element study for elastic guided wave interactions with a surface-breaking defect," *International Journal of Solid and Structures*, vol. 37, no. 30, pp. 4103–4124, 2000.

[8] CHOI, S. and STUBBS, N., "Nondestructive damage detection algorithms for 2d plates," in *Smart Systems for Bridges, Structures, and Highways, Proceedings of SPIE*, vol. 3, pp. 193–204, 1997.

[9] CHONDROS, T., DIMAROGONAS, A., and YAO, J., "A continuous cracked beams vibration theory," *Journal of Sound and Vibration*, vol. 215, no. 1, pp. 17–34, 1998.

[10] CHONDROS, T., DIMAROGONAS, A., and YAO, J., "Vibration of a beam with a breathing crack," *Journal of Sound and Vibration*, vol. 239, no. 1, pp. 57–67, 2002.

[11] CHRISTIDES, S., BARR, A. D. S., and BANG, H. J., "One-dimensional theory of cracked Euler-Bernoulli beams," *International Journal of Mechanical Sciences*, vol. 26, no. 11-12, pp. 339–348, 1984.

[12] CIANG, C. C. and LEE, J. R., "Structural health monitoring for a wind turbine system: a review of damage detection methods," *Measurement Science And Technology*, vol. 19, pp. 1–20, 2008.

[13] CORNWELL, P., DOEBLING, S., and FARRAR, C., "Application of the strain energy damage detection method to plate-like structures," *Journal of Sound and Vibration*, vol. 224, no. 2, pp. 359–374, 1999.

[14] DIMAROGONAS, A. D., "Vibration of cracked structures: a state of the art review," *Engineering Fracture Mechanics*, vol. 55, no. 5, pp. 831–857, 1996.

114

[15] Dixit, A. and Hanagud, S., "Comparison of strain energy based damage measure for Timoshenko and Euler-Bernoulli beams with notch like damages," in *Proceedings of the International Workshop on Structural Health Monitoring 2009*, 2009.

[16] Dixit, A. and Hanagud, S., "A damage localization method for Timoshenko And Euler-Bernoulli beams," in *51st AIAA/ASME/ASCE/AHS/ASC Structures, Structural Dynamics, and Materials Conference*, 2010.

[17] Dixit, A. and Hanagud, S., "Comments on: 'Curvature mode shape-based damage assessment of carbon/epoxy composite beams'," *Journal of Intelligent Material Systems and Structures*, vol. 21, no. 6, pp. 659–663, 2010.

[18] Dixit, A. and Hanagud, S., "Single beam analysis of damaged beams verified using a strain energy based damage measure," *International Journal of Solid and Structures*, vol. 48, no. 3-4, pp. 592–602, 2011.

[19] Dixit, A. and Hanagud, S., "Verification of Unified Framework for plate structures using Kirchhoff's plate theory," in *Proceedings of the International Workshop on Structural Health Monitoring 2011*, pp. 899–907, 2011.

[20] Dixit, A. and Hodges, D. H., "A general damage theory: Solution of nth-order equations using unified framework," *Mechanics Research Communications*, vol. 38, no. 7, pp. 486–493, 2011.

[21] Doebling, S., Farrar, C. R., and Prime, M., "Summary review of vibration-based damage identification methods," *Shock and Vibration Digest*, vol. 30, pp. 91–105, 1998.

[22] Doebling, S., Farrar, C. R., Prime, M., and Daniel, W., *Damage Identification and Health Monitoring of Structural and Mechanical Systems from Changes in Their Vibration Characteristics: A literature Review*. New York: LA-13070-MS, 1996.

[23] Fan, W. and Qiao, P. Z., "Vibration-based damage identification methods: A review and comparative study," *Structural Health Monitoring*, 2010.

[24] Griffith, A. A., ""the phenomena of rupture and flow in solids"," *Philosophical Transactions of the Royal Society of London, A*, vol. 221, pp. 163–198, 1921.

[25] Gurgoze, M., "On the eigenfrequencies of a cantilever beam with attached tip mass and a springmass system," *Journal of Sound and Vibration*, vol. 190, pp. 149–162, 1996.

[26] Happawana, G. S., Bajaj, A. K., and Nwokah, D. I., "A singular perturbation perspective on mode localization," *Journal of Sound and Vibration*, vol. 147, no. 2, pp. 361–365, 1991.

[27] Ho, Y. and Ewins, D., "Numerical evaluation of the damage index," in *Structural Health Monitoring 2000, Stanford University*, pp. 995–1011, 2000.

[28] Ho, Y. and Ewins, D., "On the structural damage identification with mode shapes," in *International Conference on System Identification and Structural Health Monitoring*, pp. 677–686, 2000.

[29] Inc., A., *Abaqus User Manual Version 6.8*. Providence, RI, USA: Abaqus, Inc., 2008.

115

[30] INGLIS, C. E., "Stresses in a plate due to the presence of cracks and sharp corners," *Trans. Inst. Naval Architects*, vol. 55, pp. 219–241, 1913.

[31] IRWIN, G., "Analysis of stresses and strains near the end of a crack traversing a plate," *Journal of Applied Mechanics*, vol. 24, pp. 361–364, 1957.

[32] JOSHI, A. and MADHUSUDHAN, B. S., "A unified approach to free vibration of locally damaged beams having various homogeneous boundary conditions," *Journal of Sound and Vibration*, vol. 147, pp. 475–488, 1991.

[33] KHAJI, N., SHAFIEI, M., and JALALPOUR, M., "Closed-form solutions for crack detection problem of timoshenko beams with various boundary conditions," *International Journal of Material Science*, vol. 51, pp. 667–681, 2009.

[34] KIM, K., RYU, J., LEE, S., and CHOI, L., "In-Situ Monitoring of Sungsan Bridge in Han River with a Optical Fiber Sensor System," in *Smart Systems for Bridges, Structures, and Highways, Proceedings of SPIE*, vol. 1, pp. 72–76, 1997.

[35] KRAWCZUK, M., "Application of spectral beam finite element with a crack and iterative search technique for damage detection," *Finite Elements in Analysis and Design*, vol. 9-10, pp. 991–1004, 2002.

[36] LAW, S. and LU, Z. R., "Crack identification in beam from dynamic responses," *Journal of Sound and Vibration*, vol. 285, pp. 967–987, 2005.

[37] LESTARI, W., *Damage of Composite Structures: Detection Technique, Dynamic Response and Residual Strength*. PhD thesis, Georgia Institute of Technology, School of Aerospace Engineering, 2001.

[38] LESTARI, W., QIAO, P., and HANAGUD, S., "Curvature mode shape-based damage assessment of carbon/epoxy composite beams," *Journal Of Intelligent Material Systems And Structures*, vol. 18, pp. 189–208, 2007.

[39] LI, Q. S., "Vibratory characteristics of timoshenko beams with arbitrary number of cracks," *Journal of Engineering mechanics*, vol. 129, no. 11, pp. 1355–1359, 2003.

[40] LOYAA, J., RUBIOB, L., and FERNANDEZ-SAVEZA, J., "Natural frequencies for bending vibrations of Timoshenko cracked beams," *Journal of Sound and Vibrations*, vol. 290, no. 11, pp. 640–653, 2006.

[41] LUO, H. and HANAGUD, S., "An integral equation for changes in the structural characteristics of damaged stuctures," *International Journal of Solids and Structures*, vol. 34, pp. 4557–4579, 1997.

[42] LUO, H. and HANAGUD, S., "Detection of debonding in thermal protective system titles by using nonlinear structural dynamic response," in *Structural Dynamics, and Materials Conference, an Exhibit*, 1998.

[43] MAGRAB, E. B., *Vibration of elastic structural members*. Alphen aan den Rijn, The Netherlands: Sijthoff and Noordhoff International Publisher B.V., 1979.

[44] MAN, X., MCCLURE, L., WANG, Z., FINCH, R., ROBIN, P., and JANSEN, B., "Slot depth resolution in vibration signature monitoring of beams using frequency shift," *The Journal of the Acoustical Society of America*, vol. 95, no. 4, pp. 2029–2037, 1994.

116

[45] MEIROVITCH, L., *Principles and Techniques Of Vibrations*. New Jersey: Prentice-Hall International, 1997.

[46] MODENA, C., SONDA, D., and ZONTA, D., "Damage localization in reinforced concrete structures by using damping measurements," in *Damage Assessment of Structures, Proceedings of the Internationa Conference on Damage Assessment of Structures, DAMAS 99*, pp. 132–141, 1999.

[47] MONTALVAO, D., MAIA, N. M. M., and RIBEIRO, A. M. R., "A review of vibration-based structural health monitoring with special emphasis on composite materials," *Shock and Vibration Digest*, vol. 38, no. 4, pp. 295–326, 2006.

[48] NAYFEH, A., *Problems in Perturbation*, pp. 1–2. New York: Wiley, 1985.

[49] OOIJEVAAR, T., LOENDERSLOOT, R., WARNET, L., BOER, A., and AKKERMAN, R., "Vibration based structural health monitoring of a composite t-beam," *Composite Structures*, vol. 92, pp. 2007–2015, 2010.

[50] OSTACHOWICZ, W. and KRAWCZUK, M., "Analysis of the effect of cracks on the natural frequencies of a cantilever beam," *Journal of Sound and Vibrations*, vol. 150, pp. 191–201, 1991.

[51] PANDEY, A., BISWAS, M., and SAMMAN, M., "Damage detection from changes in curvature mode shapes," *Journal of Sound and Vibration*, vol. 145, no. 2, pp. 321–332, 1991.

[52] QIAN, G. L., GU, S. N., and JIANG, J. S., "The dynamic behavior and crack detection of a beam with a crack," *Journal of Sound and Vibration*, vol. 138, pp. 233–243, 1991.

[53] QIAO, P., LU, K., LESTARI, W., and WANG, J., "Curvature mode shape-based damage detection in composite laminated plates," *Composite Structures*, vol. 80, pp. 407–428, 2007.

[54] RAGHAVAN, A. and CESNIK, C. E., "Review of guided-wave structural health monitoring," *Shock and Vibration Digest*, vol. 39, no. 2, pp. 91–114, 2007.

[55] SADRNEJAD, S. A., DARYAN, A. S., and ZIAEI, M., "Vibration equations of thick rectangular plates using mindlin plate theory," *Journal of Computer Science*, vol. 5, no. 11, pp. 838–842, 2009.

[56] SCHULZ, M., NASER, A., THYAGARAJAN, S., MICKENS, T., and PAI, P., "Structural health monitoring using frequency response functions and sparse measurements," in *Proceedings of the International Modal Analysis Conference*, pp. 760–766, 1998.

[57] SHARMA, V., *Damage Index Estimation in Beams and Plates Using Laser Vibrometry*. PhD thesis, Georgia Institute of Technology, School of Aerospace Engineering, 2008.

[58] SHARMA, V., HANAGUD, S., and RUZZENE, M., "Damage index estimation in beams and plates using laser vibrometry," in *Proceedings of the 2005 International Workshop on Structural Health Monitoring*, 2005.

[59] SHARMA, V., RUZZENE, M., and HANAGUD, S., "Perturbation methods for the analysis of the dynamic behavior of damaged plates," *International Journal of Solids and Structures*, vol. 43, pp. 4648–4672, 2006.

[60] SHEN, M. H. and PIERRE, C., "Natural modes of Euler-Bernoulli beams with symmetric cracks," *Journal of Sound and Vibration*, vol. 138, pp. 115–134, 1990.

[61] SHI, Z. Y., LAW, S. S., and ZHANG, L. M., "Structural damage detection from modal strain energy change," *Journal of Engineering Mechanics*, vol. 126, no. 12, pp. 1216–1223, 2000.

[62] SOHN, H., FARRAR, C. R., HEMEZ, F. M., SHUNK, D. D., STINEMATES, D. W., and NADLER, B. R., *A review of structural health monitoring literature : 1996-2001.* Los Alamos National Laboratory Report, LA-13976-MS, 2003.

[63] STASZEWSKI, W., BOLLER, C., and TOMLINSON, G., *Health Monitoring of Aerospace Structures: Smart Sensor Technologies and Signal Processing.* England: John Wiley and Sons, Inc., 2004.

[64] SWAMIDAS, A. S. J., YANG, X., and SESHADRI, R., "Identification of cracking in beam structures using timoshenko and euler formulations," *Journal of Engineering Mechanics*, vol. 130, no. 11, pp. 1297–1308, 2004.

[65] TAKEHASHI, I., "Vibration and stability of non-uniform cracked timoshenko beam subjected to follower force," *Computer and Structures*, vol. 71, pp. 585–591, 1999.

[66] THOMPSON, W. T., "Vibration of slender bars with discontinuities in stiffness," *Journal of Applied Mechanics*, vol. 16, pp. 203–207, 1949.

[67] WANG, J. and QIAO, P., "Vibration of beams with arbitrary discontinuities and boundary conditions," *Journal of Sound and Vibration*, vol. 308, no. 1-2, pp. 12–27, 2007.

[68] WANG, M., XU, F., and LLOYD, G., "A systematic numerical analysis of the damage index method used for bridge diagnostics," in *Smart Structures and Materials 2000: Smart Systems for Bridges, Structures and Highways, Proceedings of SPIE*, vol. 3, pp. 154–164, 2000.

[69] WEST, W., "Illustration of the use of modal assurance criterion to detect structural changes in an orbiter test specimen," in *Proc. Air Force Conference on Aircraft Structural Integrity*, pp. 1–6, 1984.